Study on Assessment of Water Resources in Agricultural Watershed in Northwestern Cambodia Facing Climate and Land Use Changes
(気候変動と土地利用変化の影響を考慮したカンボジア北西部農業流域の水資源評価に関する研究)

Hokkaido University Graduate School of Agriculture

Frontiers in Environmental Sciences Doctor Course

CHEY Vanna

Frontiers in Environmental Sciences

CHEY Vanna

ABSTRACT

Economic and population growth have expanded agricultural land, and the sustainability of water and natural resources like forest preservation has become a concern for future development. Cambodia's water resources depend on abundant freshwater from the Mekong River and Tonle Sap Great Lake. However, the northwestern part of the nation, the largest rice production area, has faced significant influence on water resources, leading to water scarcity, flooding, and droughts. Additionally, limited information is available to analyze these issues. This study aims to identify and predict the impacts of land use and climate change on water resources and examine problems and countermeasures for future agricultural water use.

There are always concerns about water deficits in cultivating rice at the onset of the dry season. First, this study evaluated the irrigation water resources in the upper Sangker River basin for agricultural production. The study used the Soil and Water Assessment Tool (SWAT) model to estimate stream water volume, and its performance was assessed using statistical metrics. It was calibrated for the period from 2007 to 2013 and validated for the period from 2014 to 2018. Flow rates in the main irrigation canals were also measured from June 2018 to October 2019 to evaluate the actual irrigation water supply by comparing supplied water volume and irrigation water demand. The SWAT model provided reliable river discharge estimates, as confirmed by statistical metrics (NSE = 0.69, RSR = 0.55). The results showed that water shortage rates exceeded 20% of the monthly water requirement between April and June, 2014 to 2017. The actual irrigation water supply during the study period showed rates of water shortage of 52% and 41% in the two main canals, respectively, at the headwork during the wet season months (September and October). The findings suggest the need for regular maintenance of water infrastructure to provide a sustainable water supply to paddy fields.

After a meticulous evaluation of agricultural water use, this study utilized remote sensing and GIS modelling techniques for analyzing satellite data from 2014, 2018, and 2022. Integrating the cellular automata (CA)-Markov model and GIS tools allowed for predicting land use changes by 2030 considering policy intervention. The model's simulation, which compared actual and predicted land use in 2022 for accuracy assessment, revealed a stark contrast in outcomes with and without a land use policy. Without a policy, built-up areas will increase, and natural forest cover will decrease by 2030. However, with a policy, the model

predicted an increase in forest cover by 2030 despite some areas being allocated for industrial agriculture. These findings underscore the transformation in land cover in the upper Sangker River basin and reiterate the crucial role of forest conservation in preserving ecosystem services and water cycles.

The final part of this study focused on evaluating the impact of land use and climate variability on water resources in the Upper Sangker River basin using the SWAT model. It projected changes in rainfall and temperature from the Coordinated Regional Climate Downscaling Experiment-Southeast Asia (CORDEX-SEA). The dynamic changes in land use within the watershed and the projected land use for 2030 were derived from the previous section. The study revealed that land use changes resulted in increasing trends in mean annual (30. 9%), wet season (39.7%), and dry season (9.8%) river discharge comparing the simulation period (1986–2001). However, the combined effects of land use and climate change scenarios for the projection period (2030–2045) indicated a significant shift in river discharge patterns between wet and dry seasons. The mean annual streamflow decreased from 30.9% to 5.7% and 3.2% for RCP4.5 and RCP8.5, respectively, comparing the simulation period. Seasonal analysis showed that average streamflow in the wet season continued to increase by 23.3% (RCP4.5) and 10.9% (RCP8.5) but decreased by -36.9% (RCP4.5) and -15.5% (RCP8.5) in the dry season. Furthermore, there is an expected slight increase in water yield and surface runoff, while evapotranspiration is likely to experience the most significant decrease in agricultural land for both climate scenarios (RCP4.5 and RCP8.5). The impact of climate change outweighs that of land use change. Reforestation efforts within land use development projects will minimize impacts on water resources. This study highlights the importance of reforestation in the upper catchment area to enhance basin water resources and mitigate flood risks.

Overall, the results reveal essential factors affecting water resources in the Upper Sangker River Basin under climate change and land use change. Based on these results, this study suggests the need to promote water-efficient agricultural practices, cultivate climate-resilient crops, and make significant investments in conserving and restoring natural resources.

ACKNOWLEDGEMENT

I would like to express my heartfelt gratitude to the following individuals and organizations who have played a significant role in my academic journey:

First and foremost, I am deeply thankful to my supervisor, Dr. Yamamoto Tadao, for his exceptional mentorship and guidance during my PhD. His trust in me and encouragement to independently write my thesis and research articles have been invaluable. I am also grateful to Professor Takashi Inoue, Professor Hirano Takashi, and Professor Toma Yo for their insightful comments and suggestions on my PhD dissertation.

I extend my sincere thanks to the Ministry of Education, Culture, Sports, Science and Technology (MEXT) of Japan for their financial support through a scholarship program, without which this journey would not have been possible. Additionally, I am grateful to the Ministry of Water Resources and Meteorology of Cambodia for their endorsement.

I am particularly thankful to Dr. Ram Avatar for his invaluable ideas and inspiration throughout my life in Japan. His support has been a source of strength during academic and leisure times.

Last but not least, I want to acknowledge the unwavering support and kindness of my mother, brothers, and sisters. I am especially grateful to my wife, Chhun Phalla, and my daughter, Vanna Sokuntevy, for their constant love and encouragement. Their support has been instrumental in making this journey possible.

Table of Contents

LIST OF FIGURES

LIST OF TABLES

LIST OF ABBREVIATION

AVGWLF: ArcView Generalized Watershed Loading Function

BCM : Billion cubic meters

CP : Cropping Pattern

CA : Cellular Automata

DEM : Digital Elevation Model

FAO : Food and Agriculture Organization

FWUC: Farmer Water Users Community

GDP : Gross Domestic Product

GCM : Global Climate Model

GIS : Geographical Information System

IW : Irrigation Water

ID : Irrigation Demands

JICA : Japan International Cooperation Agency

MRC : Mekong River Commission

MCM : Million cubic meters

MOWRAM: Ministry of Water Resources and Meteorology

N : North

PDWRAM : Provincial Department of Water Resources and Meteorology

RMSE : Root Mean Square Error

RCM : Regional Climate Model

RCP : Representative Concentration Pathway

RUSLE: Revised Universal Soil Loss Equation

SUFI-2: Sequential Uncertainty Fitting-Version 2

SWAT : Soil and Water Assessment Tool

SWAT-CUP: SWAT Calibration and Uncertainty Programs

SCS : Soil Conservation Service

TSC : Technical Service Center for Irrigation and Meteorology

UTM : Universal Transverse Mercator

USRB : Upper Sangker River Basin

WGS : World Global System

WGEN: Weather Generator

Chapter 1 Introduction

1.1 Background of research

The agricultural sector is vital to Cambodia's economy and food security as it promotes rural socio-economic development and equity. In 2021, it contributed 20.7% to the GDP and employed 31.2% of the total population (Sok et al., 2022). With 60.6% of the total population living in rural areas, agriculture is their primary source of food security (Sok et al., 2022). However, Cambodian agriculture is mainly rainfed and susceptible to climate-related risks (Monin, 2021). As Cambodia's economy grows, there is increasing stress on water and forest resources. The cultivation of energy crops and deforestation have reduced forest cover to 57% over the past decade. This has led to concerns about water scarcity for drinking, agriculture, industry, and energy, and has also heightened competition between sectors and upstream-downstream regions in river basins (TSC & JICA, 2014). In addition to the impact of climate change, deforestation and land-use changes in river basins contribute to droughts and floods (TSC & JICA, 2014).

Cambodia is known for its abundant freshwater resources, with the Mekong River and Tonle Sap Great Lake being the main sources (Sithirith, 2017; Sagara, 2021). Despite contributing minimally to climate change, Cambodia is highly vulnerable to its impacts, such as floods and droughts, particularly drought (MoE, 2013; Monin, 2021). Cambodian farmers face seasonal challenges, dealing with droughts in the dry season and floods in the wet season due to heavy rains. Rainfall patterns have been changing, resulting in longer droughts, shorter rainy seasons, and occasional flash floods (MoE, 2013). Additionally, rainfall distribution and river discharges in Cambodia are highly seasonal and variable, following a natural pattern of wet and dry seasons (Sagara, 2021). Major environmental changes are expected to occur due to climate change in many regions worldwide (IPCC, 2007), with the majority of these changes affecting the hydrological cycle. Drought and flood events are anticipated to become more frequent and intense (Sok et al., 2021). Hence, understanding hydrological changes and having information on water resources amidst changing land use and climate features is crucial for establishing mechanisms for present and future basin water management..

Insufficient water supply is becoming a growing concern in Cambodia and other parts of the world (Brika et al., 2018; Wheida and Verhoeven, 2007). Climate change, increasing population, rapid urbanization, and declining water quality have led to water scarcity being considered one of the most significant threats to society and a limitation for sustainable development (Chen et al., 2016). Irrigation plays a crucial role in agricultural production in most countries and has put significant pressure on water resources and river ecosystems due to the large amount of water used for irrigation. Additionally, rapid urbanization has led to a growing demand for urban water use, particularly domestic water consumption, creating tension in urban water supply and demand (Wu and Tan, 2012). Water scarcity can be broadly defined as a mismatch between the demand for fresh water and its availability, measured in physical terms. Water shortages can also occur even where infrastructure exists if water distribution is unequal (Jaeger et al., 2017). While much of the literature examining the impacts of climate change on water security focuses on quantifying physical water scarcity, it's important to note that this is just one aspect of the issue.

Land use and land cover (LULC) change is considered to be a significant factor impacting the hydrological cycle (Elfert and Bormann, 2010; Chim et al., 2021). Major factors contributing to land use change include demographic changes, climatic variability, political actions (Elfert and Bormann, 2010), and socio-economic factors (Wang et al., 2021; Handavu et al., 2019). The transformation of land use over time influences various components of the hydrologic budget such as evaporation, surface runoff, infiltration, and groundwater recharge (Ozturk et al., 2013; Lin et al., 2007). The conversion of vegetation cover impacts the annual water balance in a watershed by reducing annual evapotranspiration (ET) and increasing streamflow and base flow (Schilling et al., 2008). LULC modification directly affects ecosystems and their associated services, particularly water yield (Li et al., 2018).

Climate change is a significant factor that is expected to impact the hydrological cycle, leading to substantial consequences for water availability (Hagemann et al., 2013). Observations of global warming have resulted in changes to regional water resources, affecting precipitation, temperature, and energy balance (IPCC, 2007a). All aspects of the

global water cycle have been altered due to climate change in recent decades (Douville et al., 2021), leading to millions of people experiencing hydrological conditions that were previously unfamiliar. According to the IPCC 6th Assessment Report, heavy precipitation has likely increased on a continental scale across North America, Europe, and Asia. Furthermore, the intensity of heavy precipitation has increased in many regions (high confidence), including much of North America, most of Europe, most of the Indian sub-continent, parts of northern and southeastern Asia, much of southern South America, parts of southern Africa, and parts of central, northern, and western Australia (Dunn et al., 2020; Sun et al., 2020). Regarding evapotranspiration (ET), Douville et al. (2021) conclude with high confidence that global terrestrial annual ET has increased since the early 1980s, driven by both increasing atmospheric water demand and vegetation greening (medium confidence), and can be partly attributed to anthropogenic forcing (high confidence). Regional changes in ET depend on changes in both the climate and the properties of the land surface and ecosystems. Trends in annual streamflow have generally followed observed changes in regional rainfall and temperature since the 1950s (Jiménez Cisneros et al., 2014). Climate change has caused changes in local and regional streamflow in various parts of the world, but there is no clear signal in the global mean. Stream flows have shown decreasing trends between the 1950s and 2010s in parts of western and central Africa, eastern Asia, southern Europe, western North America, and eastern Australia, and increasing trends in northern Asia, northern Europe, and northern and eastern North America (Trang, 2016; Gudmundsson et al., 2017; Gudmundsson et al., 2019; Li et al., 2020b; Masseroni et al., 2020). In tropical regions like Asia, the frequency and magnitude of extreme events are projected to change. It is important to understand the magnitude of these projected changes and assess their potential impact. Floods and droughts in Cambodia may be influenced by changing climate.

Assessing the impact of climate and land use changes on water resources is best done through simulating the hydrological conditions expected under projected weather conditions in a specific area (Gosain et al., 2006). Hydrological models are commonly used for evaluating water resources, particularly for studying the effects of climate change

(Hagemann et al., 2013) and land use change. There is a wide array of hydrological models available to simulate streamflow and predict the impact of land management practices on water, sediment, and agricultural chemical yields. These models include empirical models (Artificial Neural Network), conceptual models (Hydrologiska Byrans Vattenavdelning - HBV, Topographic hydrologic model - TOPMODEL), and physically based models (Soil and Water Assessment Tool - SWAT, Systeme Hydrologique European - MIKE SHE, Areal Nonpoint Source Watershed Environment Response Simulation - ANSWERS). Physically based models like SWAT or MIKE SHE are capable of simulating streamflow under changing environmental conditions, such as climate change or land use and land cover changes (LULCC). However, these models require intensive data inputs due to their physically based approach. Conducting a hydrological modeling case study in Cambodia is challenging due to low data availability. SWAT, a spatially distributed hydrological model (Arnold et al., 1998; Gassman et al., 2007), is selected as it is the most widely used to simulate water resources under changing environmental conditions, such as climate change or land use and land cover changes (LULC) (Zhang et al., 2020; Bhatta et al., 2019; Narsimlu et al., 2013). Many researchers have conducted separate studies on the potential impact of LULC change on hydrology (Breuer et al., 2009; Lin et al., 2007; Boongaling et al., 2018) and future climate change on water resources (Hagemann et al., 2013; Hattermann et al., 2015; Vicuna and Dracup, 2007). However, most of these studies did not consider integrating both factors in their analysis. There are still very few studies that have analyzed the combined impacts of land use and climate changes on hydrology (Trang et al., 2017; Li et al., 2009). Consequently, the combined effects of future forest cover conversion and trends under various climate change scenarios on water resources and runoff at the subbasin level remain unclear (Oeurng et al., 2019). Therefore, an integrated approach to hydrological modeling is necessary to quantify the contribution of individual land use change classes to a change in river discharge.

The study is conducted in the Upper Sangker River basin in Battambang province, Cambodia. Although, there is a need to collect detailed studies to understand the available water resources and the impact assessment of climate variability in this basin. There is

relatively little information regarding the effects of climate change on hydrology in this catchment. Specifically, there is no study on the combined impacts of land use and climate changes on water resources in the Sangker River basin. Monichoth et al. (2014) applied the Hydro-Crop model to assess the possible impacts of climate change on rice production in the Sangker River basin. The entire catchment of the Sangker River was analyzed by Oeurng et al. (2019) using the SWAT model to examine the effect of climate change on river flow regime. These studies investigated water-related relationships within the Sangker River basin (Vanna et al., 2021) and the impact of climate variation on future hydrological alterations (Oeurng et al., 2019; Monichoth et al., 2014), but without considering the impacts of land use and land cover changes. To address this gap, we apply a semi-distributed SWAT model to quantify the available water resources and to gain a better understanding of the hydrological processes in view of the combined influence of land use and climate change projections.

1.2 Problem statement

Water scarcity and flood events have been observed in the irrigation system. Recently, severe droughts and floods have occurred subsequently. However, little information is available to analyze these issues.

1.3 Statement of purpose

The purpose of this multicase study is to identify and predict the impacts of land use and climate change on water resources and examine problems and countermeasures for future agricultural water use. This will involve estimating irrigation needs, conducting hydrological modeling, and carrying out spatial analysis. To achieve these goals, we have outlined the following objectives:

1) Develop a distributed hydrological model to simulate river discharge and assess the impact of environmental changes.

2) Evaluate the water balance in an irrigation scheme in the upper Sangker River basin.

3) Identify and predict changes in land use and land cover (LULC) in the upper Sangker River basin.

4) Assess the impacts of projected climate and land use changes on water resources.

1.4 Research questions

To shed light on the problem, the following research questions are addressed:

1. Is the water supply sufficient to respond to the demands in an irrigation area?
2. What is the effect of environmental changes on the river flow pattern?
3. What is the seasonal flow in the river leading to flooding risks and water scarcity?

1.5 Structure of the thesis

This thesis comprises seven chapters:

1. Introduction and background information about water resources issues and the potential of the agricultural sector for Cambodia's economy.

2. Literature review of previous studies on irrigation water balance, climate change, land use change, hydrological modeling, and land use modeling.

3. Description of the study area.

4. Evaluation of water balance in an irrigation system in the study area and formulation of a hydrological model suitable for the study area.

5. Prediction of future changes in land use and land cover (LULC) in the upper Sangker River basin to assess the integrated future land use change impact on streamflow and hydrologic water balance components.

6. Assessment of the combined impacts of projected climate and land use changes on the hydrological cycle.

7. General conclusions and recommendations.

References

Breuer, L., Huisman, J. A., Willems, P., Bormann, H., Bronstert, A., Croke, B. F. W., ... & Viney, N. R. (2009). Assessing the impact of land use change on hydrology by ensemble modeling (LUCHEM). I: Model intercomparison with current land use. Advances in water resources, 32(2), 129-146.

Boongaling, C. G. K., Faustino-Eslava, D. V., & Lansigan, F. P. (2018). Modeling land use change impacts on hydrology and the use of landscape metrics as tools for watershed management: The case of an ungauged catchment in the Philippines. Land use policy, 72, 116-128.

Bhatta, B., Shrestha, S., Shrestha, P. K., & Talchabhadel, R. (2019). Evaluation and application of a SWAT model to assess the climate change impact on the hydrology of the Himalayan River Basin. Catena, 181, 104082.

Brika, B., Ghuila, H., & Mosbah, H. (2018). Municipal water shortage and related water issues in the city of Tajoura: A case study to raise public awareness. Water Conservation and Management, 10.

Chen, Z., Ngo, H. H., Guo, W., & Eslamian, S. (2016). Water shortages. Urban Water Reuse Handbook.

Douville, H., Raghavan, K., Renwick, J., Allan, R. P., Arias, P. A., Barlow, M., . . . Zolina, O., 2021: Water Cycle Changes. In: Climate Change 2021: The Physical Science Basis. Contribution of Working Group I to the Sixth Assessment Report of the Intergovernmental Panel on Climate Change. Cambridge University Press, Cambridge.

Dunn, R. J., Alexander, L. V., Donat, M. G., Zhang, X., Bador, M., Herold, N., ... & Bin Hj Yussof, M. N. A. (2020). Development of an updated global land in situ‐based data set of temperature and precipitation extremes: HadEX3. Journal of Geophysical Research: Atmospheres, 125(16), e2019JD032263.

Eyring, V., Gillett, N. P., Achutarao, K., Barimalala, R., Barreiro Parrillo, M., Bellouin, N., ... & Sun, Y. (2021). Human influence on the climate system. in climate change 2021: the physical science basis. Contribution of Working Group I to the Sixth Assessment Report of the Intergovernmental Panel on Climate Change. IPCC Sixth Assessment Report.- Sun, Q., et al., 2020: A global, continental and regional analysis of changes in extreme precipitation. J. Climate, 34 (1), 243-258, doi:10.1175/JCLI-D-19-0892.1.

Gudmundsson, L., Leonard, M., Do, H. X., Westra, S., & Seneviratne, S. I. (2019). Observed trends in global indicators of mean and extreme streamflow. Geophysical Research Letters, 46(2), 756-766.

Gudmundsson, L., Seneviratne, S. I., & Zhang, X. (2017). Anthropogenic climate change detected in European renewable freshwater resources. Nature Climate Change, 7(11), 813-816.

Gosain, A. K., Rao, S., & Basuray, D. (2006). Climate change impact assessment on hydrology of Indian river basins. Current science, 346-353.

Hattermann, F. F., Huang, S., & Koch, H. (2015). Climate change impacts on hydrology and water resources. Vol. 24, No. 2, 201–211

Handavu, F., Chirwa, P. W., & Syampungani, S. (2019). Socio-economic factors influencing land-use and land-cover changes in the miombo woodlands of the Copperbelt province in Zambia. Forest policy and economics, 100, 75-94.

Hagemann, S., Chen, C., Clark, D. B., Folwell, S., Gosling, S. N., Haddeland, I., ... & Wiltshire, A. J. (2013). Climate change impacts on available water resources obtained using multiple global climate and hydrology models. Earth System Dynamics, 4(1), 129-144.

IPCC, 2007: Climate Change 2007: Synthesis Report. Contribution of Working Groups I, II

and III to the Fourth Assessment Report of the Intergovernmental Panel on Climate Change

Adaptation options for the vulnerability of Mekong water resources Page 147

[Core Writing Team, Pachauri, R.K and Reisinger, A. (eds.)]. IPCC, Geneva, Switzerland,

104 pp.

IPCC, 2007a: Climate change 2007: Impacts, Adaptation and Vulnerability, summary for policy makers. Working Group II Contribution to the Fourth Assessment. – Report of the Intergovernmental Panel on Climate Change.

IPCC 6th AR: Climate Change 2022: Impacts, Adaptation and Vulnerability. The Working Group II contribution to the IPCC Sixth Assessment Report assesses the impacts of climate change, looking at ecosystems, biodiversity, and human communities at global and regional levels.

Jaeger, W. K., Amos, A., Bigelow, D. P., Chang, H., Conklin, D. R., Haggerty, R., ... & Turner, D. P. (2017). Finding water scarcity amid abundance using human–natural system models. Proceedings of the National Academy of Sciences, 114(45), 11884-11889.

Li, Z., Liu, W. Z., Zhang, X. C., & Zheng, F. L. (2009). Impacts of land use change and climate variability on hydrology in an agricultural catchment on the Loess Plateau of China. Journal of Hydrology, 377(1-2), 35-42.

Lin, Y. P., Hong, N. M., Wu, P. J., Wu, C. F., & Verburg, P. H. (2007). Impacts of land use change scenarios on hydrology and land use patterns in the Wu-Tu watershed in Northern Taiwan. Landscape and urban planning, 80(1-2), 111-126.

Lin, Y. P., Hong, N. M., Wu, P. J., Wu, C. F., & Verburg, P. H. (2007). Impacts of land use change scenarios on hydrology and land use patterns in the Wu-Tu watershed in Northern Taiwan. Landscape and urban planning, 80(1-2), 111-126.

Li, S., Yang, H., Lacayo, M., Liu, J., & Lei, G. (2018). Impacts of land-use and land-cover changes on water yield: A case study in Jing-Jin-Ji, China. Sustainability, 10(4), 960.

Li, L., Ni, J., Chang, F., Yue, Y., Frolova, N., Magritsky, D., ... & Walling, D. E. (2020). Global trends in water and sediment fluxes of the world's large rivers. Science Bulletin, 65(1), 62-69.

MoE. (2013). Cambodia climate change strategic plan 2014–2023.

Masseroni, D., Camici, S., Cislaghi, A., Vacchiano, G., Massari, C., & Brocca, L. (2020). 65-year changes of annual streamflow volumes across Europe with a focus on the Mediterranean basin. Hydrology and Earth System Sciences Discussions, 2020, 1-16.

Monin, N. (2021). The Impacts of Climate Change on Agriculture and Water Resources in Cambodia: From Local Communities' Perspectives (No. 125). CDRI Working Paper Series.

Narsimlu, B., Gosain, A. K., & Chahar, B. R. (2013). Assessment of future climate change impacts on water resources of Upper Sind River Basin, India using SWAT model. Water resources management, 27, 3647-3662.

Oeurng, C., Cochrane, T. A., Chung, S., Kondolf, M. G., Piman, T., & Arias, M. E. (2019). Assessing climate change impacts on river flows in the Tonle Sap Lake Basin, Cambodia. Water, 11(3), 618.

Öztürk, M., Copty, N. K., & Saysel, A. K. (2013). Modeling the impact of land use change on the hydrology of a rural watershed. Journal of Hydrology, 497, 97-109.

Sok, S., Cheb, H., Chhinh, N., & Nguonphan, P. (2022). Productivity, damages, and losses of rice in Cambodia: past, present, and future trends in the Mekong and Tonle Sap regions. In Remote Sensing of Agriculture and Land Cover/Land Use Changes in South and Southeast Asian Countries (pp. 277-295). Cham: Springer International Publishing.

Sithirith, M. (2017). Water governance in Cambodia: From centralized water governance to farmer water user community. Resources, 6(3), 44.

Sagara, J. (2021). Surface Water Resources Assessment of the Tonle Sap and Mekong Delta River Basin Groups: Improving Climate Resilience, Productivity, and Sustainability (ADB Brief 171.

Schilling, K. E., Jha, M. K., Zhang, Y. K., Gassman, P. W., & Wolter, C. F. (2008). Impact of land use and land cover change on the water balance of a large agricultural watershed: Historical effects and future directions. Water resources research, 44(7).

Sok, S., Chhinh, N., Hor, S., & Nguonphan, P. (2021). Climate change impacts on rice cultivation: a comparative study of the Tonle Sap and Mekong River. Sustainability, 13(16), 8979.

TSC & JICA. (2014). Background of the project for river basin water resources utilization. Phnom Penh: Ministry of Water Resources and Meteorology. (Unpublished)

Trang, N. T. T., Shrestha, S., Shrestha, M., Datta, A., & Kawasaki, A. (2017). Evaluating the impacts of climate and land-use change on the hydrology and nutrient yield in a transboundary river basin: A case study in the 3S River Basin (Sekong, Sesan, and Srepok). Science of the Total Environment, 576, 586-598.

Tang, Q., Oki, T., & Dai, A. (2016). Historical and future changes in streamflow and continental runoff. Terrestrial Water Cycle and Climate Change: Natural and Human-Induced Impacts; American Geophysical Union: Hoboken, NJ, USA, 17-37.

Vicuna, S., & Dracup, J. A. (2007). The evolution of climate change impact studies on hydrology and water resources in California. Climatic change, 82(3), 327-350.

Wheida, E., & Verhoeven, R. (2007). An alternative solution of the water shortage problem in Libya. Water resources management, 21, 961-982.

Wu, P., & Tan, M. (2012). Challenges for sustainable urbanization: a case study of water shortage and water environment changes in Shandong, China. Procedia Environmental Sciences, 13, 919-927.

Wang, S. W., Munkhnasan, L., & Lee, W. K. (2021). Land use and land cover change detection and prediction in Bhutan's high-altitude city of Thimphu, using cellular automata and Markov chain. Environmental Challenges, 2, 100017.

Zhang, H., Wang, B., Li Liu, D., Zhang, M., Leslie, L. M., & Yu, Q. (2020). Using an improved SWAT model to simulate hydrological responses to land use change: A case study of a catchment in tropical Australia. Journal of Hydrology, 585, 124822.

Chapter 2 Literature review

This section provides a review of background literature related to climate and LULC change impacts on hydrology. The literature review is presented in six categories: the balance of irrigation supply and demand, LULC change, modeling of LULC change, climate change, combined LULC and climate change, and hydrological modeling.

2.1 The Studies of balance between irrigation water supply and demand

Previous studies have utilized slightly different methods to analyze the equilibrium between water supply and the demand for irrigation water. However, their primary objective remains consistent: to identify the root cause of water deficits and/or assess the performance of on-farm irrigation water. When water shortages arise or significant changes are anticipated in the irrigation scheme, it is essential to conduct a comparison of irrigation needs with irrigation supply. The two most pivotal factors in irrigation planning, design, and operation are the availability of water supply and the water demand (Sakthivadivel et al., 1993).

Hussain et al. (2011) estimated the water balance between supply and demand and projected future trends in various sectors of the economy in the Indus Basin. They conducted separate analyses to determine the balance between supply and demand in the agricultural, domestic, and industrial sectors. Their findings indicated that water scarcity was increasing, and they recommended that the government develop water management strategies. The results revealed that 274 billion cubic meters (BCM) was available for use, with 130 BCM being usable and 60 BCM lost in the system. The empirical results also showed that the gross water supply for agriculture was nearly 190 BCM, while its demand was 210 BCM, resulting in a shortfall of about 20 BCM. They emphasized the importance of increasing crop yield per unit of water by employing high-efficiency irrigation methods, particularly for high-value crops such as orchards and vegetables.

The study by Shakir et al. (2010) found that there is an annual water shortage of more than 40% in the Upper Chenab Canal of Pakistan when comparing the actual water supply with crop water requirements. This shortage could be reduced slightly if the allocation of water supply could be ensured according to the Water Apportionment Accord 1991. The water deficit occurs in August and is compensated for by pumping low-quality groundwater, which increases the secondary salinity of the area. The researchers also observed large gaps between supply and demand in August and September, while there was

an excess of water in May and June. They suggested that controlling this excessive water could help reduce the shortages in other months to some extent.

In 2006, Ji et al. established a model to study the balance between water supply and demand in the middle reaches of the Heihe River basin in Northwest China. They used data from meteorology, hydrology, soil, planting, vegetation, and socio-economic development in the irrigation region. Their research found that the unified management of water resources in the basin had significant effects on regional hydrology. This included a decrease in water supply, an increase in groundwater extraction, and a steady decline in the groundwater level due to over-pumping and reduced recharges. As a result, the water supply was inadequate to meet the demands in the irrigation districts, leading to a water supply crisis in the Pingchuan irrigation district. Additionally, the study highlighted concerns about the sustainable development and utilization of water resources.

In a study conducted by Masona et al. (2018), the water supply and demand for small-scale irrigation at the Fuve-Panganai irrigation scheme in Zimbabwe were evaluated. The researchers used the relative water supply (RWS) metric, which is the ratio of water supply to water demand for crops grown using specific cultural practices on the actual irrigated area. They interviewed a random selection of 38 farmers and compared the interview results with the RWS findings. The study revealed a stable water supply over five years, with a coefficient of variation of 0.2. An RWS of 1.6 indicated that the irrigation scheme received significantly more water than needed during the winter mid-irrigation period (May to July). Both the interview survey and the RWS ratio indicated that over 90 percent of the farmers were satisfied with the irrigation management performance. However, the study also found that 37 percent of the farmers experienced water shortages due to delivery losses caused by damaged pipes and leaking water valves.

To evaluate the actual supply of irrigation water and irrigation water demand for major crops, Ullah et al. (1998) compared water supply and demand for all the outlets of Pabbi minor of Warsak gravity canal in Pakistan. The results revealed that the actual water supply was insufficient to meet crop water demands at all the outlets in the study area. This inadequacy was due to the non-availability of a sufficient amount of water, leading to a

significant portion of the command areas at the outlets being left fallow. Factors such as high temperatures and low rainfall were identified as contributing to increased water demand. However, Iqbal (1995) obtained different results. His findings indicated that the supply exceeded crop demands at the head of a minor, but in the middle, the supply was less than demand due to a larger cultivable command area. Additionally, when the latter was small, the supply exceeded demand.

It is important to ensure that all farmers in an irrigation system have a reliable water supply throughout the year. Proper distribution of water is crucial, and it's necessary to compare water supply and demand to achieve this. However, when it comes to the spatial distribution of operational parameters, simply calculating the balance between water supply and demand doesn't solve the regional problem of water resource utilization on a relatively large scale in an inland basin (Bormann et al., 1999). Furthermore, the water balance provides practitioners with a tool to evaluate source control and assess stream health based on runoff (Hussain et al., 2011).

2.2 A case study of land use and land cover (LULC) change

Numerous research studies have evaluated how changes in land use and land cover (LULC) affect the hydrology of watersheds. In particular, Boongaling et al. (2018), Daramola et al. (2022), and Garg et al. (2019) have demonstrated a significant correlation between LULC patterns and various hydrological processes, as well as the impact on soil erosion and sediment yield within watersheds.

In 2013, Ozturk et al. developed a model to study how changes in land use affect the water system in Bartin Spring, a rural watershed in northwestern Turkey. They combined a land use dynamics model with a spatially distributed three-dimensional surface–subsurface hydrologic model. By running different land use and forest management scenarios through the model, they were able to simulate the water budget. The study found that the water budget is most affected by changes in precipitation and the conversion between forest and agricultural lands, and less affected by the type of forest stands. The results also

demonstrated that the combined model is a valuable tool for evaluating the impact of land use changes on the hydrological processes within the watershed.

In 2018, Boongaling and colleagues utilized various physical, meteorological, and remotely sensed data to create a hydrological model of the Calumpang watershed in Batangas, Philippines. Their study aimed to establish a connection between landscape patterns and hydrologic processes. The results from their SWAT hydrological modeling revealed that land use and land cover (LULC) change led to a 5% increase in surface runoff, a 6% increase in sediment yield, and an 11% decrease in baseflow for the entire basin. Additionally, they found that degraded subbasins experienced a significant increase in streamflow (up to 31%) during stormy months and a reduction in baseflow (up to 26%) during dry months. On the other hand, improved sub-basins showed a decrease in stormflow (up to 4%) and an increase in baseflow (up to 5%) during dry months. Overall, their study demonstrated a strong relationship between land cover patterns and hydrologic processes.

Nut et al. (2021) conducted a study to estimate soil loss resulting from land use and land cover (LULC) changes in the Sangker catchment, Cambodia. They used the Revised Universal Soil Loss Equation (RUSLE) model within a Geographic Information System (GIS) environment. The study found that the total soil loss in the periods of 2002 and 2015 was 1.9 million tons per year and 4.5 million tons per year, respectively. Additionally, the research indicated that the highest soil loss values (ranging from 14.3 to 62.9 tons per hectare per year) were observed in the central, southwestern, and upland parts of the catchment.

Nomano et al. (2018) conducted a study to assess the influence of Land Use and Land Cover (LULC) changes on sediment load in the Carapelle watershed, located in Southern Italy. The study employed a combination of satellite remote sensing, Geographic Information Systems (GIS), and hydrological modeling. The findings revealed that the high erosion rates observed in 2011 did not show significant variations in the S1 scenario. Under this scenario, numerous areas exhibited substantial soil erosion, exceeding 10 Mg ha^{-1}

year^{-1}, which poses a significant threat to soil fertility. The study emphasized the critical importance of modeling the potential impact of future land use changes on soil erosion.

All these studies have revealed a robust correlation between land cover and river discharge, soil erosion, and sediment yield within watersheds. The transformation of land cover has been found to induce alterations in hydrology, with adverse implications for the ecological integrity of the river system and local communities (Baker and Miller, 2013). Furthermore, the absence of protective land cover has predominantly led to soil erosion and depletion. Given the variability of hydrological processes and sediment transport capacity across different land cover types, it is evident that sediment export to rivers and changes in river discharge are intricately linked to land use.

2.3 Modeling of land use change

Understanding land use change is important for studying the driving forces, ecological impacts, and environmental assessments. Researchers from various fields have developed numerous land use models. These models represent the complexity of the land use system. Commonly used models for estimating land use change include the Markov model, Cellular Automata, Artificial Neural Network (ANN), Cellular Automata-Markov model (CA-Markov), Conversion of Land Use and its Effects at Small regional extent model (CLUE-S), Land Change Modeler (LCM), and Raster-Based Land Change Modeling Tool (GEOMOD) (Zhang et al., 2013; Lacono et al., 2015; Ahmad et al., 2023; Saputra and Lee, 2019; Subedi et al., 2013; Kucsicsa et al., 2019; Pontius et al., 2001).

Islam et al. (2021) utilized the CLUE-S model to forecast changes in land use across the southeastern region of Bangladesh, integrating a non-spatial demand module and geospatially explicit distribution. Land cover data from 2010, 2015, and 2017 were employed as datasets. The simulated maps for 2015 and 2017 were found to be generally accurate compared to the actual land use, with error matrix and Kappa indices showing 62.38% (0.6101) and 71.64% (0.7106) accuracy, respectively, confirming the success of the model simulation. According to their predictions, built-up areas would expand by 100%, 65.3%, and 34.2%, respectively, compared to all other land-use types. The study also

concluded that the scientific information derived from the simulations demonstrated that the model approach is suitable for formulating relevant land use policies.

Wu et al. (2006) used the Markov model to predict land use changes in Beijing, China. They analyzed land use dynamics using satellite remote sensing and geographic information systems (GIS). The study projected future land use over the next 20 years and compared the results of the Markov model with those of a regression model. The researchers found that the Markov chain model effectively described and projected land use and land cover changes, but it required restrictive assumptions. However, combining remote sensing and GIS technologies with the Markov and regression models was found to be useful for describing, analyzing, and predicting land use changes.

Wang et al. (2021) utilized a CA-Markov model to simulate the spatiotemporal dynamics of land use and land cover changes in the city of Thimphu in Bhutan. Their study predicted future changes, indicating a considerable transformation in the landscape of Thimphu city over the study period, with the trend expected to continue until 2050. The results showed a significant 12.77% increase in the built-up area from 2002 (52.88%) to 2018 (65.5%), along with a slight increase in the cover of bare ground. Conversely, there was a drastic decline in forest cover (15.25%) and agriculture (1.01%). The study suggests an urgent need to implement effective planning, particularly to protect existing forest and water resources from further degradation.

In 2013, Subedi et al. used a hybrid approach called the CA-Markov model to forecast land use changes in the Saddle Creek Drainage Basin in Florida. When the model was evaluated, the comparison between actual and predicted land use showed a satisfactory level of prediction accuracy. The model projected a significant increase in urban areas (from 47.3% to 49.4%) and transportation facilities (from 3.7% to 5%) from 2006 to 2015. In contrast, agricultural areas are expected to decrease from 14.4% to 12.3% during the same period.

Rashmi and Lele (2010) conducted a study to evaluate GEOMOD's ability to forecast future changes in forest cover and to analyze the spatiotemporal patterns of forest cover

change in the Kanakapura area and neighboring regions of the Western Ghats located in India. The results showed that GEOMOD accurately predicted the forest cover for the year 2000, closely matching the actual data. Additionally, it projected a further 3% loss of forest cover by the year 2015. The study emphasized the advantage of GEOMOD in requiring minimal data and being able to predict changes using estimated cell numbers.

Chim et al. (2019) utilized the LCM model to identify and forecast land use changes in the Upper Siem Reap River, Cambodia. They analyzed land use patterns, specifically annual deforestation from 1988 to 2018, and projected potential land use scenarios 40 and 80 years into the future. Their findings revealed a significant decrease in forest cover at a rate of 1.22% over the past three decades. They also indicated a projected continuous increase in deforestation and a decrease in forest cover in the future (by the years 2058 and 2098). Additionally, their study highlighted the impact of land use changes on the water supply for the Angkor temple complex (a World Heritage Site) and the surrounding population.

The hybrid model known as the CA-Markov model has been selected for the current study to predict future land use and land cover changes up to the year 2030. This model is widely used by scholars to understand systematic landscape changes, meet land management needs, and predict the future impact of land use and land cover changes on the earth's system (Tadese et al., 2021; Hamad et al., 2018; Nouri et al., 2014).

2.4 A case study of climate change

The impact of climate change on hydrological systems, including temperature and precipitation patterns, has been documented over several decades. Extensive research has been conducted worldwide to study the effects of climate change on surface water, groundwater, and nutrients (Jiang et al., 2007; Swain et al., 2022; Chiew et al., 1995; Herawati, 2015; Raulino et al., 2021).

In a study conducted by Mengistu et al. (2021), the impact of climate change on water resources in the Upper Blue Nile (Abay) River Basin in Ethiopia was assessed using a regional climate model (RCM), specifically the COSMO Climate Limited-area Model

(CCLM), coupled with the SWAT hydrological model. The findings from the climate change projection revealed a rise in mean annual temperature and a reduction in precipitation across most parts of the Basin. The SWAT Model simulations were established from 1981-2010 as the baseline and (2010–2039, 2040–2069, and 2070–2099) as the future climate scenarios. The study concluded that while surface runoff is expected to increase by up to 14%, this will not lead to an overall increase in the total water yield of the basin. In fact, the total water yield of the Basin is estimated to decrease by -1.7 to -6.5% and -10.7 to -22.7% for simulations forced by RCP4.5 and RCP8.5 scenarios, respectively.

In a study conducted by Ashofteh et al. (2013), the researchers examined the effects of climate change on the inflow volume to a reservoir and downstream water demand in an East Azerbaijan river basin in Iran. They analyzed three climate change scenarios and utilized the HadCM3 model to project temperature and rainfall scenarios for the period 2026–2039, based on the A2 emission scenario. Additionally, the researchers employed the IHACRES hydrological model. The study revealed that according to the HadCM3 model, temperatures are expected to increase by 0.5 to 2.7°C, while rainfall is projected to fluctuate by -36% to 76% compared to the base period. Monthly temperature and rainfall data for the future were used as input for the IHACRES model to simulate monthly runoff for the future. The results indicated a 0.7% decrease in the average long-term annual runoff volume relative to the base period.

Luo et al. (2013) conducted a study to assess the effects of climate change on hydrology and water quality in the northern Coastal Ranges and western Sierra Nevada, California. They used the Soil and Water Assessment Tool (SWAT) model to simulate the impact of climate change on water supply and ecosystem stressors. The results of the study showed that an increase in the annual average air temperature led to a proportional increase in stream temperature. The researchers also discovered that reduced streamflow during the summer, coupled with higher projected air temperatures in summer compared to winter, would result in elevated stream temperatures during the summer months, creating unfavorable conditions for cold water fish species.

Andersen et al. (2006) conducted a study to evaluate the impact of climate change on hydrology and nutrient levels in the lowland Gjern River basin in Denmark. They utilized the ECHAM4/OPYC General Circulation Model (IPCC A2 scenario) dynamically downscaled by the Danish HIRHAM regional climate model (25 km grid) to predict climate change for two-time periods: 1961–1990 (control) and 2071–2100 (scenario). Statistical models were employed to incorporate the influence of altered hydrology on nutrient losses from land to surface waters. The findings from HIRHAM indicated a projected increase in mean annual precipitation of 47 mm (5%) and a rise in mean annual air temperature of 3.2 °C (43%). The mean annual runoff from the river basin was projected to increase by 27 mm (7.5%, $p < 0.05$) when comparing the scenario to the control. Regarding nutrients, the study revealed simulated mean annual changes in TN loads in a loamy and a sandy sub-catchment of + 2.3 kg N ha− 1 (8.5%) and + 1.6 kg N ha− 1 (6.9%), respectively.

In a study conducted by Graham et al. (2007), the impacts of climate change on hydrology in northern Europe were evaluated using an ensemble of regional climate models and an offline hydrological model. The researchers utilized climate change scenarios from seven RCMs, two GCMs, two global emissions scenarios, and two RCMs of varying resolution. Two different approaches to transfer climate change from the RCMs to hydrological models were examined. The findings revealed an overall increase in river flow, earlier spring peak flows, and an augmented hydropower potential. While the two approaches to the hydrological impacts model yielded similar mean results, they exhibited considerably different seasonal dynamics.

2.5 A case study of the combined impact of climate and land use change

It is crucial to comprehend the combined impact of climate and land use change on water to develop sustainable water resource plans (Zhang et al., 2018) and management strategies (Kim et al., 2013). Li et al. (2009) conducted a study to analyze the effects of land use change and climate variability on hydrology in an agricultural catchment on the Loess Plateau of China. Using the SWAT model, they evaluated the impacts of land use

change and climate variability on surface hydrology, including runoff, soil water, and evapotranspiration. The results demonstrated that the SWAT model is an effective tool for assessing the influence of environmental changes on surface hydrology. Their findings revealed that both land use change and climate variability led to a decrease in runoff by 9.6% and 95.8%, respectively, and a decrease in soil water content by 18.8% and 77.1%. Additionally, land use change resulted in an 8.0% increase in evapotranspiration, while climate variability caused a decrease of 103.0%. Furthermore, the study observed that overall climate variability had a more significant impact on surface hydrology compared to land use change.

In a study conducted by Tu (2009), the combined effects of climate and land use change on streamflow and water quality in eastern Massachusetts, USA were investigated. Using a GIS-based ArcView Generalized Watershed Loading Function (AVGWLF) watershed simulation model, future changes in streamflow and nitrogen load were simulated under various climate and land use change scenarios in the watersheds of eastern Massachusetts. The findings revealed that the seasonal distributions of streamflow and nitrogen load are more significantly influenced by climate change and land development than the average annual amounts of streamflow and nitrogen load.

In a study conducted by Kim et al. (2013), the researchers investigated the individual and combined effects of anticipated climate and land use/land cover (LULC) changes on stream flow in the Hoeya River Basin, South Korea. They constructed three scenarios (solely climate change, solely LULC change, and combined climate and LULC change) and utilized the Soil and Water Assessment Tool (SWAT) model to simulate the future period. The findings revealed that under the climate change scenario, streamflow increased in spring and winter but decreased in summer and autumn. Conversely, LULC change led to increased high flow during wet periods but decreased low flow in dry periods. Notably, the combined scenario produced results similar to the climate change scenario, albeit with more pronounced seasonal variations in streamflow.

Trang et al. (2016) conducted an assessment of the influence of climate and land use changes on the hydrology and nutrient yield in the 3 basins (Sekong, Sesan, and Srepok

River basins) located in the southeastern part of the Mekong Basin. They utilized the SWAT model to comprehend the processes and outcomes of pollution (nutrient yield) as well as the hydrological patterns. Future scenarios for three periods: 2030s (2015–2039), 2060s (2045–2069), and 2090s (2075–2099) were created using an ensemble of five GCMs (General Circulation Model) simulations: HadGEM2-AO, CanESM2, IPSL-CM5A-LR, CNRM-CM5, and MPI-ESM-MR, driven by the climate projection for RCPs (Representative Concentration Pathways) RCP4.5 (medium emission) and RCP8.5 (high emission) scenarios, along with two land-use change scenarios. The findings from their study suggest that the region is likely to experience warmer and wetter conditions under both emission scenarios. It is predicted that discharge and nutrient yield will increase during the wet season and decrease during the dry season. Overall, the annual discharge and nutrient yield are projected to rise over the twenty-first century, indicating the susceptibility of the 3S River Basin to climate and land-use changes.

López-Moreno et al. (2014) conducted a study on the influence of climate and land use changes on water availability and reservoir management in the Upper Aragón River, Spanish Pyrenees. They used the Regional Hydro-Ecologic Simulation System (RHESSys) to model streamflow. Regional climate models (RCMs) indicated a projected trend of warming and drying in the basin from 2021 to 2050, resulting in a 13.8% decrease in annual streamflow, particularly in late spring and summer. The combined effects of forest regeneration and climate change are anticipated to reduce annual streamflow by 29.6%, with significant decreases in all months except January and February, where the decline will be more moderate. The study highlighted the importance of further research and the adoption of water-saving technologies, practices, and a legal framework to safeguard the supply and quality of water resources.

The findings of the above studies indicate that the combined influence of climate and land use changes have amplified the impact of land development and water resources. This compounded effect is expected to significantly affect riparian ecosystems due to alterations in river hydrology and geomorphological processes. Changes in land use, land cover, and climate regimes can exert substantial influence on the natural processes within a watershed

ecosystem, thereby carrying long-term implications for both economic and ecological processes. As a result, it is imperative to conduct a thorough assessment of the hydrologic responses to these changes in order to safeguard water resources and environmental quality.

2.6 Hydrological modeling

The interaction of climate, land use, and infrastructure, influenced by changing hydrological conditions, continues to present significant challenges to the hydrological research and water management communities (Peel and Bloschl, 2011). Hydrological modeling serves as a valuable tool for comprehending the Earth's environmental system and enhances decision-making in water resource planning, flood prediction, irrigation practices, groundwater development, and more (Pandi et al., 2021). Various hydrological models fall into the categories of empirical, conceptual, and physically based models, each offering suitable options for small and large-scale applications.

In a study conducted by McMichael et al. (2006), the MIKE SHE model, a spatially distributed hydrological model, was utilized to estimate monthly streamflow in a semi-arid shrubland catchment in central California. The results from MIKE SHE simulations for seven leaf area index (LAI) input scenarios, including the baseline LAI sequence used during model calibration and testing, revealed that differences in predictive uncertainty between scenarios were generally less than ±10%. Additionally, Singh et al. (1999) also employed MIKE SHE to simulate the hydrological water balance of a small watershed in the western part of the Midnapore district of West Bengal, India. Their objective was to develop an irrigation plan, and the results demonstrated the necessity of supplemental irrigation for paddy cultivation to achieve its potential yield, despite frequent rainfall during the kharif season. This study showcased the practicality of employing a comprehensive hydrological modeling system for managing water resources for agricultural purposes within a watershed.

In a study conducted by Muttiah et al. (2002), the SWAT model was employed to evaluate the impact of variability in soils and climate on the mean and variance of water balance components in six different watersheds in Texas. The research indicated that the

mean soil water storage (SW) exhibited high sensitivity to scale increase from 1:250,000 to 1:240,000m, while the sensitivity of mean evapotranspiration (ET) remained relatively consistent.

Similarly, Wang et al. (2009) utilized the SWAT model to assess the influence of human activities and climate change on the monthly water balance in the northern part of China. The findings revealed that human activities contributed to a 68.6% decrease in runoff in the Chao River basin, suggesting that human activities are the primary cause of declining streamflow.

In another study, Ahn, Jeong, and Kim (2016) employed an integrated modeling framework, incorporating a water balance network model (MODSIM) and SWAT, to evaluate the threat of drought on agricultural water supplies in South Korea under climate change. The research demonstrated that the maximum shortage rate of agricultural water was projected to reach 38.2% by the 2040s. The intensified future drought levels were predominantly attributed to the increasingly concentrated rainfall distribution throughout the year under a monsoonal climate, as outlined in the IPCC climate scenarios.

Furthermore, Perry (2014) applied the SWAT model to simulate runoff in a mountainous catchment in South Africa. The study highlighted the potential of the SWAT hydrological model for application in mountainous, semi-arid catchment areas and concluded that SWAT was capable of accurately simulating streamflow.

Grillakis et al. (2010) utilized a conceptual model similar to HBV to assess its applicability for flash flood forecasting in the Sora river basin in Slovenia. Their study demonstrated the effectiveness of a simple conceptual rainfall-runoff model in capturing the internal dynamics of flash flood events and its potential for forecasting flash floods. The simulated results provided a comprehensive understanding of the model's performance in the case study basin simulations. The analysis of the Zelezniki subcatchment exhibited strong model performance in terms of peak discharge, watershed response time, and internal watershed dynamics.

In a separate study, Huang et al. (2019) employed the HBV model structure and calibration procedure to improve the simulation of potential evapotranspiration (EP) and discharges in mainland Norway. The EP results showed favorable agreement with the measured data. Overall, the HBV model demonstrated good performance in accurately reproducing daily discharge for most calibration catchments, with a median daily NSE of 0.68, PBIAS of -3%, KGE of 0.70, and monthly NSE of 0.80. This research highlighted the appropriateness of the model setup for climate and land use impact studies, indicating its potential to provide more reliable projections of changes in discharge and hydrological components in Norway.

In a study conducted by Akhter (2017), artificial neural network (ANN) methodology was used to evaluate the impact of climate change on the river Jhelum basin in the State of Jammu & Kashmir, India. The model analyzed monthly temperature and precipitation data from 1979 to 2009 at four different meteorological stations - Srinagar, Pahalgam, Qazigund, and Gulmarg within the river Jhelum basin. The study then predicted the future average annual temperature and precipitation levels up to the year 2100. The results indicated that by the end of the 21st century, the mean annual temperature of the Jhelum river basin is projected to increase by 1.43°C under the A1B scenario, while total annual precipitation is expected to decrease substantially by 30.88%. Under the A2 scenario, the average annual temperature is forecasted to increase by 1.56°C, and total annual precipitation is predicted to decrease by 35.32%.

In a study by Wang et al. (2016), the Hydrologic Engineering Center's Hydrologic Modeling System (HEC-HMS) was utilized to simulate runoff in the semi-arid region of northwestern China, specifically in the Hailiutu watershed. The model was calibrated for the period of 1978-1992. The results indicated that the model consistently underestimated winter and spring hydrographs, as well as some summer flows. The continuous runoff model for the Hailiutu watershed inadequately represented runoff volume and peak runoff, including peak volume and time of peak. Consequently, due to the unsatisfactory calibration results, model validation could not be achieved. In a separate study, Skhakhfa and Ouerdachi (2016) examined the effectiveness of the HEC-HMS for flood estimation modeling in the El Berda watershed, located in the northeast of Algeria. The results

demonstrated that the HEC-HMS model exhibited the highest efficiency when calibrated with specific parameters based on objective functions (percent error in peaks). The model showed an 8.8 percent difference between observed and simulated discharges, with an R2 value of 0.87 and a Nash-Sutcliffe efficiency value of 0.99.

Xue et al. (2018) conducted a simulation of water movement in the Manas River Basin (MRB) using an enhanced semi-distributed Topographic hydrologic model (TOPMODEL) that incorporated a snowmelt model and a topographic index algorithm. The findings indicated that the improved TOPMODEL demonstrated acceptable performance, producing runoff simulations in the MRB that were comparable to observed data. However, uncertainties in the simulated results were attributed to various factors such as model parameters, structure, climate, and human influence.

Numerous hydrological models serve as robust tools for examining hydrology and conducting impact assessments of environmental changes on surface water. However, these models are constrained by their high data requirements, particularly the physically based approaches such as HEC-HMS, SWAT, and MIKE SHE.

References

Akhter, M. (2017). Application of ANN for the Hydrological Modeling. International Journal for Research in Applied Science & Engineering Technology, 5(7), 203-213.

Andersen, H. E., Kronvang, B., Larsen, S. E., Hoffmann, C. C., Jensen, T. S., & Rasmussen, E. K. (2006). Climate-change impacts on hydrology and nutrients in a Danish lowland river basin. Science of the Total Environment, 365(1-3), 223-237.

Ashofteh, P. S., Haddad, O. B., & A. Mariño, M. (2013). Climate change impact on reservoir performance indexes in agricultural water supply. Journal of Irrigation and Drainage Engineering, 139(2), 85-97.

Ahmad, M. N., Shao, Z., Javed, A., Islam, F., Ahmad, H. H., & Aslam, R. W. (2023). the cellular automata approach in dynamic modelling of land use change detection and future simulations based on remote sensing data in Lahore Pakistan. Photogrammetric Engineering & Remote Sensing, 89(1), 47-55.

Ahn, S. R., Jeong, J. H., & Kim, S. J. (2016). Assessing drought threats to agricultural water supplies under climate change by combining the SWAT and MODSIM models for the Geum River basin, South Korea. Hydrological Sciences Journal, 61(15), 2740-2753.

Boongaling, C. G. K., Faustino-Eslava, D. V., & Lansigan, F. P. (2018). Modeling land use change impacts on hydrology and the use of landscape metrics as tools for watershed management: The case of an ungauged catchment in the Philippines. Land use policy, 72, 116-128.

Baker, T. J., & Miller, S. N. (2013). Using the Soil and Water Assessment Tool (SWAT) to assess land use impact on water resources in an East African watershed. Journal of hydrology, 486, 100-111.

Bormann, H., Diekruger, B., Renschler, C., and Richter, O. (1999). Regionalization scheme for the simulation of regional water balance using a physically based model system. Phys Chem Earth, 24, 43-48.

Chiew, F. H. S., Whetton, P. H., McMahon, T. A., & Pittock, A. B. (1995). Simulation of the impacts of climate change on runoff and soil moisture in Australian catchments. Journal of hydrology, 167(1-4), 121-147.

Chim, K., Tunnicliffe, J., Shamseldin, A., & Ota, T. (2019). Land use change detection and prediction in upper Siem Reap River, Cambodia. Hydrology, 6(3), 64.

Daramola, J., Adepehin, E. J., Ekhwan, T. M., Choy, L. K., Mokhtar, J., & Tabiti, T. S. (2022). Impacts of land-use change, associated land-use area and runoff on watershed sediment yield: implications from the Kaduna Watershed. Water, 14(3), 325.

Graham, L. P., Andréasson, J., & Carlsson, B. (2007). Assessing climate change impacts on hydrology from an ensemble of regional climate models, model scales and linking methods–a case study on the Lule River basin. Climatic Change, 81(Suppl 1), 293-307.

Garg, V., Nikam, B. R., Thakur, P. K., Aggarwal, S. P., Gupta, P. K., & Srivastav, S. K. (2019). Human-induced land use land cover change and its impact on hydrology. HydroResearch, 1, 48-56.

Grillakis, M. G., Tsanis, I. K., & Koutroulis, A. G. (2010). Application of the HBV hydrological model in a flash flood case in Slovenia. Natural Hazards and Earth System Sciences, 10(12), 2713-2725.

Herawati, H. (2015). Impact of climate change on streamflow in the tropical lowland of Kapuas River, West Borneo, Indonesia. Procedia Engineering, 125, 185-192.

Huang, S., Eisner, S., Magnusson, J. O., Lussana, C., Yang, X., & Beldring, S. (2019). Improvements of the spatially distributed hydrological modelling using the HBV model at 1 km resolution for Norway. Journal of hydrology, 577, 123585.

Hamad, R., Balzter, H., & Kolo, K. (2018). Predicting land use/land cover changes using a CA-Markov model under two different scenarios. Sustainability, 10(10), 3421.

Hussain, I. Hussain, Z. Sail, MH. Akram, W. Farhan, M. F. (2011). Water balance, supply and demand irrigation efficiency of indus basin. Paskistan Economic and Social Review, 49, No 1, 13-38.

Iacono, M., Levinson, D., El-Geneidy, A., & Wasfi, R. (2015). A Markov chain model of land use change. TeMA-Journal of Land Use, Mobility and Environment, 8(3), 263-276.

Islam, S., Li, Y., Ma, M., Chen, A., & Ge, Z. (2021). Simulation and prediction of the spatial dynamics of land use changes modelling through CLUE-S in the southeastern region of Bangladesh. Journal of the Indian Society of Remote Sensing, 49(11), 2755-2777.

Ji, X., Kang, E., Chen, R., Zhao, W., Xiao, S., and Jin, B. (2006). Analysis of water resources supply and demand and security of water resources development in irrigation regions of the middle reaches of the Heihe River basin, Northwest China. J. Integr. Agri., 5, 130-140.

Jiang, T., Chen, Y. D., Xu, C. Y., Chen, X., Chen, X., & Singh, V. P. (2007). Comparison of hydrological impacts of climate change simulated by six hydrological models in the Dongjiang Basin, South China. Journal of hydrology, 336(3-4), 316-333.

Kim, J., Choi, J., Choi, C., & Park, S. (2013). Impacts of changes in climate and land use/land cover under IPCC RCP scenarios on streamflow in the Hoeya River Basin, Korea. Science of the Total Environment, 452, 181-195.

Kucsicsa, G., Popovici, E. A., Bălteanu, D., Grigorescu, I., Dumitraşcu, M., & Mitrică, B. (2019). Future land use/cover changes in Romania: regional simulations based on CLUE-S model and CORINE land cover database. Landscape and ecological engineering, 15, 75-90.

Li, Z., Liu, W. Z., Zhang, X. C., & Zheng, F. L. (2009). Impacts of land use change and climate variability on hydrology in an agricultural catchment on the Loess Plateau of China. Journal of hydrology, 377(1-2), 35-42.

López-Moreno, J. I., Zabalza, J., Vicente-Serrano, S. M., Revuelto, J., Gilaberte, M., Azorín-Molina, C., ... & Tague, C. (2014). Impact of climate and land use change on water

availability and reservoir management: Scenarios in the Upper Aragón River, Spanish Pyrenees. Science of the total environment, 493, 1222-1231.

Luo, Y., Ficklin, D. L., Liu, X., & Zhang, M. (2013). Assessment of climate change impacts on hydrology and water quality with a watershed modeling approach. Science of the total environment, 450, 72-82.

Mengistu, D., Bewket, W., Dosio, A., & Panitz, H. J. (2021). Climate change impacts on water resources in the upper Blue Nile (Abay) river basin in Ethiopia. Journal of Hydrology, 592, 125614.

Muttiah, R. S., & Wurbs, R. A. (2002). Scale-dependent soil and climate variability effects on watershed water balance of the SWAT model. Journal of hydrology, 256(3-4), 264-285.

Masona, E., Shimizu, K., and Yoshioka, Y. 2018. An evaluation of water demand and supply for a small scale irrigation scheme in Zimbabwe. Int. J. Environ. Rural Dev., 9-2, 41-46.

McMichael, C. E., Hope, A. S., & Loaiciga, H. A. (2006). Distributed hydrological modelling in California semi-arid shrublands: MIKE SHE model calibration and uncertainty estimation. Journal of Hydrology, 317(3-4), 307-324.

Nut, N., Mihara, M., Jeong, J., Ngo, B., Sigua, G., Prasad, P. V., & Reyes, M. R. (2021). Land use and land cover changes and its impact on soil erosion in Stung Sangker catchment of Cambodia. Sustainability, 13(16), 9276.

Nouri, J., Gharagozlou, A., Arjmandi, R., Faryadi, S., & Adl, M. (2014). Predicting urban land use changes using a CA–Markov model. Arabian Journal for Science and Engineering, 39, 5565-5573.

Öztürk, M., Copty, N. K., & Saysel, A. K. (2013). Modeling the impact of land use change on the hydrology of a rural watershed. Journal of Hydrology, 497, 97-109.

Peel, M. C., & Blöschl, G. (2011). Hydrological modelling in a changing world. Progress in Physical Geography, 35(2), 249-261.

Perry, K. A. (2014). Application of the SWAT hydrological model in a small, mountainous catchment in South Africa. University of Pretoria (South Africa).

Pontius Jr, R. G., Cornell, J. D., & Hall, C. A. (2001). Modeling the spatial pattern of land-use change with GEOMOD2: application and validation for Costa Rica. Agriculture, Ecosystems & Environment, 85(1-3), 191-203.

Pandi, D., Kothandaraman, S., & Kuppusamy, M. (2021). Hydrological models: a review. International Journal of Hydrology Science and Technology, 12(3), 223-242.

Romano, G., Abdelwahab, O. M., & Gentile, F. (2018). Modeling land use changes and their impact on sediment load in a Mediterranean watershed. Catena, 163, 342-353.

Raulino, J. B., Silveira, C. S., & Lima Neto, I. E. (2021). Assessment of climate change impacts on hydrology and water quality of large semi-arid reservoirs in Brazil. Hydrological Sciences Journal, 66(8), 1321-1336.

Rashmi, M. K., & Lele, N. (2010). Spatial modeling and validation of forest cover change in Kanakapura region using GEOMOD. Journal of the Indian Society of Remote Sensing, 38, 45-54.

Saputra, M. H., & Lee, H. S. (2019). Prediction of land use and land cover changes for North Sumatra, Indonesia, using an artificial-neural-network-based cellular automaton. Sustainability, 11(11), 3024.

Swain, S., Taloor, A. K., Dhal, L., Sahoo, S., & Al-Ansari, N. (2022). Impact of climate change on groundwater hydrology: a comprehensive review and current status of the Indian hydrogeology. Applied Water Science, 12(6), 120.

Singh, R., Subramanian, K., & Refsgaard, J. C. (1999). Hydrological modelling of a small watershed using MIKE SHE for irrigation planning. Agricultural water management, 41(3), 149-166.

Subedi, P., Subedi, K., & Thapa, B. (2013). Application of a hybrid cellular automaton–Markov (CA-Markov) model in land-use change prediction: a case study of Saddle Creek Drainage Basin, Florida. Applied Ecology and Environmental Sciences, 1(6), 126-132.

Skhakhfa, I. D., & Ouerdachi, L. (2016). Hydrological modelling of wadi Ressoul watershed, Algeria, by HEC-HMS model. Journal of Water and Land Development, 31(1), 139.

Shakir, A.S. Khan, N.M., Qureshi, M.M. (2010). Canal water management: case study of upper Chenab canal in Pakistan. Irrig. Drain., 59, 76-91.

Sakthivadivel, R. Merrey, DJ and Fernando, N. (1993). Cumulative relative water supply: A methodology for assessing irrigation system performance. Irrigation and Drainage Systems, 7, 43-67.

Tu, J. (2009). Combined impact of climate and land use changes on streamflow and water quality in eastern Massachusetts, USA. Journal of Hydrology, 379(3-4), 268-283.

Trang, N. T. T., Shrestha, S., Shrestha, M., Datta, A., & Kawasaki, A. (2017). Evaluating the impacts of climate and land-use change on the hydrology and nutrient yield in a transboundary river basin: A case study in the 3S River Basin (Sekong, Sesan, and Srepok). Science of the Total Environment, 576, 586-598.

Tadese, S., Soromessa, T., & Bekele, T. (2021). Analysis of the current and future prediction of land use/land cover change using remote sensing and the CA-markov model in Majang forest biosphere reserves of Gambella, southwestern Ethiopia. The scientific world journal, 2021, 1-18.

Ullah, E I., Khan, H., Khan, S.A. (1998). An assessment of the crop water demand and irrigation water supply at Pabbi minor of warsak gravity canal. Abbottabad, Pakistan.

Wang, S. W., Munkhnasan, L., & Lee, W. K. (2021). Land use and land cover change detection and prediction in Bhutan's high altitude city of Thimphu, using cellular automata and Markov chain. Environmental Challenges, 2, 100017.

Wu, Q., Li, H. Q., Wang, R. S., Paulussen, J., He, Y., Wang, M., ... & Wang, Z. (2006). Monitoring and predicting land use change in Beijing using remote sensing and GIS. Landscape and urban planning, 78(4), 322-333.

Wang, M., Zhang, L., & Baddoo, T. D. (2016). Hydrological modeling in a semi-arid region using HEC-HMS. Journal of Water Resource and Hydraulic Engineering, 5(3), 105-115.

Wang, G., Xia, J., & Chen, J. (2009). Quantification of effects of climate variations and human activities on runoff by a monthly water balance model: A case study of the Chaobai River basin in northern China. Water resources research, 45(7).

Xue, L., Yang, F., Yang, C., Wei, G., Li, W., & He, X. (2018). Hydrological simulation and uncertainty analysis using the improved TOPMODEL in the arid Manas River basin, China. Scientific reports, 8(1), 452.

Zhang, D., Fu, M., Tao, J., Hu, L., & Yang, X. (2013). Scenario simulation of land use change in mining city based on CLUE-S model. Transactions of the Chinese Society of Agricultural Engineering, 29(12), 246-256.

Zhang, L., Cheng, L., Chiew, F., & Fu, B. (2018). Understanding the impacts of climate and landuse change on water yield. Current Opinion in Environmental Sustainability, 33, 167-174.

Chapter 3 Description of the study site

This chapter depicts the location of the study area and the physical characteristics including climate, soil, and natural vegetation of the upper Sangker River basin. Furthermore, it also describes the water infrastructure that existed in the study area.

3.1 Location of study site

The study was conducted in the Upper Sangker River basin (USRB), located in Battambang province in northwestern Cambodia, between the latitudes of 13.0957° North and the longitude of 103.2022° East. The basin covers a total drainage area of 3,062 km^2 (Figure 3-1). This transboundary river basin stretches across Battambang province, Pailin, and Pursat province, with the most upstream areas covering approximately 392 km^2 and 173 km^2, respectively, and sharing a border with Thailand. The elevation in this area ranges from 13 to 1,400 meters above sea level.

Sangker River is one of the main tributaries, representing the largest river basin in Battambang province with a distance of about 250 km. It travels through 6 districts and 27 communes before draining into the Tonle Sap Great Lake. Some tributaries join the river on both sides of the riverbanks throughout its traverse from the upstream to the Tonle Sap Great Lake.

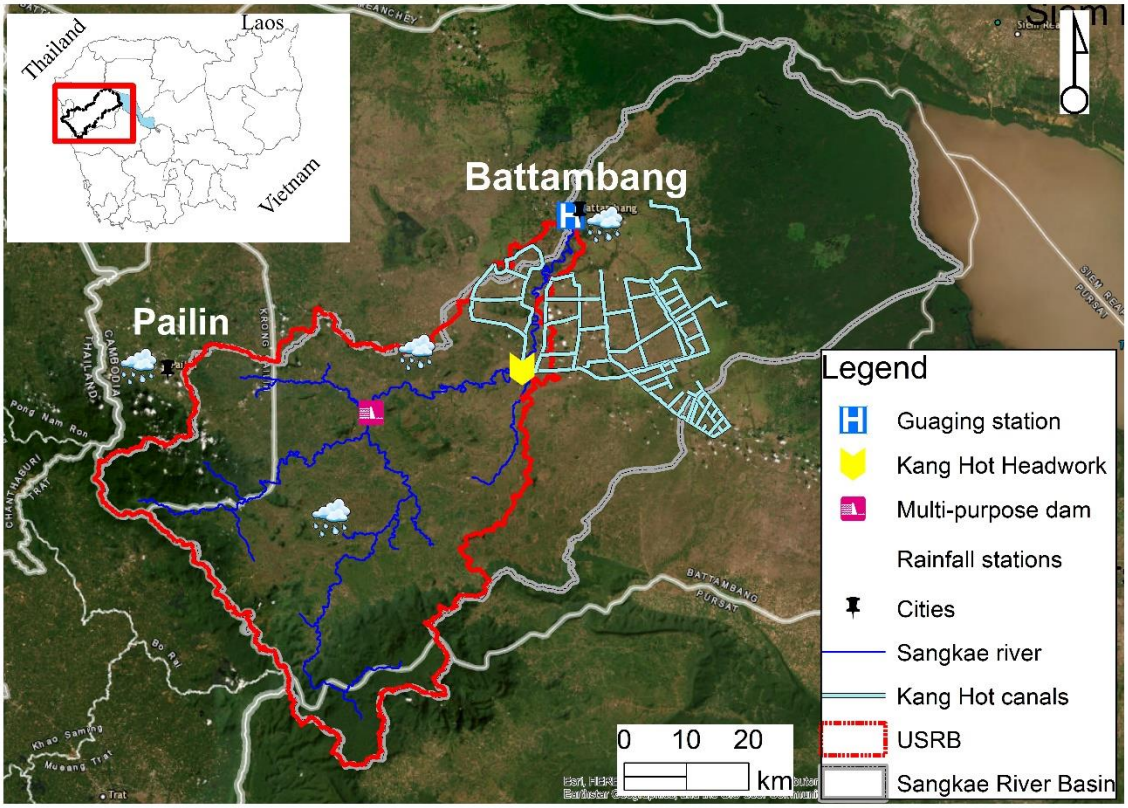

Figure 3-1 Location map of the Upper Sangker River basin representing in red line.

3.2 Climate

The region is governed by a tropical monsoon climate, characterized by two distinct seasons: dry and rainy (Sourn et al., 2021). The rainy season, brought by the southwest monsoon, lasts from May to October and is marked by heavy rain and high humidity. Following this, the dry season spans from November to April, with winds blowing from the northeast to the southwest. Approximately 80% of the annual rainfall occurs during the rainy season. There is a brief dry interval of 1-2 weeks between June and July due to high anti-cyclone circulation. Rainfall varies with altitude, with mean annual rainfall ranging from 695 mm around Tonle Sap Great Lake to 1787 mm in the mountainous areas. The mean annual temperatures range from 23°C for the minimum to 33°C for the maximum. The average annual humidity stands at 79%, with December being the most humid month on average and March the least humid.

3.3 Land use and land cover

In the upper catchment area, the land use and land cover comprise 53.13% natural forest, 44.41% agriculture, 2.03% built-up land, and 0.44% water bodies, based on the 2010 Mekong River Commission (MRC) land use data (see Figure 3-2). The Phnom Samkos Wildlife Sanctuary and Samlot Multiple Use Area, which are protected areas (PAs) associated with the Sangker River system, are the primary sources of heavy rainfall collection.

3.4 Soil characteristics

According to the FAO-UNESCO Soil Map of the World, the catchment is predominantly characterized by Distric Nitosols in the upland area (middle part of the catchment), whereas the mountain regions are dominant by Orthic Acrisols. Gleyic Luvisols mainly cover the semi-upland area.

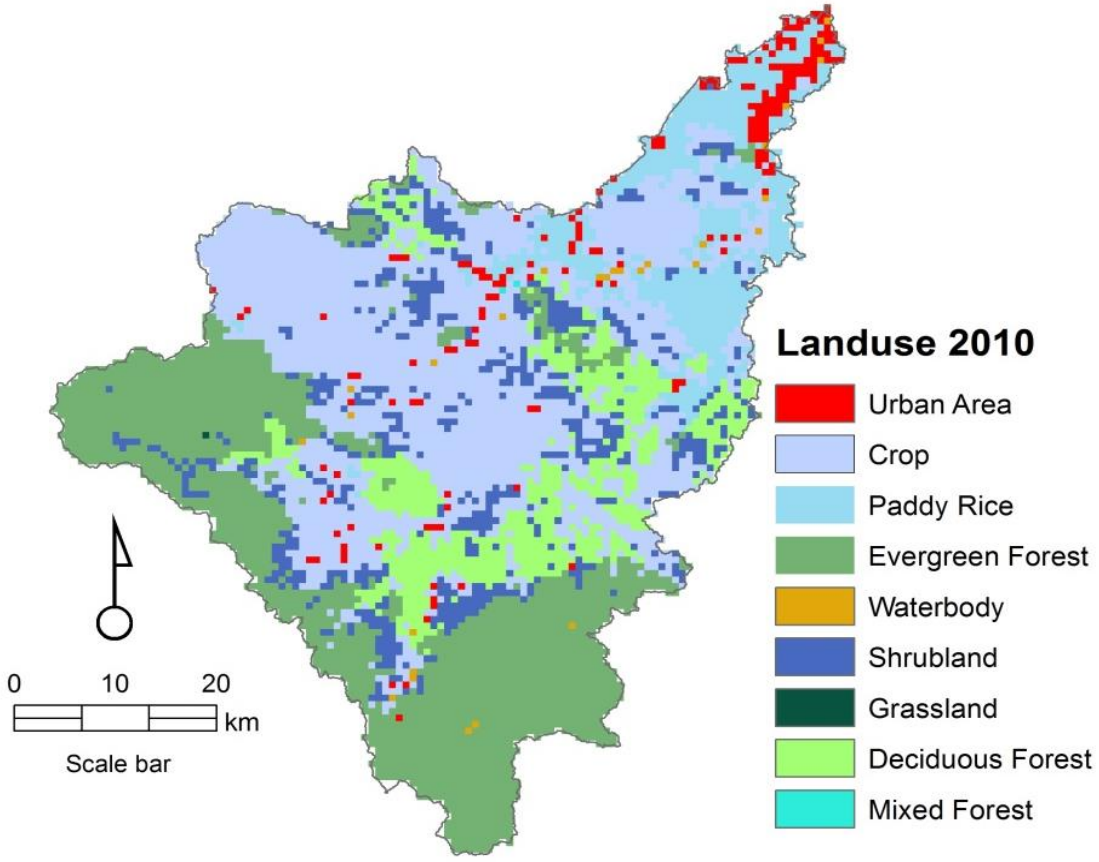

Figure 3-2 Map of land use in the upper Sangker river basin in 2010.

3.5 Irrigation scheme and infrastructure

The Kang Hot irrigation project area is located in the middle of the Sangker River, approximately 47 km from Battambang city. It is the largest irrigation scheme in the study area, covering a total command area of 72,000 ha. Water is drawn from the Sangker River via the Kang Hot headworks and distributed to the paddy fields through the left and right main canals, covering irrigated areas of 11,200 ha and 42,000 ha respectively (Kodoma, 2018) (Figure 3-3). The scheme was originally constructed during the Khmer Rouge regime, but it fell into disrepair, relying solely on rainfall for rice cultivation. However, the irrigation scheme was rehabilitated, and in 2013, the headworks were completely reconstructed within the river to store and increase water levels for agricultural purposes

(Figure 3-4). This development significantly improved irrigation and drainage across five districts, including Banan, Moung Russey, Koh Kra'lor, Sangker district, and Battambang City.

Upstream from the headworks, approximately 40 km along the river, there is a dam known as the "Battambang Multipurpose Dam," which was completed in June 2018. This dam was constructed to store water for agricultural and domestic use, prevent floods, generate electricity, and serve as a recreational area. The dam has a water storage capacity of about 193.43 million cubic meters and can irrigate an agricultural land area of 47,000 ha.

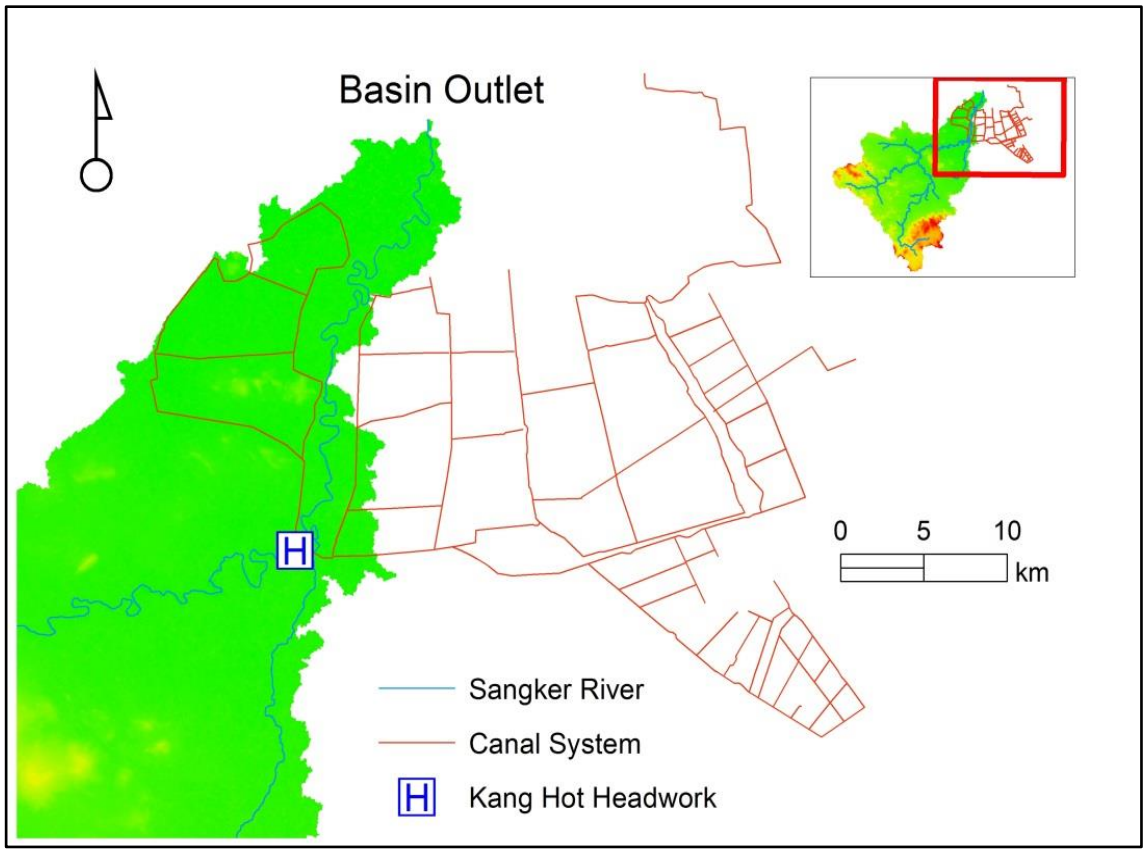

Figure 3-3 Location map of Kang Hot irrigation scheme

Figure 3-4 Kang Hot headwork site

Figure 3-5 Battambang multipurpose dam site

References

Kodoma, M. (2018). Practical use of water balance models in the Sangker and Prekthnoat River basins. Ministry of Water Resources and Meteorology, Phnom Penh, Cambodia. (Unpublished)

Sourn, T., Pok, S., Chou, P., Nut, N., Theng, D., Rath, P., ... & Prasad, P. V. (2021). Evaluation of land use and land cover change and its drivers in Battambang Province, Cambodia from 1998 to 2018. Sustainability, 13(20), 11170.

Chapter 4 Evaluation of the water balance in the irrigation system.

4.1 Introduction

Many river basins worldwide are facing perceived water shortages because of increasing demands for water from all sectors. In Cambodia, increasing water demands and competitiveness among sectors and between upstream and downstream of the river system are also becoming crucial, and the concern is that the country will face highly restricted water resources (Technical Service Center & JICA, 2014). Accordingly, the shortage of agricultural water is becoming a serious problem in the river basins, and the streamflows appear to be decreasing. Contributing 22% of gross domestic product collectively, agriculture, forestry, and fishing are essential to the growth of Cambodia's economy, and of the 80% of Cambodian people who live in rural areas, 65% rely on those three sectors (USAID, 2019). The Royal Government of Cambodia continues to enhance the management of water resources, develop irrigation systems, and undertake repair and maintenance of the irrigation infrastructure where required. Furthermore, headwork and multipurpose dams have been constructed in the river basins to meet the increased demand for water and flood control. The Sangker River basin in northwest Cambodia is one of the largest agricultural production areas in the nation and faces similar water resource issues. An irrigation project has been implemented in this area, but improved management is required to solve the water deficit problems.

The state-of-the-art method for estimating water deficiency is to analyze the balance between the water supply and the demand for irrigation water (IW). Masona et al. (2018) revealed a shortfall in IW use by applying the relative water supply (RWS), the ratio of water supply to water demand; an RWS of 1.6 showed that the targeted scheme received much more water than its IW demands. To assess water deficits in the Heibe River basin of China, Ji et al. (2006) established a model of the balance between water supply and demand based on meteorological, hydrological, land use, and socioeconomic data. They found that the water supply was insufficient to meet the water demands of the various irrigation districts, and indeed the Pingchuan irrigation district in China has already experienced a water supply crisis. By comparing the actual water supply with crop water requirements, Shakir et al. (2010) revealed an annual water shortage of more than 40% in the Upper

Chenab Canal of Pakistan. However, with regard to the spatial distribution of operational parameters, calculating the supply-and-demand balance of water resources does not resolve the regional problem of water-resource utilization on a relatively large scale in an inland basin (Bormann et al., 1999). Therefore, the present study considers the water balance of a regional scheme by incorporating a physically hydrologic-based model.

In the present study, the Soil and Water Assessment Tool (SWAT) hydrological model is used because of its widespread use in predicting runoff and sediment yield (Arnold et al., 1998). Herein, SWAT is used to estimate the streamflow at the headwork of the main canals. These streamflow data are then used to evaluate the deficit of water resources in the irrigation project area. The present results could help to identify the root of the water shortages that occur frequently not only in the irrigation project area but also across the river basin.

This chapter aimed to define the available stream water in the irrigation project area and identify the extent to which the water supply of the system is in deficit and/or excess. The specific objectives are (i) to assess the surplus (excess) and deficiency of IW from the Sangker River at the Kang Hot headwork point and (ii) to evaluate the actual IW uses and the demand in the Kang Hot Irrigation Project area.

4.2 Methods

4.2.1 Study area

The study area for this chapter is covered the Upper part of the Sangker River basin. See Chapter 3 section 3.1 for details.

4.2.2 SWAT hydrological modeling

4.2.2.1 SWAT description

The SWAT model was used in this study to simulate streamflow for a specific time period. SWAT is a continuous-time model and is designed to predict the impact of management on water, sediment, and agricultural chemical yields in ungauged watersheds (Gassman et al., 2007). It operates on a daily time step and is efficient enough to run for

many years. The watershed is delineated using the Digital Elevation Model (DEM). The watershed in the SWAT model is divided into multiple subbasins, which are then further subdivided into hydrologic response units (HRUs) that consist of unique land use, management, topographical, and soil characteristics (Abbaspour et al., 2015). The water in each HRU in SWAT is stored in four storage volumes: snow, soil profile (0–2 m), shallow aquifer (typically 2–20 m), and deep aquifer. Surface runoff from daily rainfall is estimated using a modified Soil Conservation Service (SCS) curve number method, which estimates the amount of runoff based on local land use, soil type, and antecedent moisture condition (Abbaspour et al., 2007). Peak runoff predictions are based on a modification of the Rational Formula (Chow et al., 1988). Channel routing is simulated using the variable storage or Muskingum method. SWAT provides three methods to simulate potential evapotranspiration (PET) including: (1) Penman-Monteith requires solar radiation, air temperature, relative humidity, and wind speed, (2) Priestley-Taylor requires solar radiation, air temperature, and wind speed, (3) Hargreaves requires only air temperature. Groundwater is water in the saturated zone of the earth materials under pressure greater than atmospheric pressure (Neitsch et al., 2011). SWAT simulates shallow and deep aquifers in each subbasin.

Water balance is the driving force behind all the processes in SWAT and the simulation of basin hydrology is separated into the land phase, which controls the amount of water, sediment, nutrient, and pesticide loadings to the main channel in each subbasin, and the in-stream or routing phase, which is the movement of water, sediments, etc., through the channel network of the watershed to the outlet (Arnold et al., 2012). The hydrological cycle is climate driven and provides moisture and energy inputs, such as daily precipitation, maximum/minimum air temperature, solar radiation, wind speed, and relative humidity, that control the water balance (Arnold et al., 2012).

4.2.2.2 SWAT data inputs

The SWAT model requires inputting the basic data including a Digital Elevation Model (DEM), Soil, Land use/land cover, hydrological, and meteorological data to run.

Digital Elevation Model (DEM)

The digital elevation model (DEM) was created using data from the ASTER GDEM globe map. This data was released jointly by the Ministry of Economy, Trade and Industry (METI) of Japan and the United States National Aeronautics and Space Administration (NASA). The GDEM v2 covers the Earth's land surfaces between 83° North and 83° South with a spatial resolution of about 30 meters, providing coverage for approximately 99% of Earth's land area. The DEM was utilized to outline the watershed boundary (see Figure 4-1) and sub-basins, and to digitize the stream network, as well as analyze the drainage patterns of the land surface terrain.

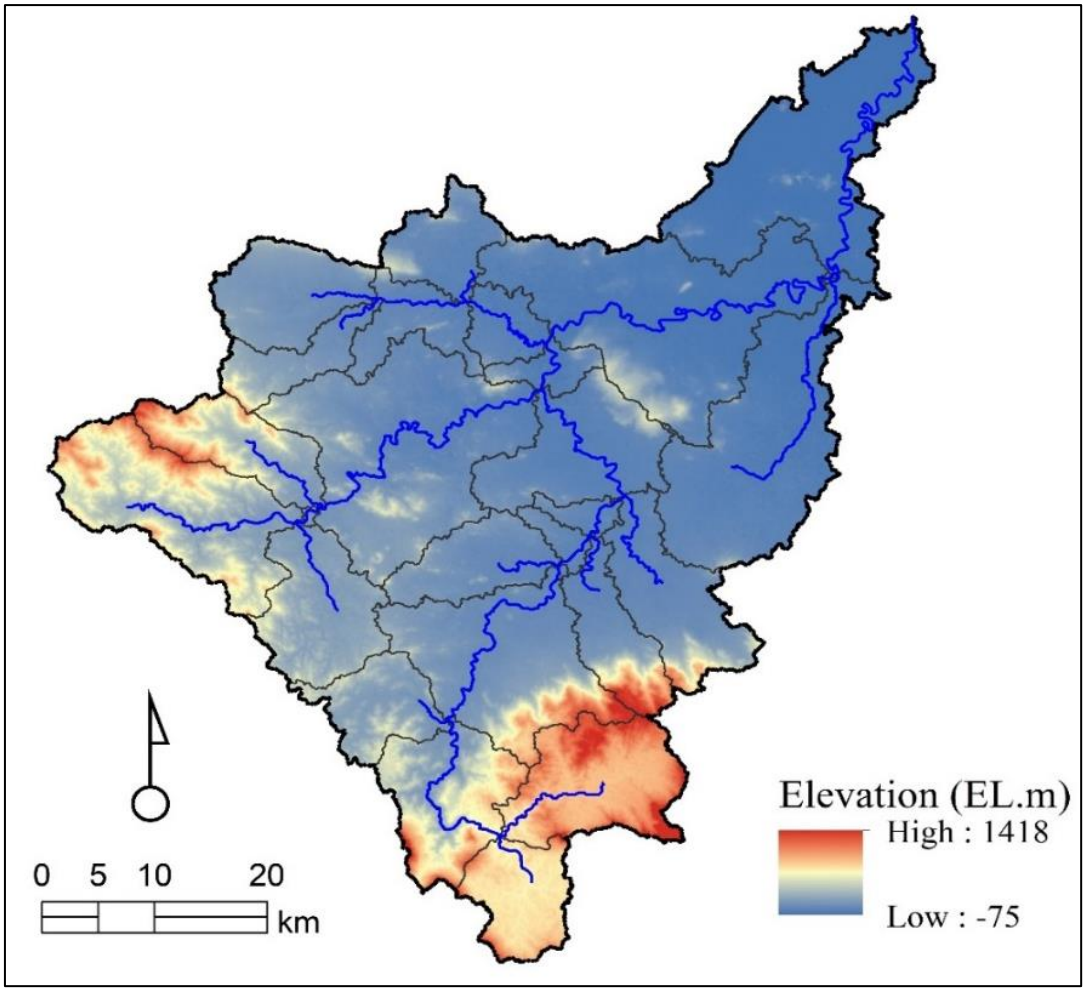

Figure 4-1 Map of elevation in the study area

Soil

The digital soil data used in the study was extracted from the FAO-UNESCO soil map of the world (DSMW). Knowledge about the soil profile is crucial for simulating the hydrological characteristics of the river basin. In the study area's basin, clay is the predominant soil type, and other areas are covered by clay loam located at higher and lower elevations (see Figure 4-2). Table 4-1 shows soil properties such as bulk density (Sol_BD), saturated hydraulic conductivity (Sol_K) soil hydrologic groups (HYDGRP) used in the SWAT modeling.

Table 4-1 Soil characteristics used for the SWAT model.

Soil name	Texture	Sol_BD	Sol_K	HYDGRP	Fractions in the soil mass		
					Clay	Silk	Sand
Lg39-3ab-4408	Clay loam	1.1	20.48	C	31	28	41
Nd65-3ab-4544	Clay	1.1	23.48	C	41	32	27
Ao90-2-3c-4284	Clay loam	1.3	7.27	D	30	30	39

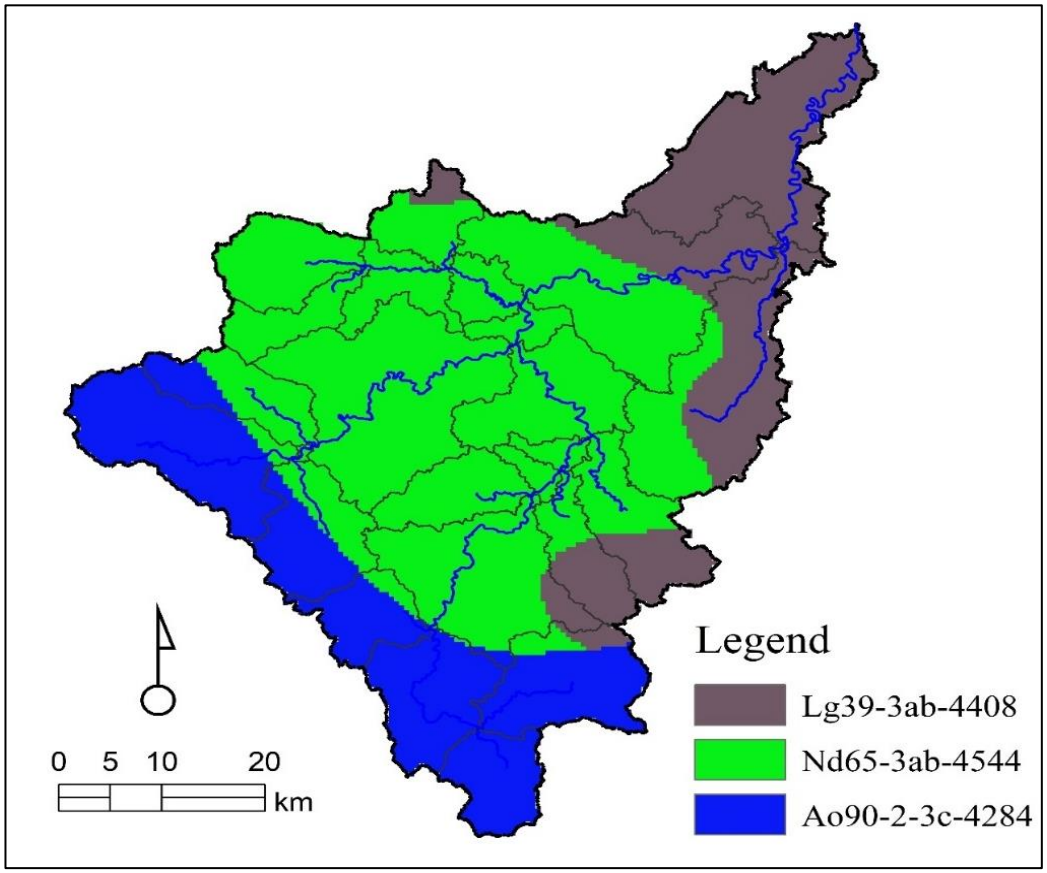

Figure 4-2 Soil properties of the study area

Land Use and Land Cover

The land use and land cover data were obtained from the Mekong River Commission in 2010 (Figure 3-2). The data was classified into nine types of land use: Built-up areas, Farmlands, Paddy fields, Evergreen Forest, Shrubland, Water, Grassland, Deciduous Forests, and Mixed Forests. In the river basin, farmland was the dominant land cover, accounting for 35% of land use. The upper part of the basin is predominantly covered with evergreen forest, comprising about 25% of the area. Paddy fields, the main crop in the study area, make up 15% of the land. All spatial datasets are projected using the WGS-1984 UTM Zone 48 N in ArcGIS.

Hydrological Data

The daily observed river flow data of the Sangker River from 2007 to 2018 were obtained from the Ministry of Water Resources and Meteorology, where the gauging station is in Battambang City at the Samdach Techo Hun Sen Bridge (Figure 4-3). These data were used to perform SWAT model calibration, validation, and sensitivity analysis.

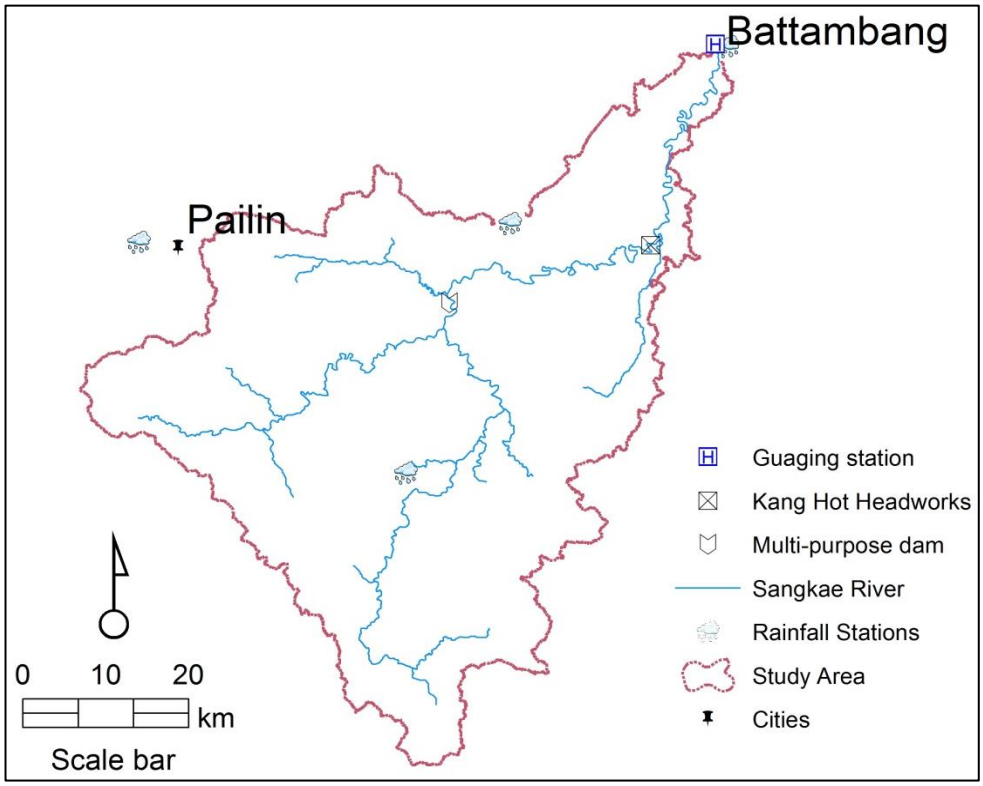

Figure 4-3 Location map of hydrological and meteorological stations

Meteorological Data

In the Sangker River basin, four meteorological stations (Figure 4-3) have recorded daily rainfall, temperature, wind speed, relative humidity, and solar radiation data from 2005 to 2018. This data was obtained from the Department of Meteorology, Ministry of Water Resources and Meteorology (MOWRAM). The SWAT model requires preprocessed daily meteorological data. To do this, the SWAT Weather Database was used to create WGEN (Weather Generator) statistics, which allows for the storage and processing of daily weather data for use with the SWAT model in this study.

4.2.2.3 SWAT model setup and data processing

In this study, we established the SWAT with the basin outlet at the Samdach Hun Sen Bridge as a gauging station in Battambang City (see Figure 4-3). We used 30-meter-resolution DEM data (ASTER-GDEM 2) in the ArcSWAT2012 interface to delineate the watershed and sub-basins within the basin. The catchment area covers 3,062 km^2, which represents 51% of the entire Sangker River basin (refer to Figure 3-1). We defined a sub-basin as a drainage area with a threshold of 5,000 hectares, resulting in 26 sub-basins that were further subdivided into 123 hydrological response units based on slope, soil, and land use. These parameters were obtained from the FAO-UNESCO Soil Map and the Mekong River Commission (MRC). We then clipped and overlapped this data 100% onto the watershed of the study area. The land use, soil, and slope layers were reclassified and overlaid to correspond with the parameters in the SWAT database. The Hargreaves method was originally derived from eight years of cool season Alta fescue grass lysimeter data from Davis, California (Hargreaves, 1975), and was applied to simulate the potential evapotranspiration in the study area because this method requires only rainfall and temperature data. One total potential evapotranspiration is determined, actual evaporation must be calculated. SWAT first evaporates any rainfall intercepted by the plant canopy. Next, SWAT calculates the maximum amount of transpiration and the maximum amount of sublimation/soil evaporation using an approach like that of Richtie (1972).

The available meteorological data of daily rainfall and temperature data at the four stations

obtained from the Ministry of Water Resources and Meteorology (MOWRAM) for 14 years (2007–2018) had to be preprocessed by the SWAT model. The streamflow data collected from MOWRAM at the Samdach Hun Sen Bridge between 2007 and 2018 will be used for model calibration (2007–2013) and validation (2013–2018). The first two years will serve as an equilibration period to set up initial conditions and will not be considered in the analysis, referred to as the 'Warm-up period'.

4.2.2.4 Manual calibration

It is crucial to carefully consider evapotranspiration, baseflow, and surface runoff when analyzing the SWAT output. The model's foundation lies in realistic hydrology. Manual calibration involved adjusting the most sensitive parameters, including the runoff curve number (CN2), the base flow recession constant (ALPHA_BF), and the soil evaporation compensation factor (ESCO), which impact surface runoff, groundwater, and evapotranspiration, respectively.

Manual calibration requires comparing simulated and measured data, using expert judgment to determine necessary adjustments to variables, and evaluating the reasonableness of the results (Gassman et al., 2007). Additionally, the analyst's experience and hydrological knowledge play a crucial role in defining parameters to balance the hydrological cycle. Abbaspour et al. (2015) provided a useful guideline for SWAT model manual calibration by adjusting the most sensitive parameters.

4.2.2.5 Model calibration and validation

Prior to the calibration and validation process in the SWAT model, the most sensitive parameters for the study area were identified. Sensitivity analysis involves determining how changes in model inputs affect the model output (Arnold et al., 2012). In SWAT-CUP, two methods of sensitivity analysis are commonly used: (i) local, by changing one parameter value at a time, and (ii) global, by allowing all parameter values to vary.

When many parameters are used in manual calibration, especially for complex hydrologic models, manual calibration can be labor-intensive, and automated calibration methods are preferred. Calibration involves better parameterizing a model to match local conditions.

This is done by comparing the predicted streamflow (output) for assumed conditions with observed stream water.

Model validation is the process of showing that a specific model for a particular site can make sufficiently accurate simulations using the parameter values from the calibration period without any changes.

In this study, the SUFI-2 algorithm in the SWAT-CUP software package was used for model calibration, validation, sensitivity, and uncertainty analysis (Abbaspour, 2011). The SWAT calibration of the Sangker River basin used 11 parameters (Table 4-2) after testing the sensitivity among 21 parameters using the one-at-a-time method in SWAT-CUP (Abbaspour, 2015). The one-at-a-time analysis involved making a single change while keeping other parameters constant at some value.

Table 4-2 Input parameters for SWAT calibration

No	Input Parameter	Definition	Range
1	CN2.mgt	Moisture condition II curve number	-0.2 to 0.2
2	CH_N2.rte	Manning's "n" value for the main channel	0 to 0.3
3	CH_K2.rte	Effective hydraulic conductivity in the main channel	0 to 500
4	RCHRG_DP.gw	Aquifer percolation coefficient	0 to 1
5	GW_REVAP.gw	Revap coefficient	0.02 to 0.2
6	GWQMN.gw	Threshold water level in shallow aquifer	0 to 5000
7	GW_DELAY.gw	Delay time for aquifer recharge	0 to 500
8	SLSOIL.hru	Hillslope length	0 to 150
9	SOL_AWC.sol	Available water capacity	0 to 1
10	SOL_BD.sol	Bulk density	0.9 to 2.5
11	HRU_SLP.hru	Average slope steepness	0 to 1

The model was calibrated automatically with a monthly time step in SWAT-CUP. Four iterations were carried out for model calibration, with each iteration involving 1000 simulations to determine the most sensitive parameters by making changes to the SWAT input parameters.

4.2.2.6 SWAT model evaluation

In SUFI-2, the variability of input parameters is depicted as uniform distributions, representing the range of possible values. The uncertainty in model outputs is quantified by the 95% prediction uncertainty (referred to as 95PPU), calculated at the 2.5% and 97.5% levels of the cumulative distribution of output variables obtained through Latin hypercube sampling (Abbaspour, 2007). This approach allows for a thorough understanding of the potential variability in the model's predictions. The effectiveness of the calibration and validation was assessed using the "*P-factor*" and "*R-factor*" indices. The *P-factor* means the percentage of observations covered by the 95PPU, ranges from 0 to 1, with a value of 1 indicating that the measured data is entirely within the model prediction uncertainty. For discharge, a *P-factor* greater than 0.7 or 0.75 is considered sufficient. The *R-factor* is the ratio of the average width of the prediction uncertainty band to the standard deviation of the measured variable, ranging between 0 and infinity. The *R-factor* of zero is a simulation that exactly corresponds to measured data. In each step of calibration, ten different objective functions in SUFI-2 allow the user to judge the performance of the model calibration and validation such as the coefficient of determination (R^2), Nash-Sutcliff efficiency (NSE), and the root mean square error (RSR), and so on. In this study, during the calibration procedure, *NSE*, and *RSR* were set as the objective function to indicate how well the plot of observed versus simulated data fits.

$$R - factor = \frac{1}{n\sigma}\sum_{n=1}^{n}(X_u - X_L) \tag{4.1}$$

where n is the number of observations, σ is the standard deviation of the observed streamflow, with X_u and X_L representing the upper 97.5th and lower 2.5th percentile of the simulated 95PPU, respectively.

The *NSE* is calculated, as shown in equation 4.2 (Nash and Sutcliffe, 1970):

$$NSE = 1 - \left[\frac{\sum_{i=1}^{n}(Q_i^{obs} - Q^{sim})^2}{\sum_{i=1}^{n}(Q_i^{obs} - Q^{mean})^2}\right] \tag{4.2}$$

where Q_i^{obs} is the *i*th streamflow observation, Q_i^{sim} is the *i* th simulated streamflow for the constituent being evaluated, Q^{mean} is the mean of observed streamflow data, and *n* is the total number of observations. It has a range from -∞ to 1. A value of 1 signifies perfect quality, which is what practitioners aim for. Negative *NSE* values indicate inadequate model performance. In the context of optimization, the *NSE* is a quantity to be maximized.

The *RSR* is computed as the ratio of the *RMSE* and the standard deviation of the observed data. It is computed as in equation 4.3:

$$RSR = \frac{RMSE}{STDEV_{obs}} = \frac{\sqrt{\sum_{i=1}^{n}(Q_i^{obs} - Q^{sim})^2}}{\sqrt{\sum_{i=1}^{n}(Q_i^{obs} - Q^{mean})^2}} \tag{4.3}$$

No comprehensive guideline is available to evaluate the accuracy of simulated data compared to observed flow. Morisai et al. (2007) reviewed the previous studies and suggested a general performance rating for recommending statistics for the SWAT model shown in Table 4-3.

Table 4-3 Performance ratings for recommending statistics for a monthly time step.

Performance rating	Nash-Sutcliffe efficiency	*RSR*
Very good	$0.75 < NSE \leq 1.0$	$0.0 < RSR \leq 0.50$
Good	$0.65 < NSE \leq 0.75$	$0.50 < RSR \leq 0.60$
Satisfactory	$0.50 < NSE \leq 0.65$	$0.60 < RSR \leq 0.70$
Unsatisfactory	$NSE \leq 0.50$	$RSR > 0.70$

4.2.3 Canal discharge measurement

Discharge refers to the volume of water moving down a canal or stream per unit of time, typically expressed in cubic meters per second. In this study, discharge measurements were carried out to estimate the actual water supply volume in both the right and left main canals. These measurements were conducted along the main water intake canals to the left

and right of the Sangker River near the headwork (refer to Figure 3-3 & Figure 3-4). The two main canals have a trapezoidal shape, as illustrated in Figure 4-4.

The canal discharge measurements were calculated directly by measuring the flow velocity using the Current-Meter method (refer to Figure 4-5) over ten times the difference with the surveyed canal cross-sectional geometry. The velocity was measured using the Six-Tenths Depth Method, which involved measuring the velocity at 0.6 or 60% of the depth from the water surface. The canal cross-sectional geometry was measured using a measuring tape. These flow measurements were then used to establish the H-Q curve or rating curve (the relationship between streamflow and water depth) for each gaging station, following the procedure described in the reports of Kodoma (2015).

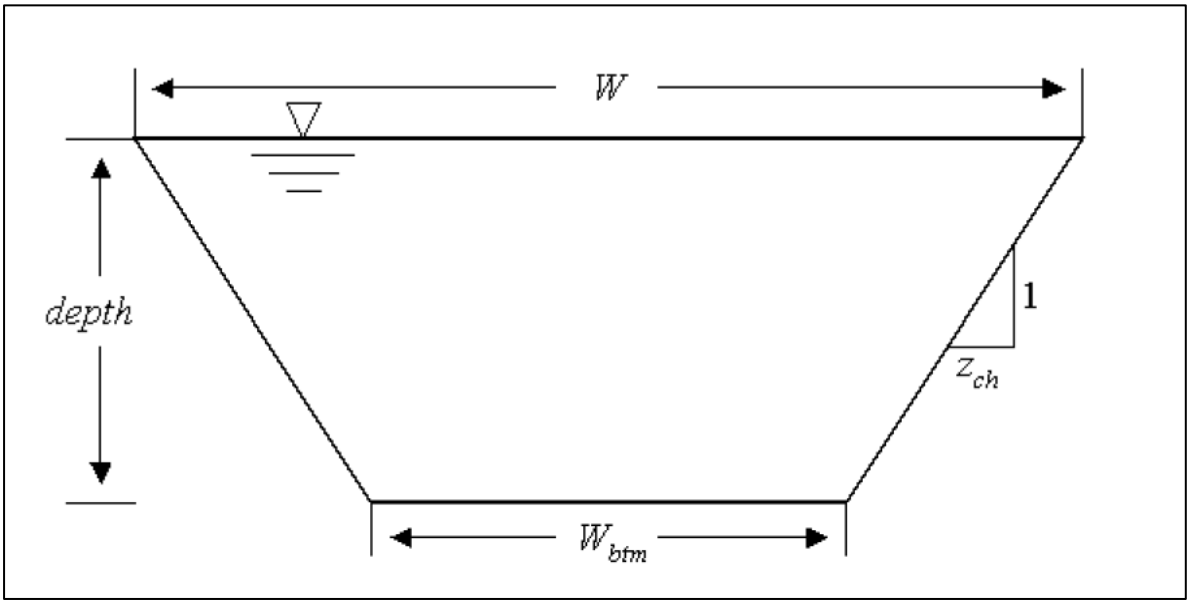

Figure 4-4 Cross section of the main canal

The canal discharge was calculated using equation (4.4):

$$Q = V \times A \tag{4.4}$$

where Q is the canal flow rate ($m^3.s^{-1}$), V is the velocity (m. s^{-1}) obtained from Current meter records, and A is the cross-sectional area of the canal (m^2).

The rating curves for the right main canal and the left main canal, which illustrate the correlation between water level and discharge, are depicted in Figure 4-6 and Figure 4-7. The equations 4.5 and 4.6 provide a detailed representation of this relationship for the right and left main canals, respectively.

$$Q = 9.96(H - 0.121)^2 \quad (4.5)$$

$$Q = 5.0176\ (H + 0.062)^2 \quad (4.6)$$

where Q is the canal flow rate ($m.s^{-1}$), and H is the water level (m).

Figure 4-5 Canal discharge measurement using the Current Meter at the Right and Left main canal.

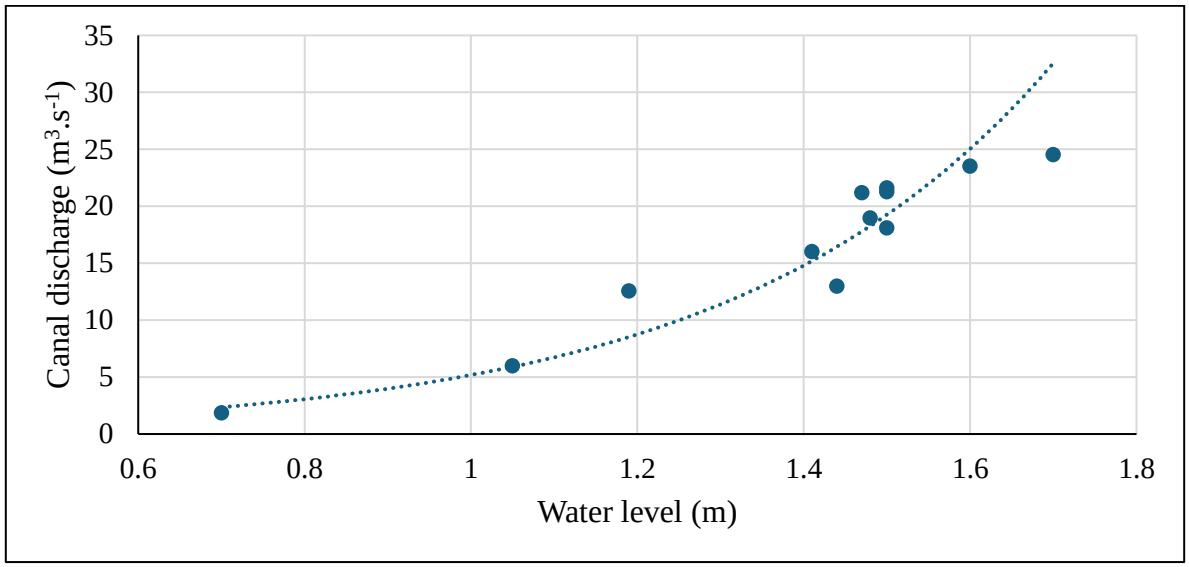

Figure 4-6 H-Q curve at the right main canal

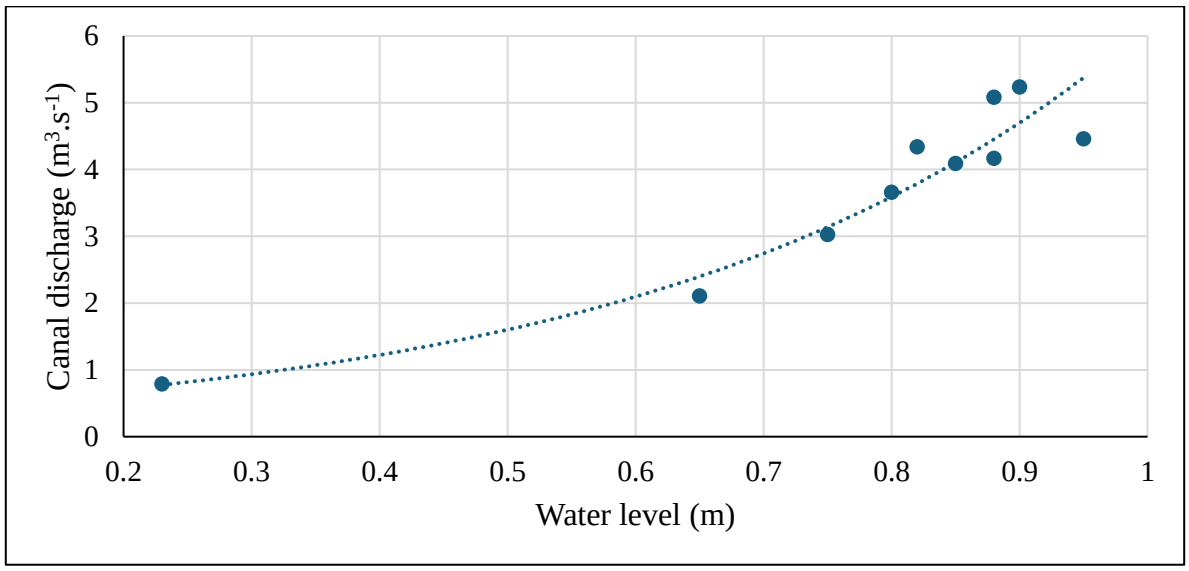

Figure 4-7 H-Q curve at the left main canal

To monitor the daily water level, HOBO U20L Water Level Loggers were placed inside the main canals to track the water surface elevation over time. Figure 4-8 and Figure 4-9 illustrate the positioning of water level loggers at the Right main canal and the Left main canal, respectively.

Figure 4-8 Installation of water level logger at the right main canal

Figure 4-9 Installation of water level logger at the left main canal

Daily and monthly discharge were determined by applying accuracy H-Q curves in equations 4.5 and 4.6 to the daily water level data obtained from the HOBO U20L Water Level Loggers.

4.2.4 Calculation of irrigation water demands

In an irrigation scheme, more than one kind of crop is grown at the same time and for a year. Thus, the calculation of irrigation water needs for a multiple cropping system is often applied. When the irrigation needs for a single cropping pattern have been computed, the irrigation needs for an entire scheme with more than one crop can be determined by adding up the irrigation requirement for each month (Brouwer et al., 1992).

In the present study, the irrigation water demands were calculated mainly for rice-based farming in the Kang Hot Project area. The unit irrigation water requirement was estimated by five days time step using Equation 4.7 based on its cropping calendar (Table 4-4):

$$IR = (ET_o \times Kc + PR + Lp - ER) / IE \qquad (4.7)$$

where *IR* is the unit irrigation water requirement.

ETo is the crop reference evapotranspiration,

Kc is the crop coefficient

PR is the percolation rate

Lp is the land preparation requirement

ER is the effective rainfall

IE is the irrigation efficiency

Crop reference evapotranspiration (*ETo*)

ETo represents the evapotranspiration rate from a reference surface, not short of water. The reference surface is a hypothetical grass reference crop with an assumed crop height of 0.12 m, a fixed surface resistance of 70 $s.m^{-1}$, and an albedo of 0.23. The reference crop completely covers the soil, is kept short, well-watered, and is actively growing under

optimal agronomic conditions. *ETo* is estimated using the FAO Penman-Monteith equation, which is recommended can be defined as:

$$ET_o = \frac{0.408\Delta(R_n - G) + \gamma \frac{900}{T + 273} u_2 (e_s - e_a)}{\Delta + \gamma(1 + 0.34u_2)} \quad (4.8)$$

where ET_o is reference evapotranspiration [mm.day^{-1}]

R_n is net radiation at the crop surface [MJ m^{-2}.day^{-1}]

G is soil heat flux density [MJ m^{-2}.day^{-1}]

T is air temperature at 2 m height [^{o}C]

u_2 is wind speed at 2 m height [m.s^{-1}]

e_s is saturation vapor pressure [kPa]

e_a is actual vapor pressure [kPa]

$e_s - e_a$ is saturation vapor pressure deficit [kPa]

Δ is slope vapor pressure curve [kPa.^{o}C^{-1}]

γ is psychometric constant [kPa.^{o}C^{-1}]

The *ETo* can be estimated through the calculation sheet in which some of the climatic parameters would be determined. The calculation procedure consists of the following steps:

1. Derivation of some climatic parameters from the daily maximum (T_{max}) and minimum (T_{min}) air temperature, altitude (z), and mean wind speed (u_2).
2. Calculation of the vapor pressure deficit ($e_s - e_a$); The saturation vapor pressure (e_s) is derived from T_{max} and T_{min}, while the actual vapor pressure (e_a) can be derived from the dewpoint temperature (T_{dew}), from maximum (RH_{max}) and

minimum (RH_{min}) relative humidity, from the maximum (RH_{max}), or from mean relative humidity (RH_{mean}).

3. Determination of the net radiation (R_n) as the difference between the net shortwave radiation (R_{ns}) and the net longwave radiation (R_{nl}). In the calculation sheet, the effect of soil heat flux (G) is ignored for daily calculations as the magnitude of the flux, in this case, is relatively small. The net radiation, expressed in MJ $m^{-2}.day^{-1}$, is converted to $mm.day^{-1}$ (equivalent evaporation) in the FAO Penman-Monteith equation by using 0.408 as the conversion factor within the equation.
4. *ETo* is obtained by combining the results of the previous steps.

The calculation procedures of all data required for the calculation of *ETo* employing the FAO Penman-Monteith equation were detailed in Chapter 3 of FAO, (1998).

Table 4-4 Cropping calendar for rice farming at Kang Hot irrigation system

Cropping Pattern	Area (ha)		Jan	Feb	Mar	Apr	May	Jun	Jul	Aug	Sep	Oct	Nov	Dec
	Left canal	Right canal												
CP-C	4,480	16,800				→	→	→	→					
CP-B	6,832	25,620								→	→	→	→	
CP-E1	1,120	4,200						→	→	→	→	→	→	
CP-E (-15)	56	210					→	→	→	→	→	→	→	
CP-E (+15)	56	210						→	→	→	→	→	→	→
CP-E2	56	210	→	→	→									→

where arrows representing the duration of rice cultivation and each abbreviation of cropping pattern stands for:

- Cropping Pattern-C: early wet rice-direct sowing (105 days)
- Cropping Pattern-B: wet season rice-transplanting (115 days)
- Cropping Pattern-E: wet season rice -direct sowing (140 days)
- Cropping pattern-E (-15 days): add wet season rice direct sowing (140 days)
- Cropping pattern-(+15days): add wet season rice direct sowing (140 days)

- Cropping pattern-E2: dry season rice-direct sowing (90 days)

Crop coefficient (*Kc*)

As the crop develops the ground cover, crop height, and leaf area change. Due to differences in evapotranspiration during the various growth stages, the *Kc* for a given crop will vary over the growing period. The growing period can be divided into four distinct growth stages: initial, crop development, mid-season, and late-season (Figure 4-10).

1. The initial stage: This is the period from sowing or transplanting until the crop covers about 10% of the ground.
2. The crop development stage: This period starts at the end of the initial stage and lasts until the full ground cover has been reached (ground cover 70-80%); it does not necessarily mean that the crop is at its maximum height.
3. The mid-season stage: This period starts at the end of the crop development stage and lasts until maturity; it includes flowering and grain-setting.
4. The late-season stage: This period starts at the end of the mid-season stage and lasts until the last day of the harvest; it includes ripening.

Given the unavailability of field measurement records, crop coefficient data from in FAO's guideline, as outlined in trusted FAO Irrigation and Drainage Paper 56 (Allen et al., 1998) and tabulated in Table 4-5. serves as a reliable reference point.

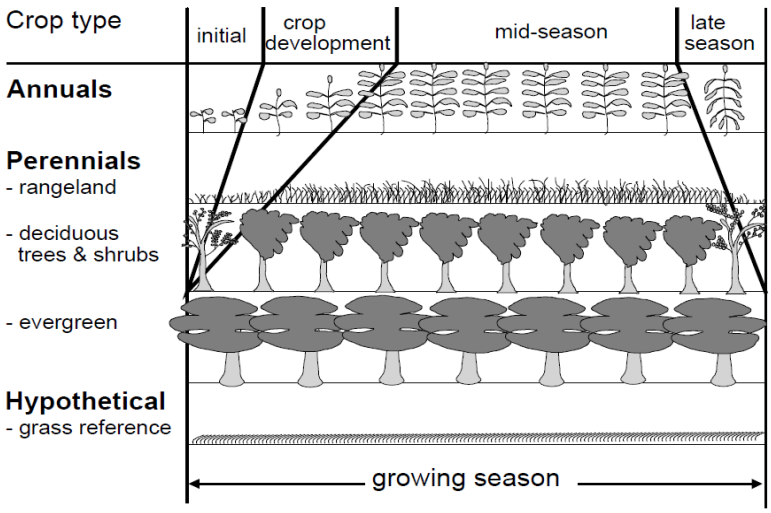

Figure 4-10 Crop growth stages for different types of crops.

Table 4-5 Crop coefficient of paddy for use with FAO Penman-Monteith ETo

Variety	Initial	Crop development	Mid season	Late season
150 days	30	30	60	30
Kc	1.05	1.15	1.20	0.90
105 days	20	30	30	25
Kc	1.05	1.15	1.20	0.90
115 days	20	30	40	25
Kc	1.05	1.15	1.20	0.90
140 days	30	30	50	30
Kc	1.05	1.15	1.20	0.90
90 days	20	20	30	20
Kc	1.05	1.15	1.20	0.90

Percolation rate (PR)

The amount of water lost due to percolation and seepage depends on the type of soil (Brouwer et al., 1992). In very heavy, well-puddled clay soils, the losses will be low, while in sandy soils, they will be high. When monitoring the water balance of flooded rice fields for irrigation system design and management, a constant seepage and percolation rate is often assumed (Bouman et al., 1994). The percolation and seepage losses typically range between 4 and 8 $mm.day^{-1}$.

In the absence of field measurement records, the percolation rate in this study area was obtained from the JICA Master Plan Study Team in 2007. The team used a dial gauge and open-ended-cylinder method in the study site. In this study area, a percolation rate of 3.5 $mm.day^{-1}$ was used to calculate the irrigation water requirement.

Land preparation requirement (Lp)

Preparing the land is crucial to ensure that the rice field is properly set for planting. A well-prepared field helps to manage weeds, recycle plant nutrients, and provide a soft soil mass for transplanting, as well as a suitable soil surface for direct seeding. When cultivating

a paddy rice crop, the water required is for preparing the rice nursery and the rice fields (Brouwer et al., 1992). The water volume needed for preparing the nursery begins one month before sowing, while the preparation of the rice fields begins about one, or sometimes two, months before the rice is transplanted. Typically, the fields are flooded, and a few days after flooding, the field is plowed. The land preparation necessary for paddy in this study was estimated based on assumptions derived from field surveys and interviews with the Agronomy Office of the Provincial Department of Agriculture (PDA) and the Provincial Department of Water Resources and Meteorology (PDWRAM). It was assumed that the amount of water required depends on the soil type, with sandy loam requiring 250 mm, clay loam requiring 200 mm, and clay requiring 170 mm.

Effective rainfall (ER)

The portion of rainwater that is stored in the root zone and utilized by plants, known as effective rainfall (Brouwer et al., 1992), may be lost through deep percolation and run-off during periods of high rainfall. Various methods for estimating effective rainfall for irrigation scheduling are employed in different countries, drawing on extensive practical knowledge and proven effectiveness within specific local conditions (Dastane, 1974). In this study, the 5-day effective rainfall for paddy fields was determined using empirical relationships developed in Japan (Dastane, 1974).

Irrigation efficiency (IE)

Irrigation efficiency is a parameter to evaluate the performance of irrigation water use from a water conservation perspective (Bos and Wolters, 1990). IE is distinguished into field application efficiency, tertiary unit efficiency, and overall efficiency.

Irrigation efficiency refers to the conveyance efficiency of the distribution system. The JICA Master Plan Study Team in 2009 supposed that PDWRAM strictly managed the canal system and water supply for fields. The irrigation efficiency was assumed. In the present study, IE was collected from the Ministry of Water Resources and Meteorology (MOWRAM) and the JICA Master Plan Study Team in 2009, as detailed in Table 4-6 and Table 4-7.

Table 4-6 Irrigation efficiency for paddy field

Item	Water loss rate (%)	Efficiency (%)	Remarks
Field application efficiency	0	100	Basin irrigation
Tertiary unit	15	85	-
Secondary canal	12	88	-
Main Canal	12	88	-
Overall efficiency	-	66	-

Table 4-7 Irrigation efficiency for upland crop

Item	Water loss rate (%)	Efficiency (%)	Remarks
Field application efficiency	20	80	Furrow irrigation
Tertiary unit	15	85	-
Secondary canal	12	88	-
Main Canal	12	88	-
Overall efficiency	-	53	-

The irrigation water demand comes from the unit irrigation water requirement multiplied by the area to be irrigated, which gives a volume of IW needed per unit time. The IW demand is computed as

$$ID = IR \times A, \tag{4.9}$$

where *ID* is the IW requirement, and *A* is the area.

The irrigation area for this calculation was described in Chapter 3 section 3.5.

4.2.5 Methods of interpretation and analysis

In the present study, the analysis of the deficit or surplus of irrigation water in the Kang Hot irrigation project area was divided into two sections. The first section analyzed the balance between available stream water and irrigation water demand. The next section compared irrigation water demand with the actual water supply. The irrigation water supply

and demand conditions were evaluated to determine whether there was an excess over demand or a deficit in supply.

4.2.5.1 Analysis of balance between available stream water and water demands

In the study area, the use of agricultural water relies on irrigation from the Sangker River, which flows down from the mountains. During the irrigation season, the area depends on the river's water supply in the absence of rainfall. The reliability of this supply is crucial for the success of the irrigation project. Therefore, after estimating the total irrigation water requirement, it is important to determine the river's flow and its reliability during the irrigation season (Brouwer et al., 1992). Consulting the hydrological service is necessary as it provides information on water resources and river discharge (Brouwer et al., 1992). Hence, in this study, the estimation of river water resources involved the use of hydrological models such as the Soil and Water Assessment Tool (SWAT).

This study also involved assessing the balance between the available streamflow at the Kang Hot Headwork and the irrigation water demands of the Kang Hot irrigation project area using a conventional equation:

$$Q_{sd} = Q_{aw} - Q_d \tag{4.10}$$

where *Qsd* is the surplus or deficit of water, *Qaw* is the available streamflow for possible water supply, *Qaw* is the irrigation water demand.

The water balance was analyzed from 2014 to 2018 using the monthly available stream minus the irrigation water requirement. The available stream water quantity was estimated by using the SWAT model. Meanwhile, the irrigation water demand was calculated as described in section 4.2.4. The irrigation water demands were slightly changing both cropping patterns and irrigation areas.

4.2.5.2 Comparing actual water supply and irrigation water demands

The study evaluated the supply and demand of irrigation water by analyzing the extent to which the irrigation water supply meets the crop demand. This analysis was based on the

flow data from the main canals near the Kang Hot irrigation project area collected between June 2018 and October 2019. The comparison of actual irrigation water supply and demand at the gaging stations on the main canals is crucial for identifying any deficits or surpluses in the system. When the actual water supply exceeds the demand, there is a surplus, and vice versa (Ullah et al., 1998). Therefore, comparing the actual irrigation water supply and demand helps in determining if there is a deficit or surplus in the supply of water. This approach is essential for evaluating the irrigation water use in the project area.

4.3 Results and Discussion

4.3.1 SWAT calibration and validation

In Figure 4-11, the results of observed and simulated streamflow at the Samdach Hun Sen Bridge gauging station in Battambang City (Figure 3-1) are presented on a monthly time scale during the calibration period from 2007 to 2013. The graphs demonstrate that the SWAT model accurately tracked the streamflow each month during the calibration period. This was supported by a statistical quantitative NSE of 0.58 and RSR of 0.64 (Moriasi et al., 2007), indicating a satisfactory model calibration. In streamflow calibration, 46% of the observed data were bracketed by the 95PPU while the *R-factor* had a value of 0.61. The hydrograph of monthly simulation versus observed streamflow generally showed similar trends. In certain years, the predicted streamflow closely matched both low streamflow and peak flows in the river basin (2007, 2008, 2009, and 2013). Additionally, the observed flow data revealed that the timing of peak flows corresponded with the timing of maximum rainfall intensity. Scatter plots during the calibration period (Figure 4-12) displayed a nearly linear relationship between the observed and simulated streamflow, which can be attributed to rainfall distribution.

In Figure 4-13, the observed and simulated streamflow at the Samdach Hun Sen Bridge gauging station in Battambang City (refer to Figure 3-1) is depicted on a monthly basis during the validation period from 2014 to 2018. The comparison of the monthly measured and simulated streamflow demonstrates accurate tracking of overall trends. In streamflow validation, 48% of the observed data were bracketed by the 95PPU while the *R-factor* had a

value of 0.75. The model effectively simulates both low river flow during the dry season and high river flow during the rainy season. Consistency between peak flows of observed and simulated flow over the years, in line with corresponding rainfall patterns, is evident. The model validation results indicate a strong agreement between observed and simulated flow output, supported by the NSE and RSR values presented in Table 4-8. Furthermore, the scatter plots during the validation period (Figure 4-14) reveal a stronger correlation between the observed and simulated streamflow. These findings emphasize the model's robust predictive capability, meeting the statistical model efficiency criteria recommended by Moriasi et al., (2007).

The comparison between the observed and predicted streamflow of the SWAT model in the Sangker River basin performed satisfactorily. This discrepancy can be attributed to uncertainty in the predictions. The uncertainties in the model are a result of processes that are accounted for in the model but cannot be fully explained within the watershed (Abbaspour, 2007). This includes factors such as the outflow from the reservoirs of the Battambang multipurpose dam and water transfer for irrigation at the Kang Hot headwork. Besides model uncertainty, there exist additional uncertainties arising from inaccuracies in input variables, such as rainfall and temperature, particularly in cases where the number of available meteorological stations is limited. The collection of rainfall data plays a crucial role in the development of rainfall-runoff models. This data, however, can be subject to uncertainties, particularly in regions with limited available data (Beven, 2012). Despite these challenges, it can be concluded that the SWAT modeling in the Sangker River watershed performed acceptably during the calibration and validation periods, as demonstrated by the evaluation using statistical indicators such as *NSE* and *RSR*.

Table 4-8 *NSE* and *RSR* values of SWAT modeling for a monthly time step at the gauging station

Quantitative statistics	Monthly calibration (2007-2013)	Monthly validation (2014-2018)	Model Evaluation	
			Calibration	Validation
NSE	0.58	0.69	Satisfactory	Good
RSR	0.64	0.55		

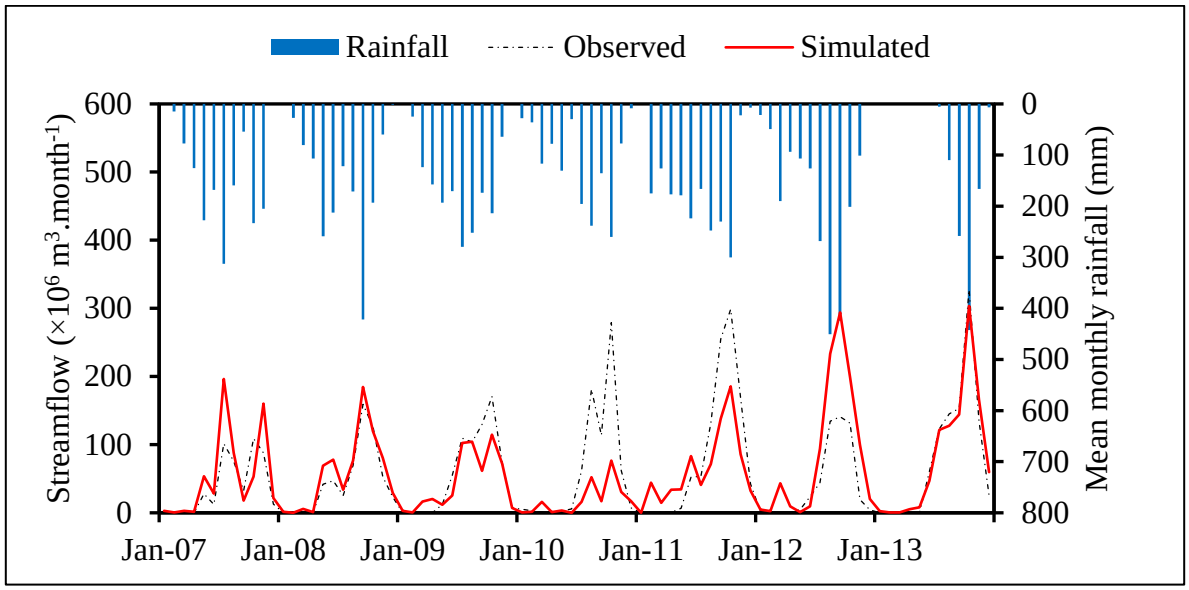

Figure 4-11 Monthly simulated and observed flow rate for model calibration period at gauging station of Sangker River

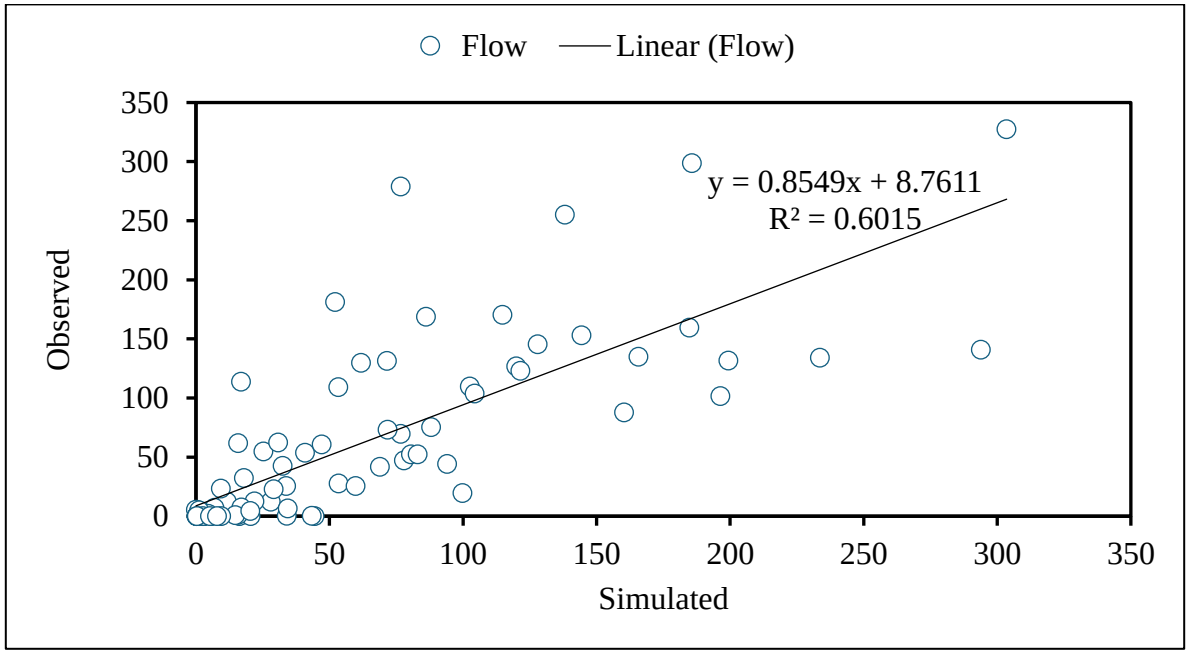

Figure 4-12 Scatter of monthly simulated and observed flow rate for model calibration.

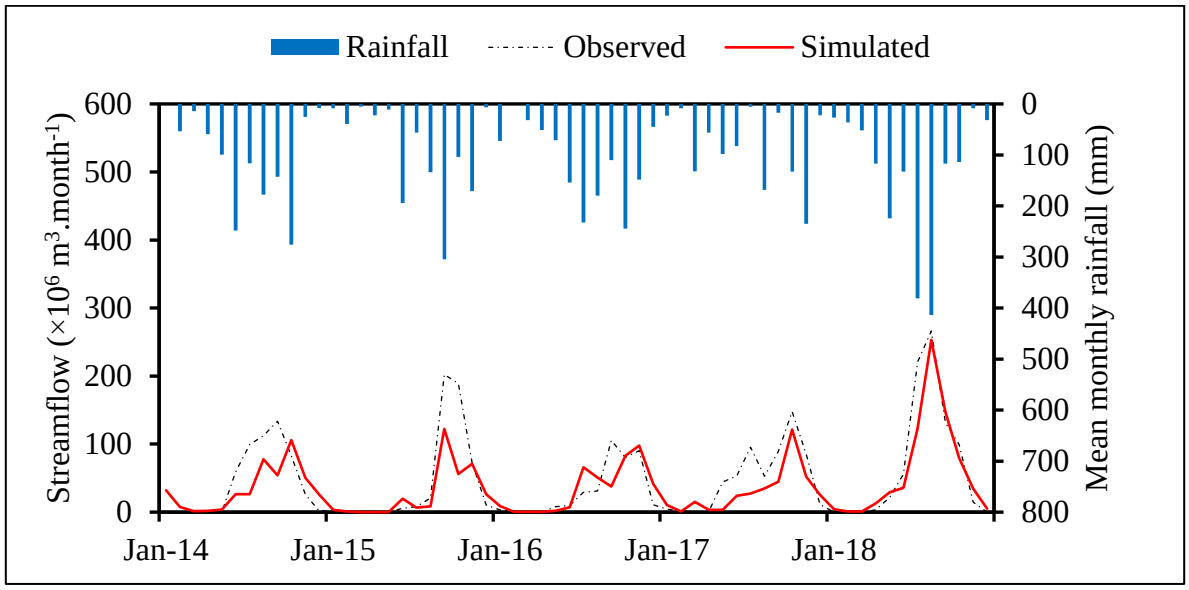

Figure 4-13 Monthly simulated and observed flow rate for the model validation period at gauging station of Sangker River

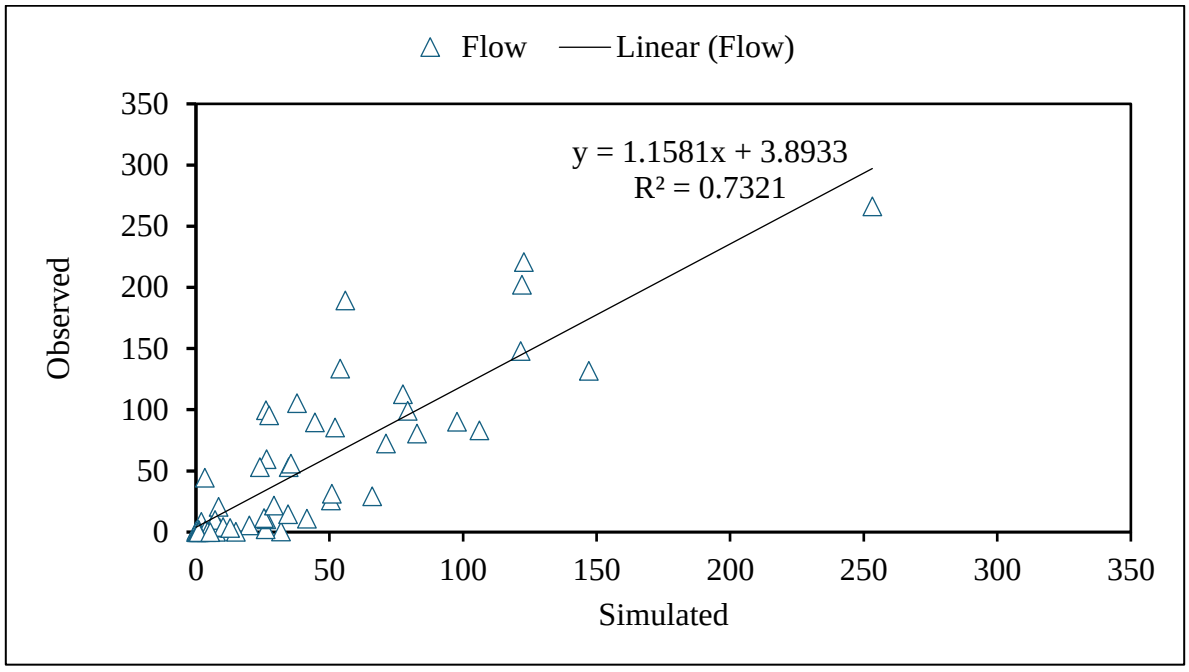

Figure 4-14 Scatter of monthly simulated and observed flow rate for model validation period at gauging station of Sangker River

4.3.2 Availability of stream water

Due to the lack of streamflow data observation at the Kang Hot headwork point, the present study utilized the SWAT model to estimate the available stream water at that location. However, the SWAT model's simulation of the stream water varied between the observed and predicted output at the Samdach Hun Sen Bridge gauging station (refer to Figure 3-1). Based on the SWAT results at the gauging station, the available water resources at the Kang Hot Headwork for the years 2014–2018 could be estimated from the simulation results database. After the SWAT simulation, several output files are generated, including the summary output file (output.std), the HRU output file (output.hru), the subbasin output file (output.sub), and the main channel or reach output file (output.rch). The flow rate at the Kang Hot headwork could be obtained from the main channel output file in the SWAT Output database resulting from the SWAT simulation. The monthly streamflow data is located in the Flow_In column in the spreadsheet format of the "output.rch" file.

Figure 4-15 illustrates the variation in river discharge at Kang Hot headworks from 2014 to 2018, measured in millions of cubic meters per month ($\times 10^6$ $m^3.month^{-1}$). The availability of water fluctuates significantly over the years and even from one year to the next. The peak flows were notably consistent with rainfall patterns. The streamflow fluctuated from 2014 to 2017, peaking at around 250×10^6 $m^3.month^{-1}$, and then doubled in 2018 to approximately 500×10^6 $m^3.month^{-1}$. Low flow consistently occurred almost every year during the dry season in April.

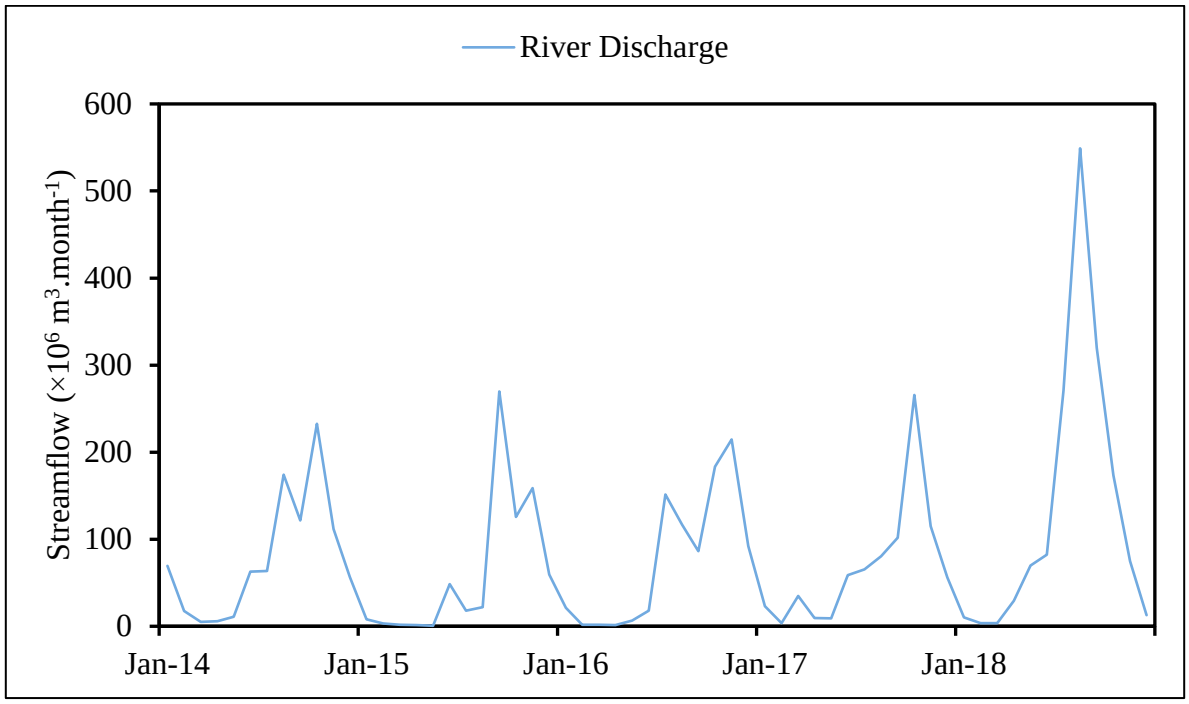

Figure 4-15 Streamflow at the Kang Hot headwork.

4.3.3 Irrigation water demands

The monthly irrigation water demand (in units of $\times 10^6$ $m^3.month^{-1}$) for a full year of rice cultivation in the Kang Hot Project area was estimated from January to December using a simplified method described in equation 4.6 and based on the irrigated crop calendar outlined in section 4.2.4. It was assumed that the irrigation water demands did not undergo significant changes in the irrigation area and cropping patterns during the study period.

Figure 4-16 and Figure 4-17 illustrate the irrigation water demand ($\times 10^6$ $m^3.month^{-1}$) for the right and left main canals from January to December. The irrigation season in the project area spanned from April to late November, with the highest irrigation demand occurring in May, June, and September to November, reaching a maximum of approximately 60×10^6 $m^3.month^{-1}$ and 15×10^6 $m^3.month^{-1}$ for the right and left main canals, respectively. The monthly average water demand was around 35×10^6 $m^3 \cdot month^{-1}$

and 10 × 10^6 m^3.$month^{-1}$ for the right and left main canals, respectively. Water demand sharply decreased from May

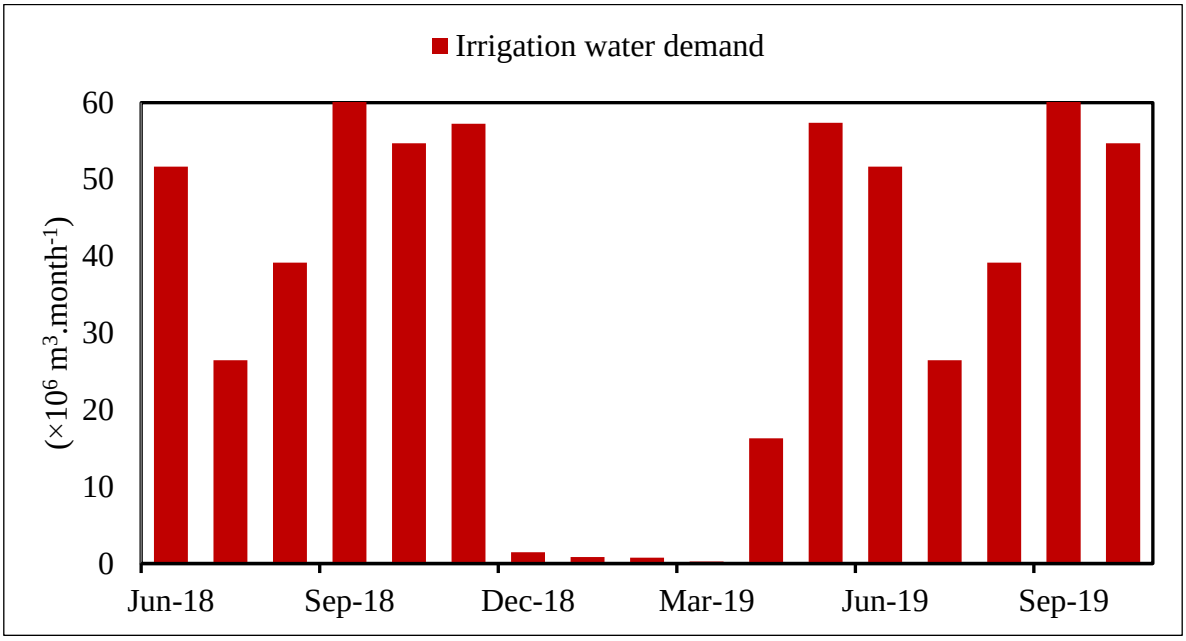

Figure 4-16 Irrigation water (IW) demand at the right main canal of Kang Hot project area

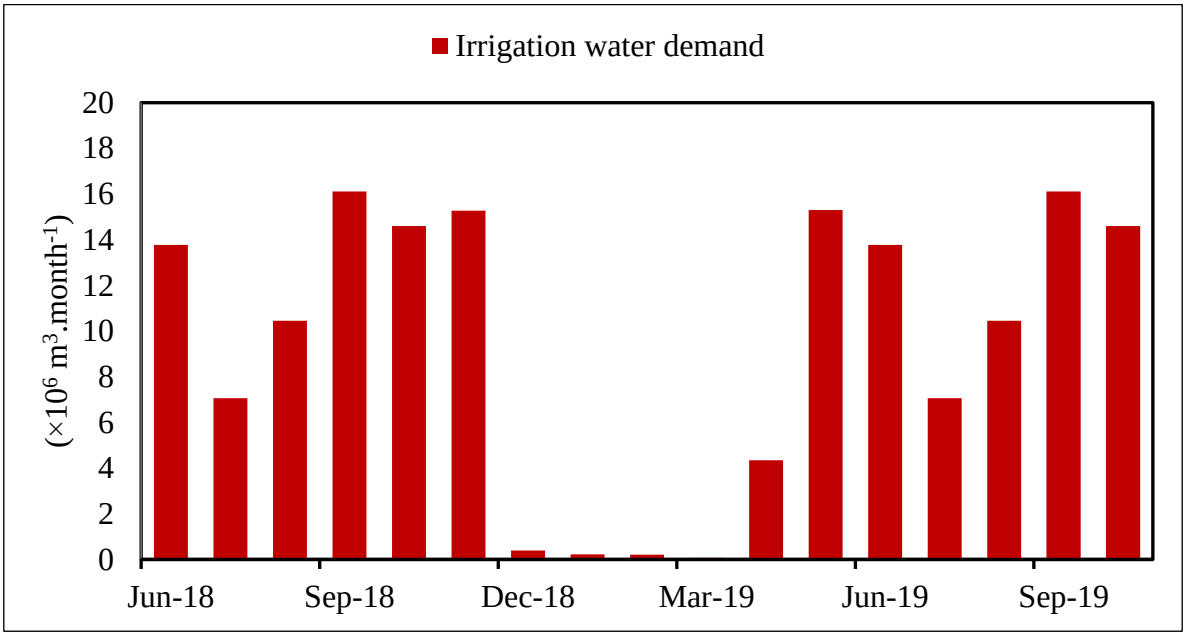

Figure 4-17 Irrigation water (IW) demand at the left main canal of Kang Hot project area

to July, with a two-fold difference in the right and left main canals, and then notably increased from July to September, remaining stable until November of that year. Water consumption between December and March was minimal due to a limited area being cultivated in the irrigation project area.

4.3.4 Actual canal water supply

The continuous canal discharge at the right and left main canals from June 2018 to October 2019 was estimated based on the equations of the H-Q curve, which represents the relationship between discharge and water level. Monthly average discharge was computed using equations 4.4 and 4.5 and observed near the headwork along the right and left main canals (see Figure 4-18 and Figure 4-19).

In 2018, the average monthly maximum volume of irrigation water supply at the right main canal was approximately 57×10^6 $m^3.month^{-1}$ and decreased to 40×10^6 $m^3.month^{-1}$ in 2019 (see Figure 4-18), occurring in June and August respectively. At the left main canal, the average monthly maximum supply volume was around 5×10^6 $m^3.month^{-1}$ in June 2018, increasing to 17×10^6 $m^3.month^{-1}$ in August 2019 (see Figure 4-19). This opposite trend was due to flood damage to the left main canal during the study period. During the field survey, we observed significant damage to the primary canal resulting from substantial discharge during the wet season. Consequently, this impairment led to a disruption in the water supply to the sub-canals and continued to the rice fields.

The water supply volume decreased significantly from June 2018 to May 2019, reaching 0.2×10^6 $m^3.month^{-1}$. However, there was a sharp increase in the water supply on both the right and left main canals in 2019 from May to August, reaching 40×10^6 $m^3.month^{-1}$ and 18×10^6 $m^3.month^{-1}$, respectively. The highest irrigation water supply was observed in August, mainly due to excess diversion at the headwork into the canal system caused by rainfall. Conversely, the minimum water supply was observed in April and May, attributed to high monthly evaporation demand, low stream water, and less rainfall, which coincided with the beginning of rice farming. This indicates a temporal and spatial variation in seasonal irrigation water supply volume.

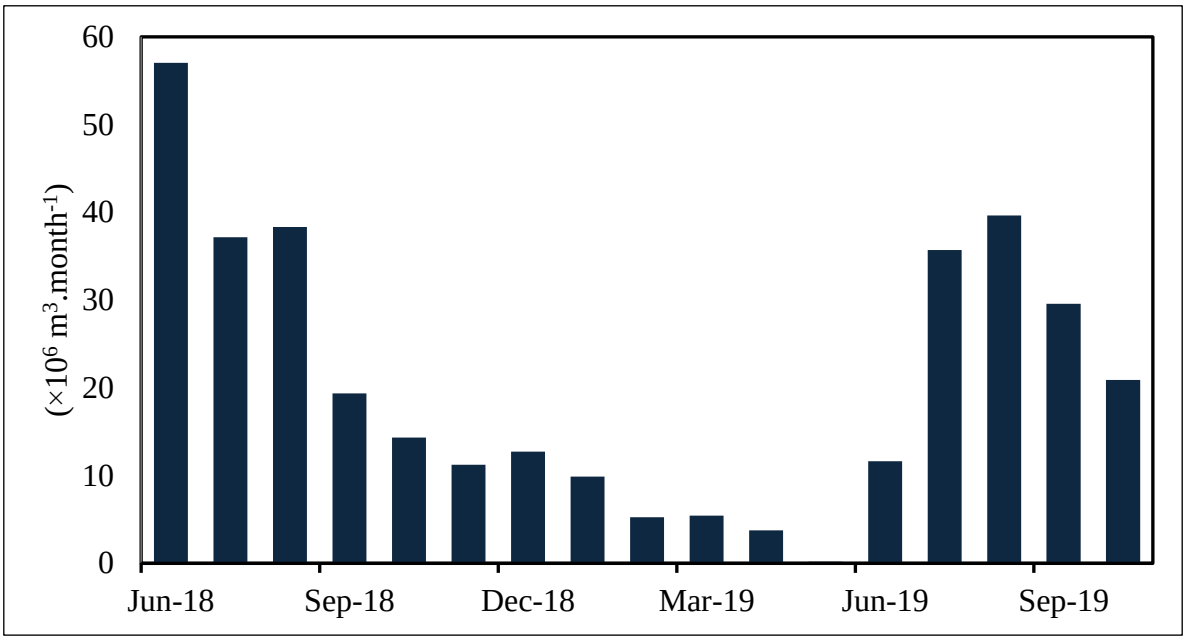

Figure 4-18 Actual volume of water supply at the right main canal

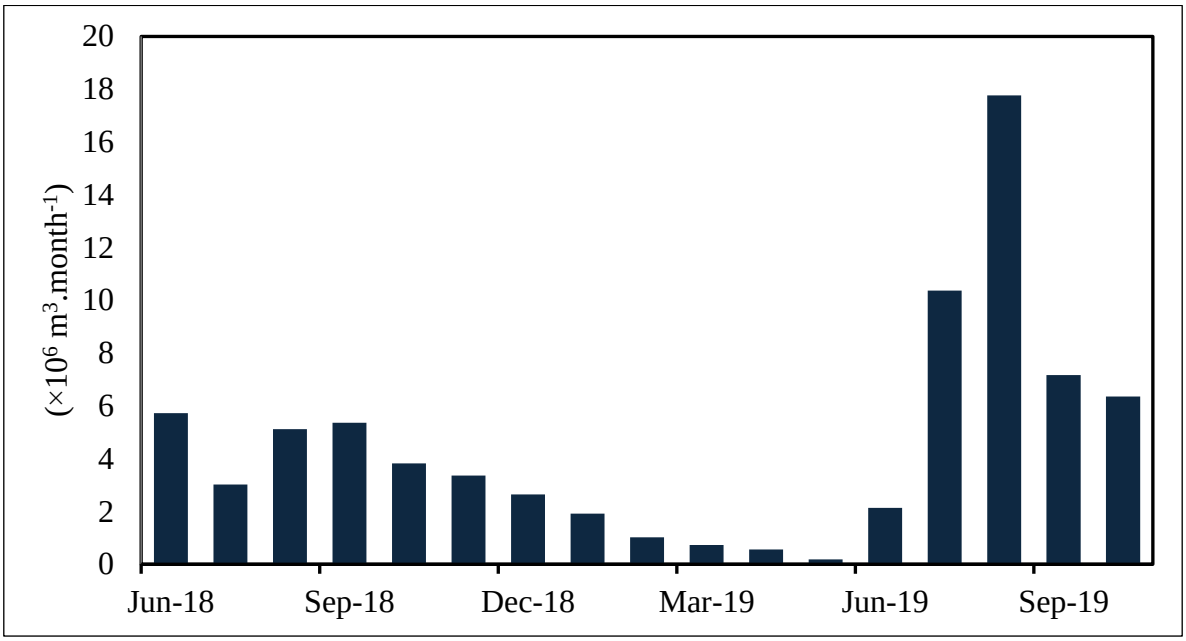

Figure 4-19 Actual volume of water supply at the left main canal

4.3.5 Analysis of balance between available stream water and IW demand

To evaluate the excess and deficiency of irrigation water from the Sangker River at the Kang Hot headwork point, Figure 4-20 shows the monthly averages of available stream water and IW demand at the headwork, and Figure 4-21 shows the observed deficit rate for the 5-year study period (2014–2018). The results show that the availability of stream water varies over a year and from 1 year to the next. Regarding the irrigation area and cropping patterns in the Kang Hot Project area during this study period, they were supposed that the IW demands did not change much. If the water shortage was less than 10–20% of the monthly requirement, the production losses are not very serious (Brouwer et al., 1992). The water balance calculation in Figure 4-21 indicates that water deficit always occurred during the April–May dry season every year from 2014 to 2017, with shortage rates of 50–99% of monthly requirements. In the dry year of 2015, the area faced five months of subsequent water scarcity (with deficiency rates of 30–99%). The stream water was surplus each year in the July–November wet season. In 2018, heavy rainfall increased the streamflow volume meaning that the stream water could meet the IW demand in a given area for the whole year.

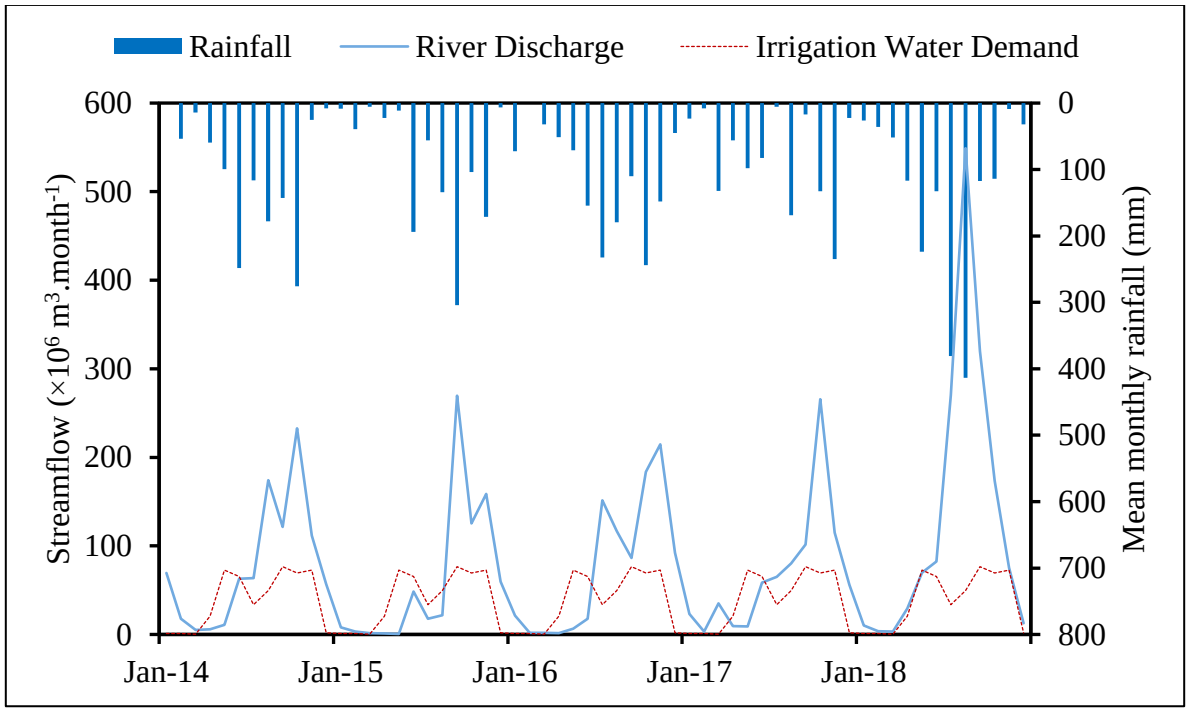

Figure 4-20 Balance of available stream water and IW demand at the Kang Hot headwork.

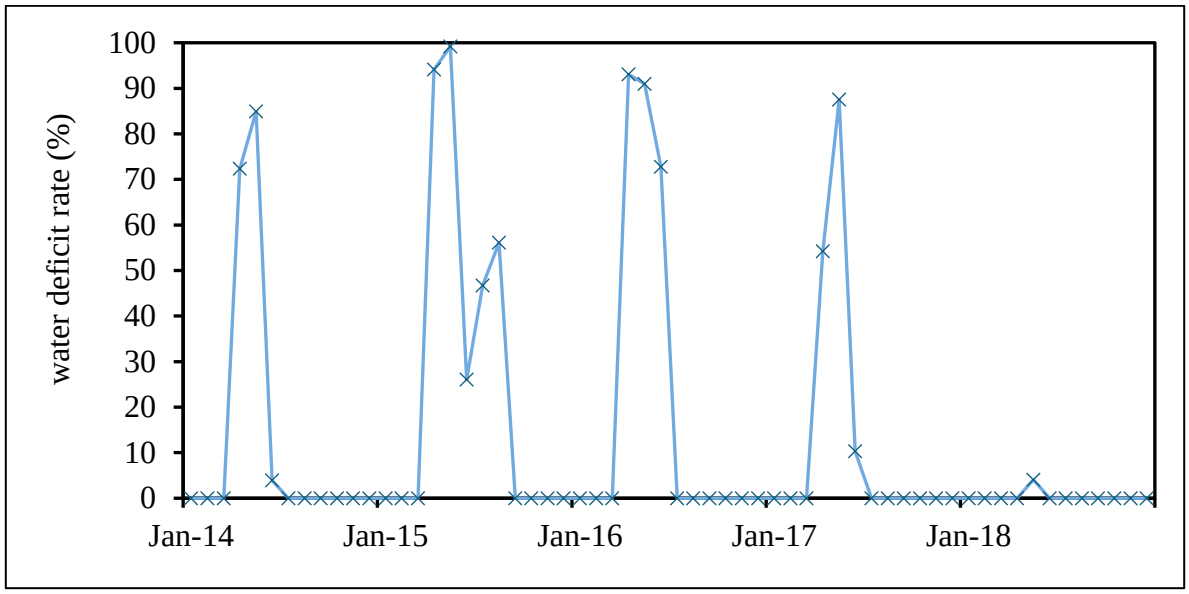

Figure 4-21 Monthly water deficit rate at Kang Hot headwork.

4.3.6 Evaluation of Actual Irrigation Water Use

The comparison between the actual volume of the canal discharge and the irrigation water demand is shown in Figure 4-22 and Figure 4-23 for the right and left main canals, respectively, as monthly averages from June 2018 to October 2019. Figure 4-24 shows the water shortage rate each month for both main canals.

The results for the actual water supply and demand balance for the right main canal (Figure 4-22) show a maximum supplied water volume of around 57 × 10^6 m^3.$month^{-1}$ in 2018, decreasing to 40 × 10^6 m^3.$month^{-1}$ in 2019. Meanwhile, the highest irrigation water demand was approximately 60 × 10^6 m^3.$month^{-1}$, corresponding to the extreme lack of water in 2019. As shown in Figure 4-24, large water shortages occurred in both 2018 (70–78% from September to November) and 2019 (over 77% from April to June). In those two years, the water supply was always less than the water demand in September and October, with the shortage rate exceeding 50%. However, the irrigation water demands every July and August during this study period were met. Overall, we conclude that the right main canal can supply around 59% of the required monthly irrigation water.

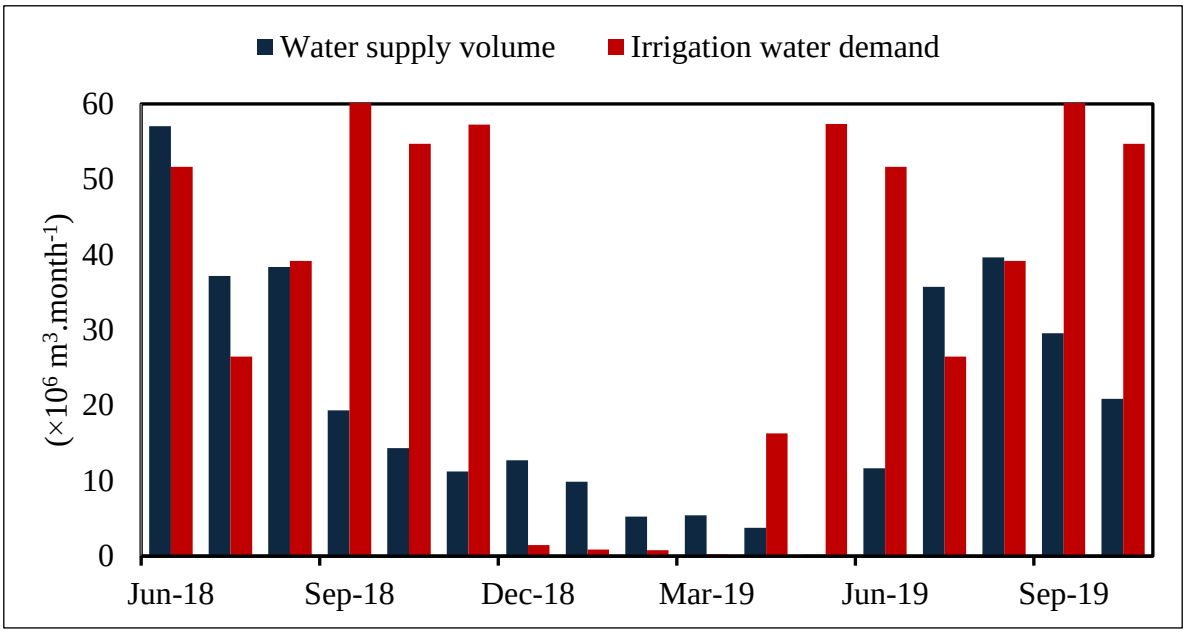

Figure 4-22 Actual irrigation water (IW) in the right main canal

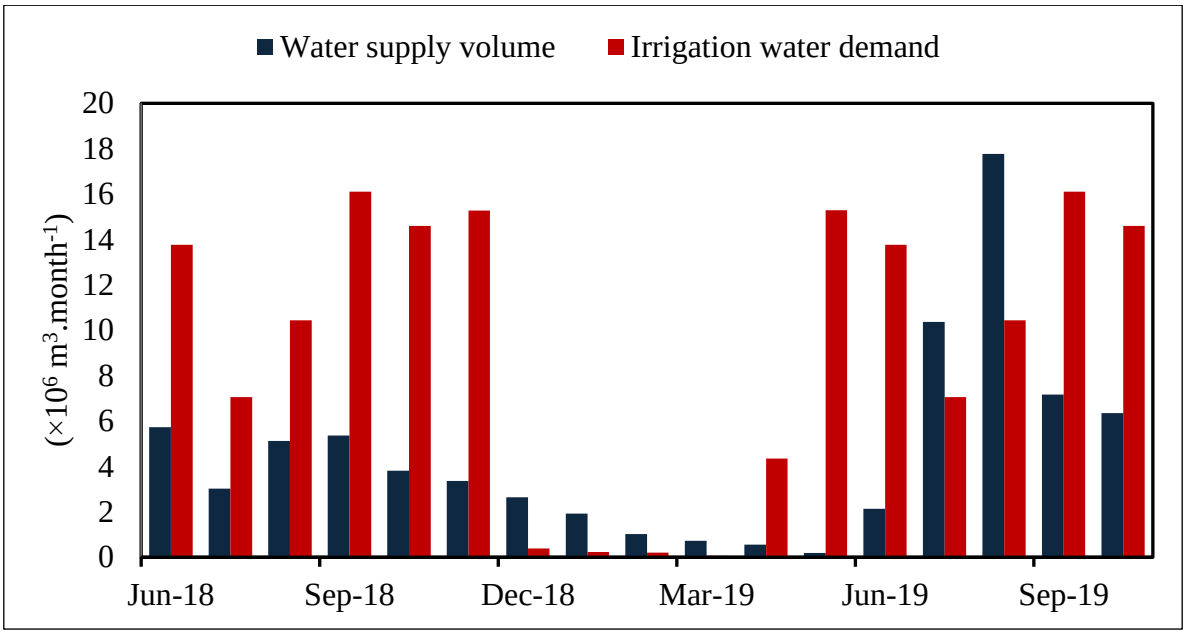

Figure 4-23 Actual irrigation water (IW) in the left main canal

Figure 4-23 shows that the maximum supplied water volume by the left main canal was around 5×10^6 $m^3.month^{-1}$ in 2018, increasing to 17×10^6 $m^3.month^{-1}$ in 2019. Meanwhile, the maximum water demand was around 16×10^6 $m^3.month^{-1}$. Similar to the right main

canal, water was also scarce in September and October for those two years, with shortage rates of 56–74% (Figure 4-24). Figure 4-24 also shows that water deficiency occurred between June and November, with 50–78% in 2018 and over 80% from April to June 2019. By 2018, the water supply in July and August was inadequate, with a shortage rate of around 51%. However, compared to that in 2019, it increased to 7×10^6 $m^3.month^{-1}$ and 12×10^6 $m^3.month^{-1}$, thereby meeting the water demands of those two months. The water volume of the left main canal can supply only 48% of the requirement.

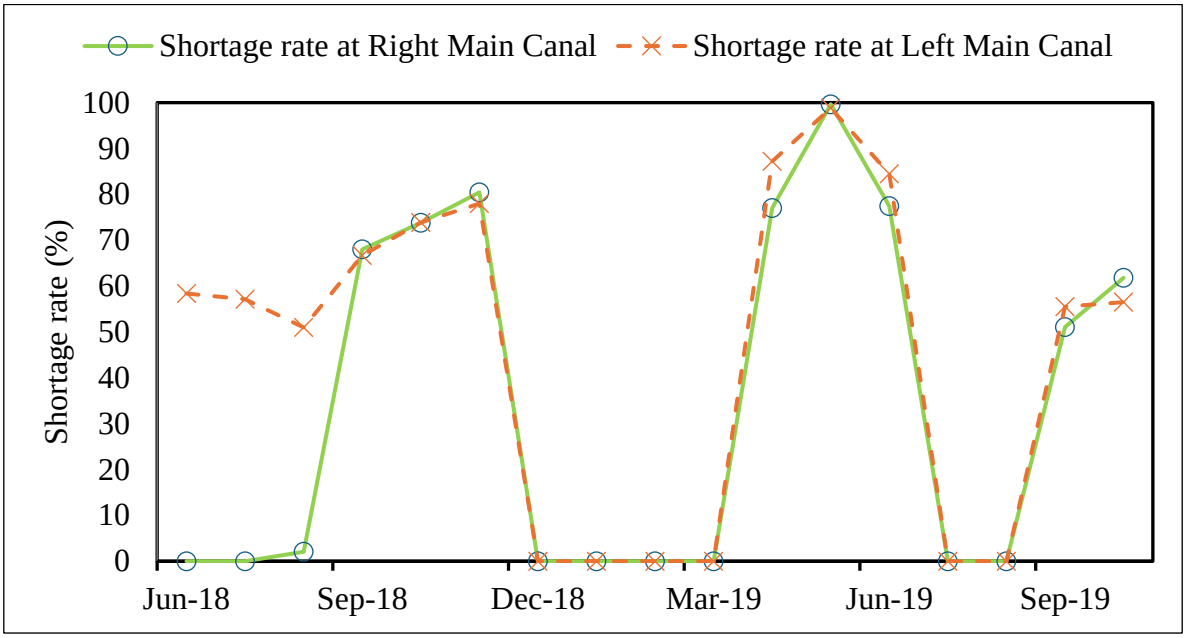

Figure 4-24 Water shortage rate in the right and left main canals

4.3.7 Cropping pattern (CP)

In the irrigation project area, the predominant cropping patterns were direct sowing-early wet season (CP-C), transplanting-wet season rice (CP-B), and direct sowing-wet season rice (CP-E). An analysis was conducted to address water deficiency by adjusting the existing cropping pattern in line with available irrigation water. CP-C, covering 40% of the irrigation area (21,280 ha) and cultivated from April to late July, was found to face water shortage issues during this period based on water balance analysis. Furthermore, the irrigation water requirement results indicated higher water consumption for CP-C compared to CP-B. CP-E also required a significant amount of water for growth. The distribution of

rice cultivation methods in their fields was adjusted. The proportion of direct sowing-early-wet-season rice decreased from 40% to 10%, while the proportion of transplanting-wet-season rice was raised from 60% to 80%. Additionally, the proportion of direct sowing-wet-season rice increased from 10% to 20% of their total cultivated area (see Figure 4-25). The results of this analysis show that the water shortage rate was reduced from 20 to 100% between April and May (2014–2017), which is at the beginning of the irrigation season (Figure 4-26).

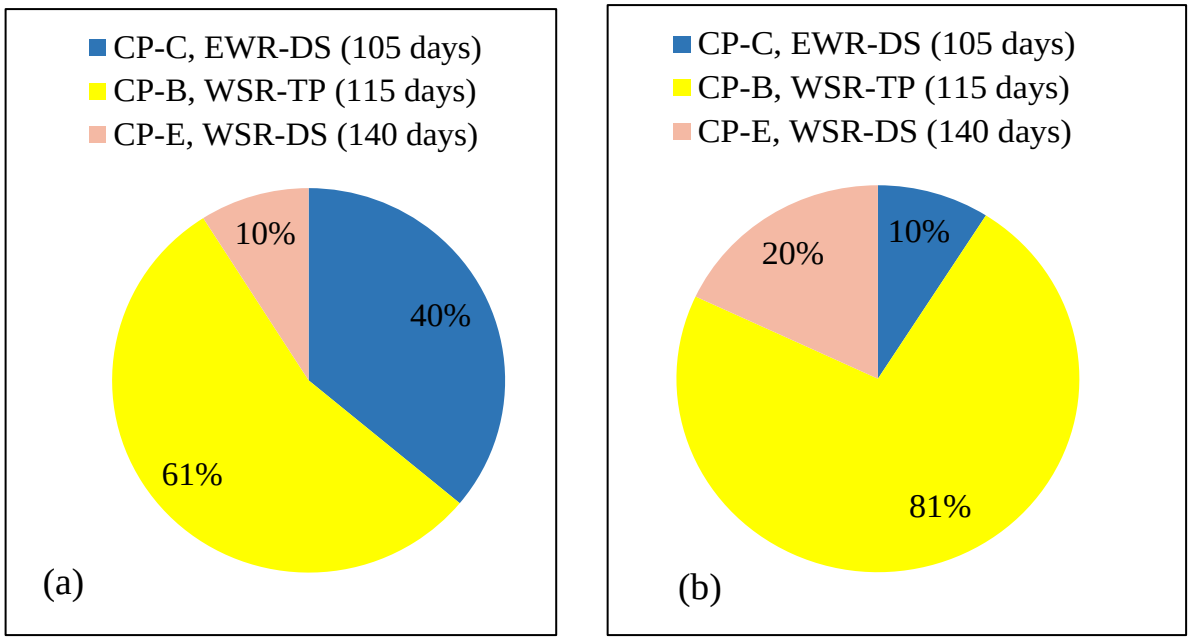

Figure 4-25 Adjustment of rice cropping patterns in percentage of physical area: current cropping patterns (a), and adjusted cropping patterns (b).

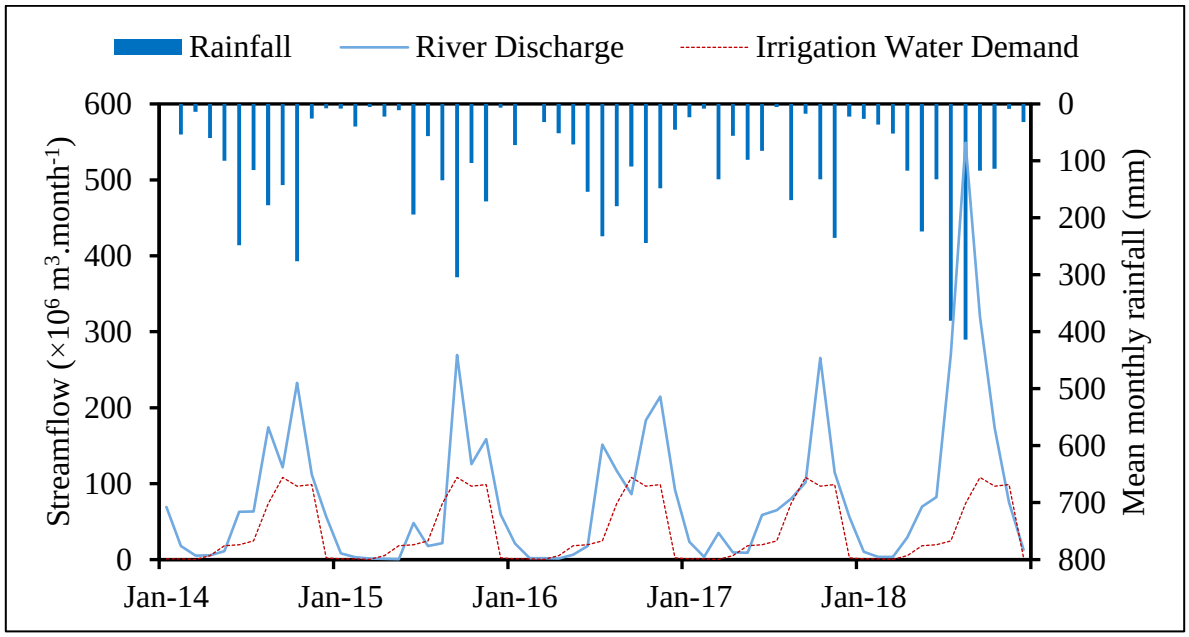

Figure 4-26 Water balance at Kang Hot headwork after cropping patterns change.

4.4 Conclusion

The results of this study show that SWAT performed well in predicting the streamflow by providing good agreement between the observed and simulated monthly flow, which is based on the statistics of NSE = 0.58/RSR=0.64 and NSE = 0.69/RSR=0.55 in the calibration and validation periods, respectively. With such good performance, SWAT can be used to estimate the river discharge at the Kang Hot headwork point as needed.

The balance between the available volume of stream water and the irrigation water demand at the Kang Hot headwork indicates that the water shortage rate was 50–99% of the monthly requirement, which occurred mainly from April to June between 2014 and 2017, and the excess water was in August–November. This excess water should be retained for utilization in the dry months. Fortunately, in 2018 the river flow was abundant due to heavy rainfall. Revising the current cropping-pattern calendar, the water deficits could be diminished from 20 to 100% of the monthly shortage rate in those shortfall months.

The actual IW use during the study period was 52% and 41%, respectively, and there was a lack of water in the left and right main canals. Also, water deficits occurred in September and October in 2018 and 2019.

The results of this study will be useful for policymakers and field technicians in irrigation planning, developing and managing the water resources in the river basin, and ensuring the sustainability of agricultural development.

4.5 Recommendation

The findings of this chapter indicate that nearly half of the irrigation project areas are experiencing water shortages, which may lead to significant challenges for water users in the community. To address this issue, the following optimal approaches are recommended:

- Introduce new paddy rice varieties that are resilient to climate change, require less water, and have shorter growth cycles. Additionally, transitioning from traditional long-duration rice varieties to medium-duration ones would be beneficial.

- It is essential to consult with the hydrologist to obtain information on available water resources in the river. This information can be utilized for future irrigation planning and consideration.

- Implement an effective water distribution plan for the irrigation system and introduce water-saving techniques.

- Considering the importance of groundwater as an alternative water source, farmers can pump groundwater for irrigation when canal water is not available.

- Enhance the functionality of the Farmer Water User Community (FWUC) by recruiting additional staff and providing them with the necessary training to ensure the efficient operation of such a large-scale irrigation system.

References

Abbaspour, K. C., Rouholahnejad, E., Vaghefi, S. R. I. N. I. V. A. S. A. N. B., Srinivasan, R., Yang, H., & Kløve, B. (2015). A continental-scale hydrology and water quality model for Europe: Calibration and uncertainty of a high-resolution large-scale SWAT model. Journal of hydrology, 524, 733-752.

Arnold, J. G., Srinivasan, R., Muttiah, R. S., & Williams, J. R. (1998). Large area hydrologic modeling and assessment part I: model development 1. JAWRA Journal of the American Water Resources Association, 34(1), 73-89.

Abbaspour, K. C., Yang, J., Maximov, I., Siber, R., Bogner, K., Mieleitner, J., ... & Srinivasan, R. (2007). Modelling hydrology and water quality in the pre-alpine/alpine Thur watershed using SWAT. Journal of hydrology, 333(2-4), 413-430.

Abbaspour, K. C., Rouholahnejad, E., Vaghefi, S. R. I. N. I. V. A. S. A. N. B., Srinivasan, R., Yang, H., & Kløve, B. (2015). A continental-scale hydrology and water quality model for Europe: Calibration and uncertainty of a high-resolution large-scale SWAT model. Journal of hydrology, 524, 733-752.

Abbaspour, K. C. (2015). SWAT calibration and uncertainty programs—a user manual. Swiss Federal Institute of Aquatic Science and Technology: Eawag, Switzerland.

Abbaspour, K.C. (2011). Swat-Cup2: SWAT Calibration and Uncertainty Programs Manual Version 2, Department of Systems Analysis, Integrated Assessment and Modeling (SIAM), Eawag. Swiss Federal Institute of Aquatic Science and Technology, Duebendorf, Switzerland. 106 p.

Arnold, J. G., Moriasi, D. N., Gassman, P. W., Abbaspour, K. C., White, M. J., Srinivasan, R., ... & Jha, M. K. (2012). SWAT: Model use, calibration, and validation. Transactions of the ASABE, 55(4), 1491-1508.

Allen, R., Pereira, L., Raes, D., and Smith, M. (1998). Guidelines for computing crop water requirements. Irrigation and Drainage Paper. 56, 300.

Bormann, H., Diekkrüger, B., Renschler, C., & Richter, O. (1999). Regionalization scheme for the simulation of regional water balances using a physically based model system. Physics and Chemistry of the Earth, Part B: Hydrology, Oceans and Atmosphere, 24(1-2), 43-48.

Bouman, B. A. M., Wopereis, M. C. S., Kropff, M. J., Ten Berge, H. F. M., & Tuong, T. P. (1994). Water use efficiency of flooded rice fields II. Percolation and seepage losses. Agricultural Water Management, 26(4), 291-304.

Brouwer, C., Hoevenaars, J. P. M., Van Bosch, B. E., Hatcho, N., & Heibloem, M. (1992). Irrigation Water Management: Training Manual No. 6: Scheme Irrigation Water Needs and Supply.

Beven, K. J. (2012). Rainfall-runoff modelling: the primer. John Wiley & Sons.

Bos, M. G. and Wolters, W. (1990). Water charges and irrigation efficiencies. Irrigation and drainage systems, 4, 267-278.

Chow, V.T., Maidment, D.R., Mays, L.W. (1988). Applied Hydrology. McGraw-Hill, New York.

Dastane, N. G. (1974). Effective rainfall in irrigated agriculture.

Gassman, P. W., Reyes, M. R., Green, C. H., & Arnold, J. G. (2007). The soil and water assessment tool: historical development, applications, and future research directions. Transactions of the ASABE, 50(4), 1211-1250.

Green, W. H. and G. A. Ampt. (1911). Studies on physics, 1. The flow of air and water through soils. Journal of Agricultural Sciences 4:11-24.

Hargreaves, G. H. (1975). Moisture availability and crop production. Transactions of the ASAE, 18(5), 980-0984.

JI, X. B., KANG, E. S., CHEN, R. S., ZHAO, W. Z., XIAO, S. C., & JIN, B. W. (2006). Analysis of water resources supply and demand and security of water resources

development in irrigation regions of the middle reaches of the Heihe River Basin, Northwest China. Agricultural Sciences in China, 5(2), 130-140.

Kodoma, M. 2015. Manual on discharge measurement by current meter and floats. Phnom Penh. Ministry of Water Resources and Meteorology, Cambodia. (Unpublished).

MASONA, E., SHIMIZU, K., & YOSHIOKA, Y. (2018). An Evaluation of Water Demand and Supply for a Small-scale Irrigation Scheme in Zimbabwe. International Journal of Environmental and Rural Development, 9(2), 41-46.

Moriasi, D. N. Arnold, J. G. Van Liew, M. W. Binger, R. L. Harmel, R. D. Veith, T. L. (2007). Model evaluation guidelines for systematic quantification of accuracy in watershed simulations. Transactions of the ASABE, 50(3), 885-900

Neitsch, S. L., Arnold, J. G., Kiniry, J. R., & Williams, J. R. (2011). Soil and water assessment tool theoretical documentation version 2009. Texas Water Resources Institute.

Ritchie, J. T. (1972). Model for predicting evaporation from a row crop with incomplete cover. Water resources research, 8(5), 1204-1213.

Shakir, A. S., Khan, N. M., & Qureshi, M. M. (2010). Canal water management: Case study of upper Chenab Canal in Pakistan. Irrigation and Drainage: The journal of the International Commission on Irrigation and Drainage, 59(1), 76-91.

TSC & JICA. (2014). Background of the project for river basin water resources utilization. Phnom Penh: Ministry of Water Resources and Meteorology. (Unpublished)

USAID. (2019). CAMBODIA: Agriculture and Food Security. Retrieved from http://www.usaid.gov/cambodia/agriculture-and-food-security.

Ullah, E I., Khan, H., Khan, S.A. (1998). An assessment of the crop water demand and irrigation water supply at Pabbi minor of warsak gravity canal. Abbottabad, Pakistan.

CHAPTER 5 Prediction of future land use changes.

5.1 Introduction

Land use/land cover has been considered the main factor in changing the hydrological cycle since it directly influences evapotranspiration and soil moisture contents (Gupta et al., 2015). In this regard, significant land use changes in Battambang Province (Cambodia) have been recently reported. For example, previous research (Sourn et al., 2021) found a considerable increase in agricultural land, with a dramatic decrease in forest cover between 1998 and 2018. These changes were driven by population growth, economic growth, landmine clearance projects, and social and economic land concessions (SLCs and ELCs, respectively). Based on the Cambodia Land Law of 2001 (Open Development Cambodia), the term SLC refers to the social purpose of allowing beneficiaries to build residential constructions and/or cultivate land belonging to the state for their subsistence. As for the term ELC, it refers to the economic purpose of allowing beneficiaries to clear the land for industrial and agricultural exploitation.

Understanding land use change has become an increasing matter of interest and concern among landscape planners and environmentalists because it influences the global environment (Subedi et al., 2013). In fact, land use/land cover mapping derived from remotely sensed data has long been an area of focus for many researchers (Civco et al., 2002; Araya and Cabral, 2010). Meanwhile, recent advancements in geographic information systems (GIS) and remote sensing tools/methods have enabled researchers to effectively model land use change (Araya and Cabral, 2010).

In general, modeling land use dynamics is a complex process (Subedi et al., 2013), due to factors such as natural settings, society, economics, culture, politics, and legal aspects (Lambin, 1997). Various models for land use simulation and prediction have been used in GIS such as statistic, dynamic, and machine learning modeling (Aburas et al., 2019). Based on historical spatio-temporal data, the cellular automata (CA)-Markov module in IDIRISI software was first used in this study to simulate and predict future land use change, due to its widespread use by scholars to understand landscape change at the global level (Wang et al., 2021). It was also used to analyze the related effects and natural resource

management strategies (Brown et al., 2000). However, this model did not consider land use policies and socio-economic factors (Subedi et al., 2013).

No previous study has attempted to simulate and predict the future change of landscape in this study area. Therefore, the present study in Chapter 5 aims to detect land use and land cover change and examine the SLCs, ELCs, and potential areas for forest communities according to the local government's 2030 master plan (Open Development Cambodia). The primary objective is to integrate the CA-Markov model and GIS-based spatial analyst tools to enhance the predictive land-use change map.

5.2 Materials and Methods

5.2.1 Study area

The study focused on the upper Sangker River basin, situated in Battambang Province (the largest agricultural area in Cambodia), with a total drainage area of 3,062 km^2 (Figure 3-1). The elevation ranges from 13 to 1,400 meters above sea level. Based on Mekong River Commission (MRC) land use data in 2010, 53.13% of land use within this basin was covered by forest, followed by agriculture at 44.41%, built-up land at 2.03%, and water bodies at 0.44%. More than one million people live in this province, with an annual population growth rate of 2.28% (Hagenlocher et al., 2016). Meanwhile, human activities have been affected in this watershed by landmine clearance, explosive remnants of war projects, and land concessions (Sourn et al., 2021). See Chapter 3, Sections 3.1 and 3.3 for more details.

5.2.2 Image classification

Image classification is the process of assigning pixels or the basic units of an image to classes (Perumal and Bhaskaran, 2010). Remote sensing in collaboration with geographic information systems (GIS) has been widely used for land use classification (Castelluccio et al., 2015; Moody and Mathur, 2004) and land development (Yeh and Li, 1999). Considering the subtle different categories for classifying imagery, two common

approaches such as unsupervised classification and supervised classification technique are presented.

5.2.2.1 Field survey

Field surveys were conducted to better understand the different types of land cover in the catchment area. Due to various field conditions, not all locations could be surveyed. Approximately 150 ground reference points were collected during the field surveys to verify the image with land use or land cover type.

Based on the land use features from the Mekong River Commission (MRC) for the year 2010, the land use and land cover inside the catchment area were classified into eight categories: evergreen forest, deciduous forest, shrublands, burned areas, farmlands, paddy rice, urban areas, and water bodies. The characteristics of each land cover type in the upper Sangker catchment were described using the land cover information catalog of the Lower Mekong Basin (Kityuttachai et al., 2016). The descriptions are as follows:

1. Evergreen Forest: Dominated by broadleaved, evergreen tree species.

2. Deciduous Forest: Characteristic of areas in the tropics affected by periodic drought, resulting in a largely deciduous forest canopy.

3. Shrublands: Characterized by vegetation-dominated shrubs and bushes.

4. Burned Area: Characterized by deposits of charcoal and ash, removal of vegetation, and alteration of vegetation structures due to slash-and-burn agriculture.

5. Annual Crops: A broad variety of crops grown yearly, with different growth cycles and the possibility of crop rotation.

6. Paddy Rice: Mainly rainfed and irrigated rice fields with three main growth stages: vegetative, and reproductive ripening phases.

7. Urban Area: Characterized by high or low human population density and vast artificial structures, with highly sealed surfaces (e.g., buildings, houses).

8. Water Body: Any significant accumulation of surface water, including lakes, rivers, streams, reservoirs, and canals.

5.2.2.2 Satellite imagery and input data

Image classification for land use and land cover (LULC) change detection in the upper Sangker was analyzed using satellite imagery. Freely available Landsat 8 (Path 127–128, Row 51) images in 2014, 2018, and 2022 for the study area were acquired from the U.S. Geological Survey (https://earthexplorer.usgs.gov/). This freely available data has a ground resolution of 30 meters. Landsat imageries were downloaded for dry season selection because of a clear sky period in which the lowest and no cloud cover existed. The Landsat images were mosaicked and composited using Bands 1–7 and projected to Universal Transverse Mercator (UTM), with a datum of the World Geodetic System 84 (WGS84) in Cambodia zone 48N using ArcGIS.

5.2.2.3 Image Classification Technique

In this research, supervised classification was utilized due to the availability of data in the study area and our prior knowledge of it. The Maximum Likelihood algorithm was employed for this purpose. Maximum likelihood classification is a widely used supervised classification technique with satellite image data and was the first rigorous algorithm to be widely adopted (Otukei and Blaschke, 2010; Ahmand and Quegan, 2012; Taati et al., 2015). As per Eastman (2012), the supervised classification technique involves the following phases:

- Creating a "training site" that represents the location of each identifiable cover type in the image.

- Digitizing polygons around each training site and assigning a unique identifier to each cover type.

- Analyzing the pixels within the training sites and creating spectral signatures for each cover type.

- Classifying the entire image by examining each pixel individually and comparing its signature with each of the known signatures.

Given our prior knowledge of the Sangker River basin, the images were subjected to hard supervised classification using the popular maximum likelihood algorithm based on signature files (Rawat and Kumar, 2015). A signature was created by using the on-screen digitizing feature to generate 5–12 vector files of the training site for each class according to the user's knowledge. Based on the MRC land use in 2010 and satellite imagery, land cover was identified, while land use was aggregated into five main classes: forest cover, farmlands, paddy fields, water bodies, and built-up areas.

5.2.2.4 Statistical Performance Evaluation

Accuracy assessment is an integral part of any classification process. The most common way to assess the accuracy of a classified map is to create a set of random points from the ground truth data and compare that to the classified data in a confusion matrix. The confusion matrix provides the basis for both describing classification accuracy and characterizing errors, which may help refine the classification or estimates derived from it (Foody, 2002).

1). Confusion matrix: involves producer accuracy, user accuracy, and overall accuracy (Jog and Dixit, 2016) and those defined as following:

- Producer accuracy: Any classification scheme can be checked for accuracy using producer accuracy. It represents the percentage of a correctly classified ground class.

$$\text{Users Accuracy} = \frac{\text{Number of Correctly Classified Pixels in each Category}}{\text{Total number of Classified Pixels in that Category (The Row Total)}} \times 100 \qquad (5.1)$$

- User Accuracy: The performance of accuracy of classification results is represented by user accuracy.

$$\text{Producer Accuracy} = \frac{\text{Number of Correctly Classified Pixels in each Category}}{\text{Total number of Reference Pixels in that Category (The Column Total)}} \times 100 \qquad (5.2)$$

- Overall accuracy: a measure of the overall behavior of the classifier is given by overall accuracy. It combines user and producer accuracy for a complete image. Overall accuracy represents the total percentage of correctly classified pixels.

$$\text{Overall Accuracy} = \frac{\text{Total Number of Correctly Classified Pixels (Diagonal)}}{\text{Total Number of References Pixels}} \times 100 \qquad (5.3)$$

2). Kappa statistics: Represented by the Kappa coefficient is measured of agreement or classified image accuracy, which ranges from zero to one. The statistical value confirms that classifier performance is good. Kappa coefficients can be defined as the equation below:

$$\text{Kappa Coefficient(T)} = \frac{(\text{TS}\times\text{TCS}) - \sum(\text{Column Total}\times\text{Row Total})}{\text{TS}^2 - \sum(\text{Column Total}\times\text{Row Total})} \times 100 \qquad (5.4)$$

where TS represents the total sample and TCS represents the total corrected sample.

In this study, stratified randoms of more than 500 points were created for each image using the Create Accuracy Assessment Points tool in ArcGIS. They were then manually checked and compared using existing land use, the Google Earth Engine, and field survey information as reference data.

5.2.3 Projection of land use change

Predicting the future LULC changes is crucial for hydrologists, environmentalists, and water policymakers to make appropriate decision policies for future development and sustainability (Sankarrao et al., 2021).

5.2.3.1 Input data and processes

To better understand of land use change analysis, land use was simply aggregated into five major classes: forest cover, farmlands, paddy fields, water bodies, and built-up areas (Table 5-1). Reclassified 2014, 2018, and 2022 images were imported as raster datasets. The datasets were converted to ASCII using geographic information system (GIS), then imported into IDIRISI software for land use simulation and prediction. First, land use simulations for 2022 and 2030 were performed with the CA-Markov model (Eastman, 2012) by inputting suitability maps, transition areas, and a transition probability matrix, all computed from the Markov chain analysis of the 2014 and 2018 images. Second, the 2018 image was set as the base map. Third, the VALIDATE module was used to assess the model's validity, which was confirmed by the statistical Kappa Index of Agreement (KIA).

Fourth, the predicted land use in 2030 was generated using the projected transition probability matrix derived from simple powering of the base matrix (Takada et al., 2010). Finally, according to the presence of a future land use policy, another land use map was created by overlaying the development areas onto the predicted land use map in 2030.

Table 5-1 Description of the simplified LULC classification

No	Simplified LULC classes	Description
1	Forest cover	Forest and natural area
2	Farmlands	Agricultural area not included in paddy fields
3	Built-up area	Residential/commercial/industrial/public facilities
4	Paddy fields	Paddy rice fields
5	Water bodies	River, reservoir, lake, and small stream

5.2.3.2 Suitability images

The concept of predictive land use suitability pertains to the suitability of a specific area for a particular land use (Eastman and Toledano, 2018). Typically, suitability images are created using multi-criteria evaluation, a widely used method for assessing and combining various "constraint and factor" criteria. Constraints are typically depicted as a Boolean image (0&1), while factors determine the degree of suitability for all geographical areas. In this analysis, water bodies and residential areas were supposed as the constraints to the development of farmland, forest cover, and paddy fields. Whereas, the built-up land was considered to be constrained by water bodies. In this research, the factors were developed empirically by analyzing the underlying dynamics of land use change between 2014 and 2018. Furthermore, multiple factors, such as proximity to roads, water bodies, canals, and existing land use, were generated and standardized on a continuous scale from 0 (least suitable) to 255 (most suitable) using a fuzzy module. The factors for each land use category were then combined using pairwise comparison in conjunction with the analytical hierarchy process (AHP) method within the weighted linear combination (WLC). In the AHP structure, the weight of each level amounts to 1 where such weights are the procedure of a pairwise comparison matrix developed by Saaty (1997) in the context of a decision-making process. In this process, each factor is rated for its importance relative to every other factor using a 9-point reciprocal scale (i.e. if 7 represents substantially more

important, 1/7 would indicate substantially less important) (see Table 5-2). The criterion factor weight for the land use classes in the study area, such as forest cover, farmlands, built-up land, and paddy fields are presented in Table 5-3, Table 5-4,

Table 5-5, and Table 5-6, respectively.

Table 5-2 The 9-point rating scale for weight determination.

1/9	1/7	1/5	1/3	1	3	5	7	9
extremely	very	strongly	moderately	equally	moderately	strongly	very	extremely

With WLC, factors are combined by applying a weight to each followed by a summation of the results to yield a suitability map defined as in equation 5.5 (Eastman, 2012).

$$S = \sum w_i x_i \tag{5.5}$$

where S = suitability, w_i= weight to factor i, x_i= criterion score to factor i.

For further details on the Markov and CA-Markov models, please refer to the following references (Subedi et al., 2013; Wang et al., 2021; Eastman, 2012; Hamad et al., 2018). The suitability and factor images utilized as input in the CA-Markov change prediction model are illustrated in Figure 5-1.

Table 5-3 The pairwise comparison procedure for the derivation of factor weights for forest cover.

	Existing forest cover	Proximity to road	DEM	Slop gradient
Existing forest cover	1			
Proximity to road	1/5	1		
DEM	1/7	2	1	
Slop gradient	1/9	1	1/2	1

Factor	Derived weight
Forest cover	0.6900
Proximity to road	0.0921
DEM	0.1409
Slop gradient	0.0771

Table 5-4 The pairwise comparison procedure for the derivation of factor weights for farmlands.

	Proximity to road	Existing farmland	Proximity to water	Slop gradient
Proximity to road	1			
Existing farmland	9	1		
Proximity to water	2	1/9	1	
Slop gradient	2	1/7	2	1
Factor	Derived weight			
Proximity to road	0.0610			
Farmland	0.7233			
Proximity to water	0.0865			
Slop gradient	0.1291			

Table 5-5 The pairwise comparison procedure for the derivation of factor weights for the built-up land.

	Residential area	Proximity to road	Slop gradient
Residential area	1		
Proximity to road	1/7	1	
Slop gradient	1/9	1/3	1
Factor	Derived weight		
Residential area	0.7854		
Proximity to road	0.1488		
Slop gradient	0.0658		

Table 5-6 The pairwise comparison procedure for the derivation of factor weights for paddy fields.

	Existing rice field	Proximity to canal	DEM	Slop gradient
Existing rice field	1			
Proximity to canal	1/3	1		
DEM	1/5	1/2	1	
Slop gradient	1/3	1/3	1/2	1
Factor	Derived weight			
Existing rice field	0.5290			
Proximity to canal	0.2355			
DEM	0.1341			
Slop gradient	0.1013			

5.2.3.3 Markov chain analysis

The Markov model is a convenient tool for simulating land use/land cover change when variations in the landscape are difficult to describe (Kumar et al., 2014). Specifically, it depicts land use/land cover change from one period to another and uses it to predict future changes. Markov chain analyzes a pair of land cover images and outputs a transition probability matrix and a transition areas matrix are presented in text files. The transition probability matrix records the probability that each land cover category will change to every other category. The transition area matrix records the number of pixels expected to change from each land cover type to each other over the specified number of time units.

The expression of Markov chain analysis is represented as: $\mathrm{S}(\mathrm{t}+1) = P_{ij} \times \mathrm{S}(\mathrm{t})$

Where, *S(t)* is the system status at the time of *t*, *S(t+1)* stands for the system status at the time of *t+1* (Wang et al., 2021, Tadese et al., 2021). Converting one state into another state of a system is called state transition. If *P* is transition probability, namely the probability of converting the current state to another state next time (Kumar et al., 2014), and can be defined as the expression below:

$$P = P_{ij} = \begin{bmatrix} P_{11} & P_{12} & \cdots & P_{1m} \\ P_{21} & P_{22} & \ldots & P_{2m} \\ \vdots & \vdots & \ddots & \vdots \\ \vdots & \vdots & \ddots & \vdots \\ P_{m1} & P_{m2} & \cdots & P_{mm} \end{bmatrix} \tag{5.6}$$

where *P* represents the probability from state *i* to state *j*.

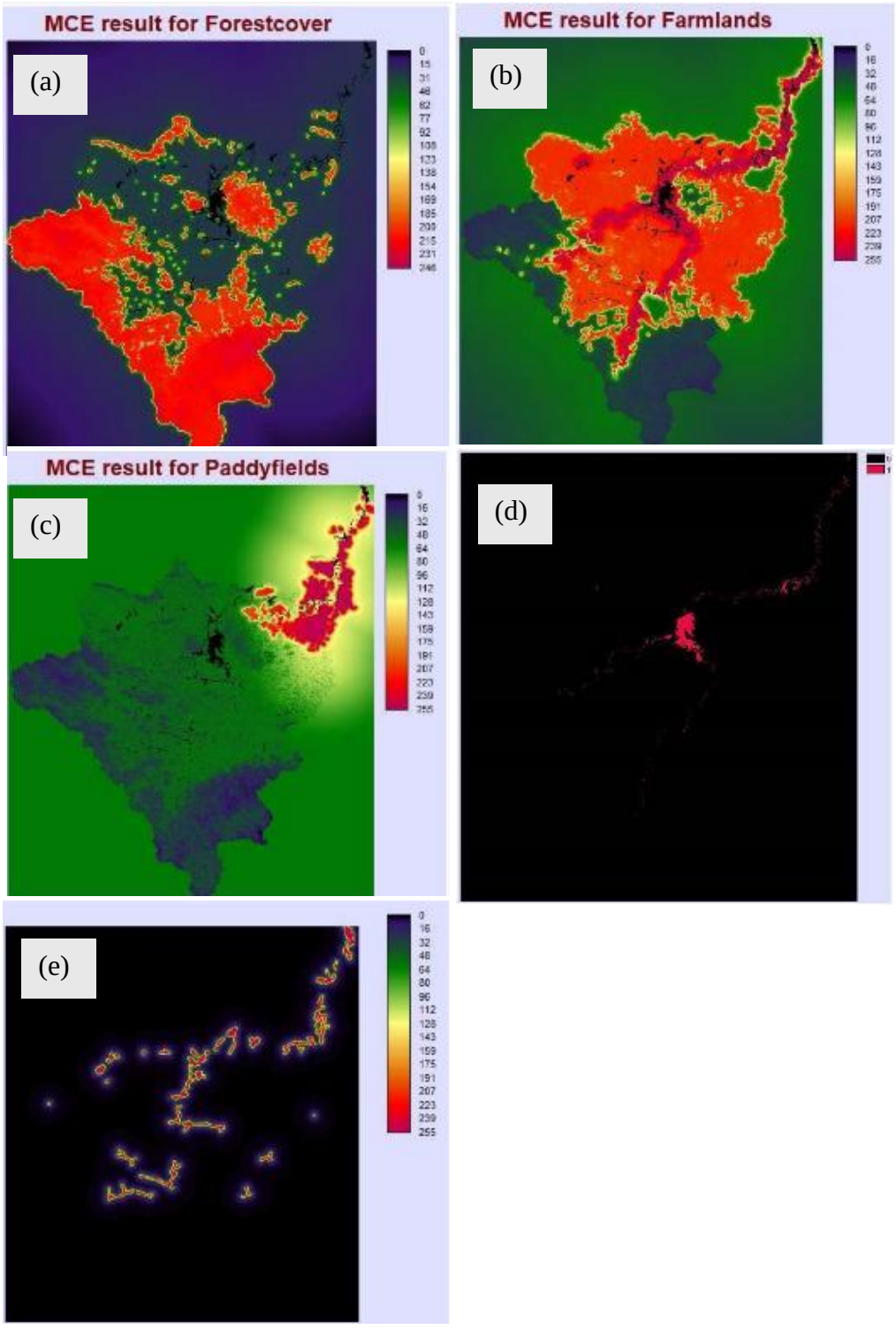

Figure 5-1 The suitability images for the upper Sangker River basin: forest cover (a) , farmlands (b), paddy fields (c), water bodies (d), and built-up land (e).

The development of a transition probability matrix of land use change from time one to time two presents the nature of changes. It is still serving as the basis for projecting to a later period (Takada et al., 2010). Table 5-7 is the transition probability matrix which presents the probability of conversions of land use from one class to another for the 2014–2018 study period. Table 5-8 is the transition area matrix representing the areal extent of change within each land use class from 2014 to 2018.

Table 5-7 Transition probabilities matrix for years 2014 to 2018

Land use classes	Forest cover	Farmlands	Built-up land	Paddy fields	Water bodies
Forest cover	0.7435	0.2510	0.0005	0.0005	0.0045
Farmlands	0.1557	0.7503	0.0162	0.0549	0.0229
Built-up land	0.0014	0.2035	0.7666	0.0251	0.0034
Paddy fields	0.0225	0.2921	0.0003	0.6851	0.0000
Water bodies	0.0710	0.1909	0.0140	0.0019	0.7222

Table 5-8 Transition area matrix for years 2014 to 2018

Land use classes	Forest cover	Farmlands	Built-up land	Paddy fields	Water bodies
Forest cover	983,902	332,170	635	720	5,912
Farmlands	281,587	1,357,053	29,344	99,221	41,385
Built-up land	55	7,800	29,378	961	130
Paddy fields	4,454	57,876	57	135,727	0
Water bodies	2,322	6,245	459	61	23,621

5.2.3.4 CA-Markov model

The CA-Markov model, as described by Eastman and Toledano in 2018, integrates cellular automata-Markov chain and multi-criteria/objective procedures for predicting land use/land cover. This model governs the temporal dynamics of different land covers through transition probability using the Markov chain. Space dynamics is controlled through local principles using the CA mechanism and according to the state of the vicinity and the transition probability of each land use (Azizi et al., 2016). The CA-Markov model allocates land based on the suitability of the land for end covers (along with a cellular automaton rule) to promote spatial contiguity (Eastman and Toledano, 2018). In addition, by using the Markov chain analysis outputs, especially the transition area file, the CA-Markov model

applies a contiguity filter to grow land use from one time to a later time. A contiguity filter of a kernel size of 5*5 pixels was applied based on suitability images to define neighborhoods of each cell of land use class. In this study, the filter used for analysis was:

0	0	1	0	0
0	1	1	1	0
1	1	1	1	1
0	1	1	1	0
0	0	1	0	0

The filter is integral to the action of the CA component to downweight the suitability of pixels that are distant from existing instances of the land cover type under consideration (Surabuddin Mondal et al., 2013; Kumar et al., 2016).

5.2.3.5 Evaluation of model performance

An important stage in the development of any predictive change model is validation. VALIDATE module in IDIRISI, provides a comparative analysis based on the Kappa Index of Agreement. Kappa is essentially a statement of proportional accuracy, adjusted for chance agreement. Based on Pontius (2000), the Kappa indexes are defined as follows:

$$\text{Kstandard} = \frac{Po-MQNL}{1-MQNL} \tag{5.7}$$

$$\text{Kno} = \frac{Po-NQNL}{1-NQNL} \tag{5.8}$$

$$\text{Klocation} = \frac{Po-MQNL}{MQPL-MQNL} \tag{5.9}$$

$$\text{Kquantity} = \frac{Po-NQML}{PQML-NQML} \tag{5.10}$$

where Po is the observed proportion correct; $MQNL$, $NQNL$ and $NQML$ are the expected proportion due to changes; and $MQPL$ and $PQML$ are the proportions correct when the classification is perfect.

5.3 Results and Discussion

5.3.1 Classification Accuracy Assessment

The three land cover maps from Landsat-8 imageries in 2014, 2018, and 2022 were generated using the Maximum likelihood algorithm (Figure 5-2, Figure 5-3, and Figure 5-4). Maximum likelihood classification is a commonly used supervised classification technique with remote sensing image data (Richards and Richards, 2022). It was the first rigorous algorithm to be widely employed. The classified images of each land cover map were compared with reference data to assess accuracy. The significance of land cover and the ability to predict the effects of land cover change are hindered by the lack of accurate land cover data (Foody, 2002). Foody (2008) noted that the 85% target accuracy for image classification is often used without thorough consideration of its appropriateness, simply due to historical tradition. This target is sometimes stated without clear justification or supporting evidence from the literature. The accuracy of the images for the years 2014, 2018, and 2022 was examined. The accuracy assessment of LULC (Land Use and Land Cover) maps, including overall accuracy and Kappa values, was conducted using the confusion matrix, and the Kappa coefficients were presented in Table 5-9. Overall, the accuracy values were high, with all values exceeding 95%, and the kappa coefficient ranged from 0.92 to 0.95.

Table 5-9 Summary of the accuracy assessment value for image classification

Year	Overall accuracy	Kappa coefficient
LULC2022	95.06	0.92
LULC2018	95.40	0.94
LULC2014	96.00	0.95

5.3.2 Land use and land cover analysis

The land use/land cover (LU/LC) maps for 2014, 2018, and 2022 were derived from Lansat-8 satellite images and are presented in Figure 5-2, Figure 5-3, and Figure 5-4, respectively. This study focused on five land use classes: forest cover, farmlands, paddy

fields, built-up areas, and water bodies, to better understand the impact of land use change on hydrology, as discussed in Chapter 6.

A comprehensive analysis of land use change from 2014 to 2018 revealed that forest cover and farmlands were the dominant land uses within the river basin. It was observed that forest cover and farmlands decreased by approximately 1.00% and 0.27%, accounting for around 3083 and 835 hectares, respectively. During this period, there was a notable increase of 0.6% in water bodies, equivalent to 1862 hectares, as depicted in Figure 5-3. This increase was attributed to the construction of a new dam, namely the Battambang multipurpose dam. Analyzing the land use and land cover change from 2018 to 2022, it was found that there was a significant decline of approximately 3.07% in forest cover, equivalent to 9413 hectares. This continued deforestation is primarily driven by factors, such as agricultural land expansion due to population growth, land concessions, and land-

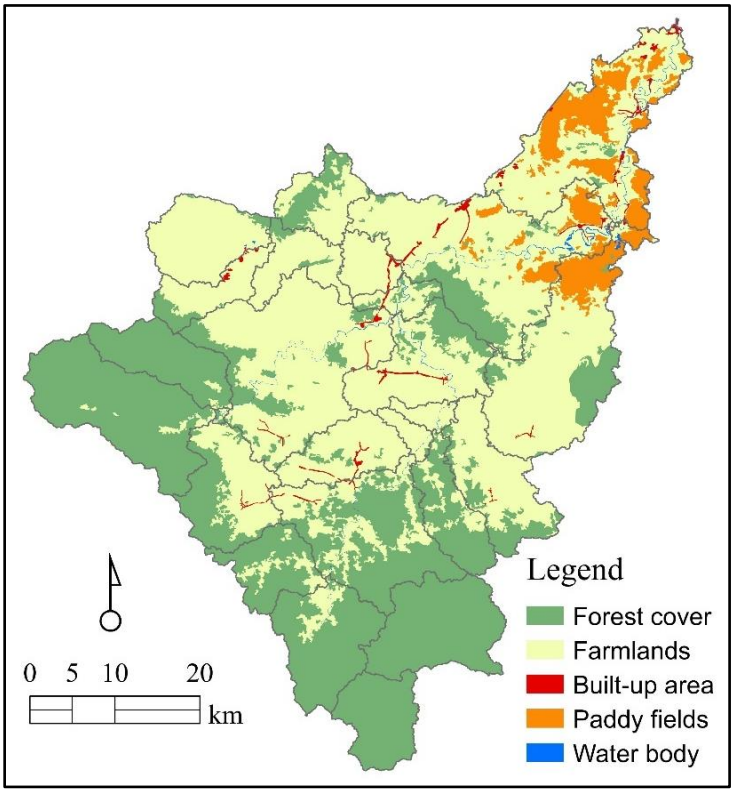

Figure 5-2 The classified land use in 2014 in the upper Sangker River basin.

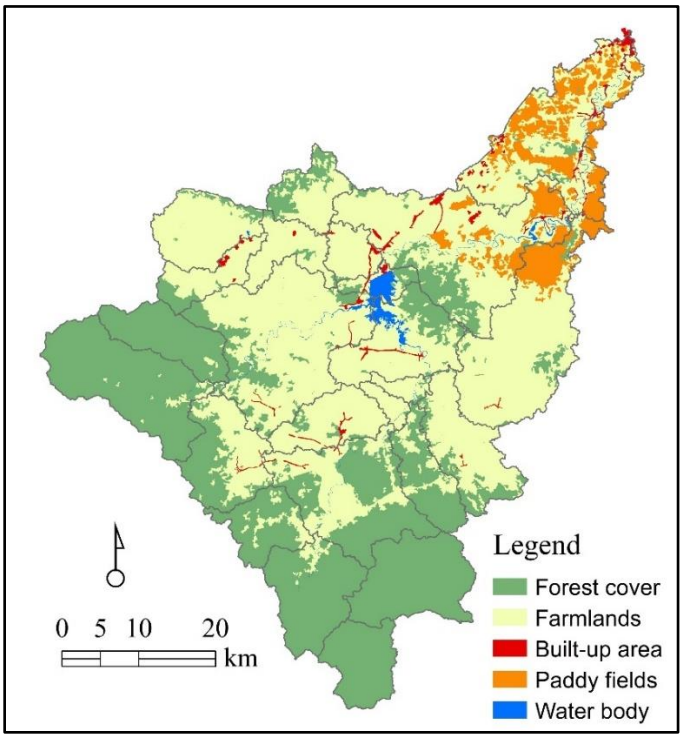

Figure 5-3 The classified land use in 2018 in the upper Sangker River basin.

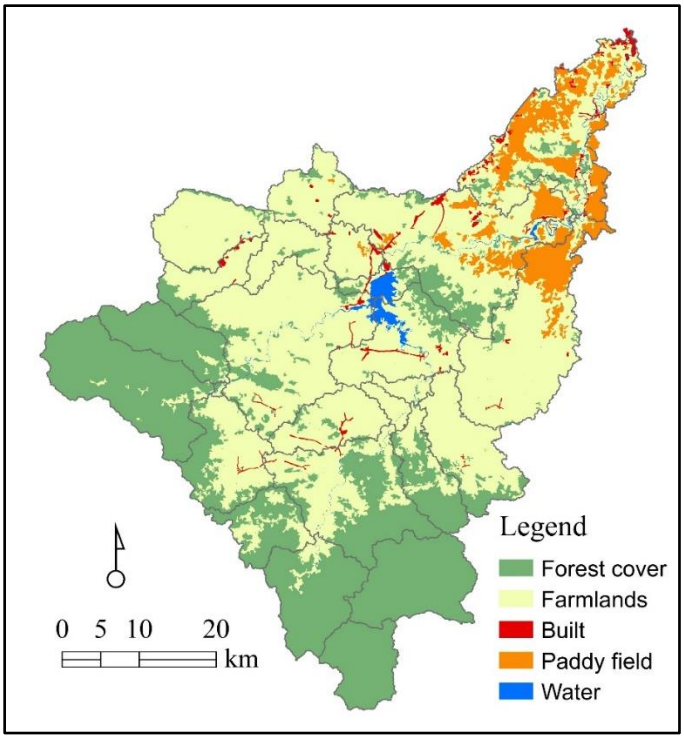

Figure 5-4 The classified land use in 2022 in the upper Sangker river basin.

mine clearance projects. On the other hand, there was an increase of about 2.32% (7098 hectares) in farmlands, despite the loss of forest cover.

5.3.3 Assessment of CA-Markov model performance

The study utilized land use data obtained from satellite imagery to characterize and forecast changes in land use and land cover. Specifically, two land use maps for the upper Sangker River basin in the years 2014 and 2018 were employed to create the 2022 land use map for the calibration of the CA-Markov model. Subsequently, the land use map generated by the CA-Markov model for 2022 underwent comparison with the observed 2022 land use map to ascertain the model's validity. Validation of the model is an essential pre-condition for research that predicts land use/land cover changes (Wang et al., 2021). Based on Figure 5-5, the actual and predicted land uses in 2022 are mostly similar, except for the forest cover class, which can be attributed to the map accuracy during image classification. Also, the model seems to have overestimated the amount of forest cover. The VALIDATE tool calculates specialized Kappa measures that distinguish between quantity and location errors in two qualitative maps. A Kappa value of 1 indicates perfect agreement, while a value of 0 indicates agreement equal to random chance.

The statistics derived from the VALIDATE module in IDIRISI software show that the Kappas for no information (Kno = 0.9407), for location (Klocation = 0.9418), for quantity (Kquantity = 0.9418), and for standard (Kstandard = 0.9145) (Table 5-10). The value of all kappa indices was larger than 0.90. According to Wang et al (2021), thus, the model was deemed valid and reliable for land use change projection.

Table 5-10 Kappa Index of Agreement to specify accurately quantity and location to predict land use map in 2022.

Statistics	Indices
Kno	0.9407
Klocation	0.9418
Kquantity	0.9418
Kstandard	0.9145

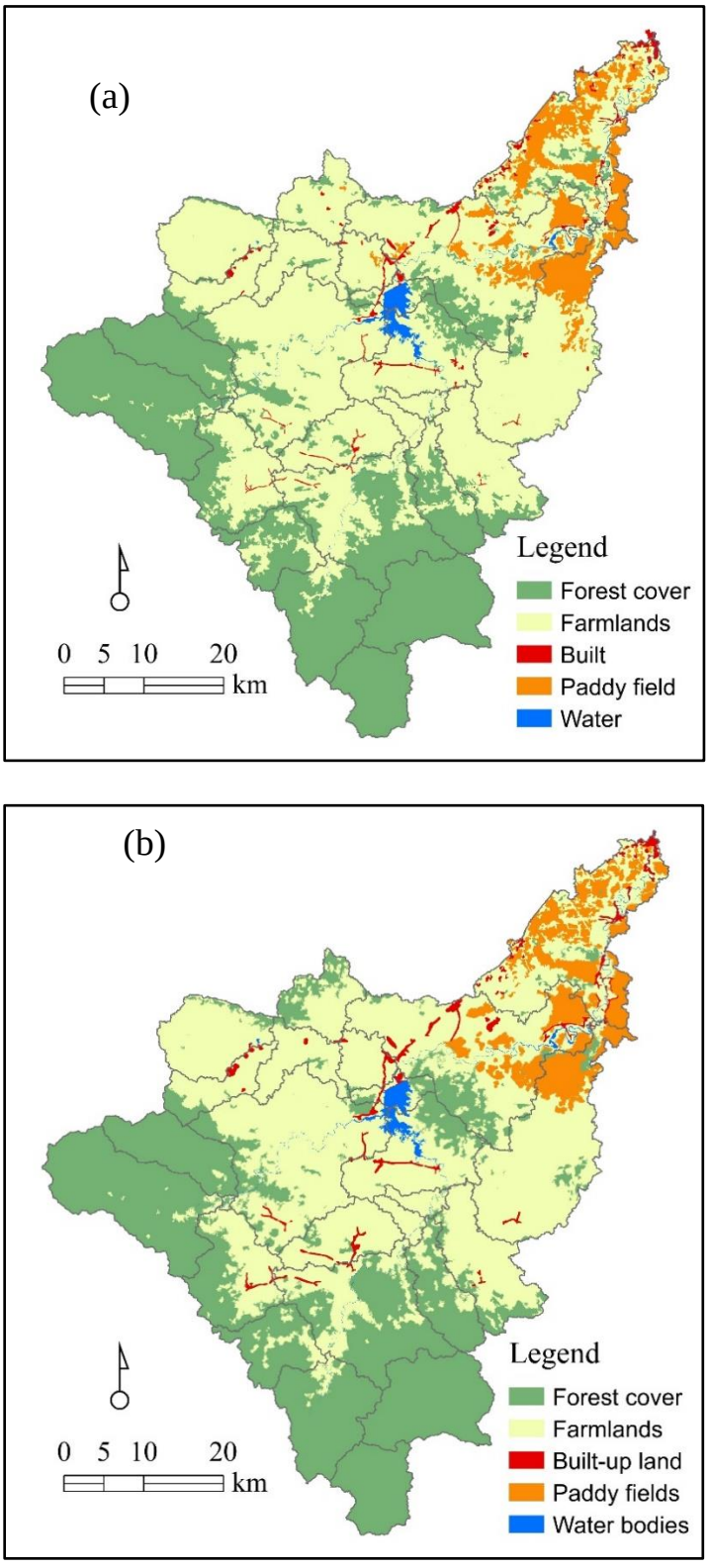

Figure 5-5 The comparison of the actual (a) and predicted (b) land use maps in 2022.

5.3.4 Prediction of future LULC of the upper Sangker river basin

The results of land use prediction maps for 2030 in the upper Sangker River basin employing the CA-Markov model are shown in Figure 5-6a and Figure 5-6b. Specifically, the model scenario without a land use policy (see Figure 5-6a) predicted that the farmlands would cover 52.12% of the total area of the upper Sangker River basin, followed by forest cover (38.42%), paddy fields (6.69%), built-up land (1.82%), and water bodies (0.95%) (Table 5-11). Additionally, forest cover and farmlands are expected to decrease in the area by 2030, compared to the land use in 2022 (Table 5-11). However, this decrease will contribute to an increase in built-up land by 0.22%. It should be noted that the decline of forest cover in the study area has been observed over the past few decades. According to previous research (Sourn et al., 2021), deforestation was observed from 1998 to 2013. Up to 2018, forest cover was mostly stable in mountainous areas, especially naturally protected areas such as the Phnom Samkos Wildlife Sanctuary and the Samlot Multiple Use Area. The expansion of agricultural land in the upper Sangker River basin will most likely reach these protected areas, reflecting the minor decline in forest cover predicted by the model.

With the land use development policy, the land use map in 2030 was achieved (see Figure 5-6b). If land use planning succeeds, then the positive impact on the natural forest cover in this basin can be seen in an increase in reforestation by 2030. In this case, our predicted land use shows that forest cover increases by 0.78%, and built-up land of high or low population density increases by 0.20% and 100%, respectively (Table 5-11). Moreover, forest cover is predicted to increase, even though some areas at most upstream parts of the river basin have been offered and allocated under ELCs. Nevertheless, the farmlands and paddy fields will decrease by 3.05% and 0.02%, respectively. Field surveys of current land use in mountain areas confirm that natural forests, even in protected areas, are being cut and burned to expand agricultural land. Therefore, it is predicted that deforestation will continue in the absence of effective land use policies. The land use policy here, however, is the planning of afforestation for forest communities by local governments. This policy is believed to help increase forest cover in the future.

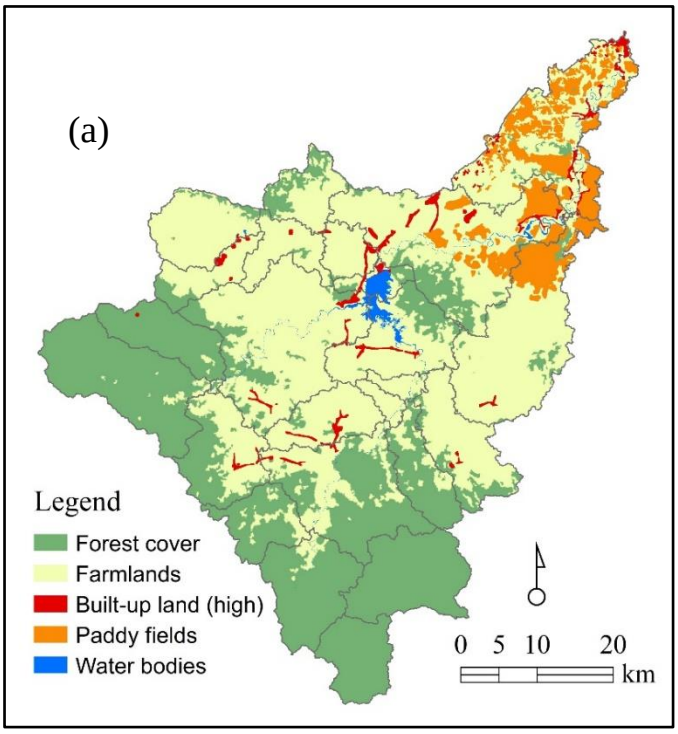

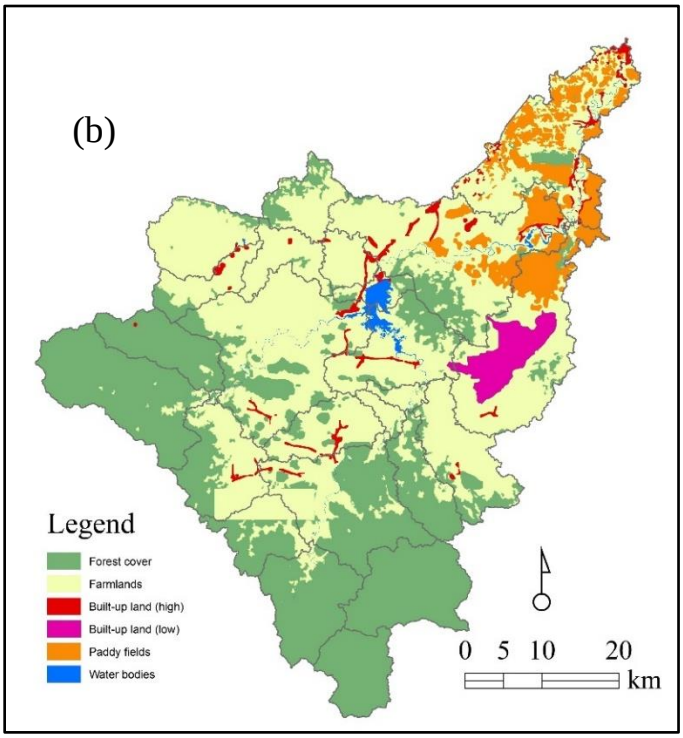

Figure 5-6 The predicted land use in 2030: without land use development policy (a); with land use development policy (b).

Overall, these decreases and increases result from government policies on land allocation. For instance, land use changes from farmlands to built-up areas of low population density appear as a new land use class. In this case, the lands were allocated under SLCs. Meanwhile, the built-up area's expansion is expected to increase, due to the increase in the number of new marriages and residential development plans. Furthermore, paddy fields will slightly decline, while water bodies will remain stable from 2018 to 2030.

Table 5-11 Predicted land use in 2030 in the upper Sangker river basin

			Without a land use policy			With a land use policy		
Land use classes	LU2022		Predicted LU 2030		Rate of changes	Predicted LU 2030		Rate of changes
	Area (ha)	Area (%)	Area (ha)	Area (%)	(%)	Area (ha)	Area (%)	(%)
Forest cover	118132.18	38.61	117678.13	38.42	−0.19	120619.33	39.39	0.78
Farmlands	159732.80	52.18	159570.39	52.12	−0.06	150436.29	49.14	−3.05
Built-up land (high density)	4914.26	1.61	5579.82	1.82	0.22	5538.65	1.81	0.20
Built-up land (low density)						6386.96	2.09	100.00
Paddy fields	20360.63	6.65	20477.64	6.69	0.03	20311.63	6.63	−0.02
Water bodies	2922.47	0.95	2909.35	0.95	0.00	2922.47	0.95	0.00
Total	306215.34	-	306215.34	-	-	306215.34	-	-

Based on the guidelines from the Ministry of Land Management, Urban Planning, and Construction, 6,386 hectares (built-up land with low population density) of state land in the Samlot district of Battambang Province and its shared border with the Koh Krala district were converted into SLCs for the poor and for retired soldiers. Specifically, these individuals were legally authorized to occupy one hectare of land with one house. This project was implemented under the Battambang Provincial Administration. Conversely, according to the Sub-degree on Reclassification of State Permanent Forest Reserve and Granting of ELCs for agro-industry investment in 2009 (Open Development Cambodia), 5,200 hectares of ELCs (see Figure 5-6b) in the Samlot district were converted from forest

for development purposes (e.g., rubber plantations). However, we found that this zoning area only experienced tree cutting.

In this study, the objective influences on land use patterns under the local government's land use development plan were successfully predicted by using the CA-Markov model. This model was effective because the land use planning focused on built-up land with low population density and farmland zoning. However, there are still challenges in predicting land use change when considering human activities (e.g., commercial and/or urban development) and investments in land use development policies.

5.4 Conclusion

This study was the first attempt to predict future land use change and the effects of government land use planning in the upper Sangker River basin of Cambodia. The prediction of land use has become a critical issue due to the uncertainty of land use policies and the availability of suitable models. The spatio-temporal land use dynamics through the CA-Markov model confirmed that it is a valuable tool for simulating and predicting future changes in the landscape. However, the model does not account for unforeseen developments that significantly influence land use change, such as land concessions and forest communities. Integrating GIS modeling that accounts for socio-economic and policy factors could improve the accuracy of land use predictions. It is hoped that our results will not only be used to assess the impact of future land use changes on the hydrological environment but also be integrated with climate change prediction models to contribute to future water demand projections.

References

Araya, Y.H. and Cabral, P. 2010. Analysis and modeling of urban land cover change in Setubal and Sesimbra Portugal. Remote Sens., 2, 1549-1563.

Aburas, M.M., Ahamad, M.S.S. and Omar, N.Q. 2019. Spatio-temporal simulation and prediction of land use change using conventional and machine learning models: a review. Environ. Monit. Assess., 191, 205.

Azizi, A., Malakmohamadi, B., & Jafari, H. R. (2016). Land use and land cover spatiotemporal dynamic pattern and predicting changes using integrated CA-Markov model.

Ahmad, A., & Quegan, S. (2012). Analysis of maximum likelihood classification on multispectral data. Applied Mathematical Sciences, 6(129), 6425-6436.

Brown, D.G., Pijanowski, B.C. and Duh, J.D. 2000. Modeling the relationships between land use and land cover on private lands in the upper Midwest, USA. J. Environ. Manag., 59, 247-263.

Castelluccio, M., Poggi, G., Sansone, C., & Verdoliva, L. (2015). Land use classification in remote sensing images by convolutional neural networks. arXiv preprint arXiv:1508.00092.

Civco, D.L., Hurd, J.D., Wilson, E.H., Song, M. and Zhang, Z. 2002. A comparison of land use and land cover change detection methods. ASPRS-ACSM Annual Conference and FIG Congress, The University of Connecticut; Volume XXII.

Eastman, J. R. (2012). Idrisi selva tutorial. Idrisi Production, Clark Labs-Clark University, 45(January), 51-63.

Eastman, J.R. and Toledano, J. (2018). Geomatic approaches for modeling land change scenarios, Springer.

Foody, G. M. (2008). Harshness in image classification accuracy assessment. International Journal of Remote Sensing, 29(11), 3137-3158.

Foody, G. M., & Mathur, A. (2004). A relative evaluation of multiclass image classification by support vector machines. IEEE Transactions on geoscience and remote sensing, 42(6), 1335-1343.

Foody, G. M. (2002). Status of land cover classification accuracy assessment. Remote sensing of environment, 80(1), 185-201.

Gupta, S.C., Kessler, A.C., Brown, M.K. and Zvomuya, F. 2015. Climate and agricultural land use change impacts on streamflow in the upper midwestern United States. Water Resour. Res., 51, 5301-5317.

Hagenlocher, M., Hölbling, D., Kienberger, S., Vanhuysse, S. and Zeil, P. 2016. Spatial assessment of social vulnerability in the context of landmines and explosive remnants of war in Battambang province, Cambodia. Int. J. Disaster Risk Reduc., 15, 148-161.

Hamad, R., Balzter, H., & Kolo, K. (2018). Predicting land use/land cover changes using a CA-Markov model under two different scenarios. Sustainability, 10(10), 3421.

Jog, S., & Dixit, M. (2016, June). Supervised classification of satellite images. In 2016 Conference on Advances in Signal Processing (CASP) (pp. 93-98). IEEE.

Kumar, S., Radhakrishnan, N., & Mathew, S. (2014). Land use change modelling using a Markov model and remote sensing. Geomatics, Natural Hazards and Risk, 5(2), 145-156.

Kumar, K. S., Kumari, K. P., & Bhaskar, P. U. (2016). Application of Markov Chain & Cellular Automata based model for prediction of Urban transitions. In 2016 International Conference on Electrical, Electronics, and Optimization Techniques (ICEEOT) (pp. 4007-4012). IEEE.

Kityuttachai, K., Heng, S., & Sou, V. (2016). Land Cover Information Catalogue of the Lower Mekong Basin. MRC Technical Paper, (58), 83.

Lambin, E.F. 1997. Modelling and monitoring land-cover change processes in tropical regions. Prog. Phys. Geogr., 21, 375–393.

Open Development Cambodia. Economic land concessions. https://bit.ly/3ZdIOtx.

Open Development Cambodia. Battambang provincial land use plan for vision. https://bit.ly/3X2XIB8; Volume 2030.

Otukei, J. R., & Blaschke, T. (2010). Land cover change assessment using decision trees, support vector machines and maximum likelihood classification algorithms. International Journal of Applied Earth Observation and Geoinformation, 12, S27-S31.

Open Development Cambodia. Law on Land (2001), https://bit.ly/3i9aqj7.

Pontius Jr, R. G. (2000). Comparison of categorical maps. Photogramm. Eng. Remote Sens, 66(20), 0.

Perumal, K., & Bhaskaran, R. (2010). Supervised classification performance of multispectral images. arXiv preprint arXiv:1002.4046.

Richards, J. A., & Richards, J. A. (2022). Remote sensing digital image analysis (Vol. 5). Berlin/Heidelberg, Germany: springer.

Rawat, J. S., & Kumar, M. (2015). Monitoring land use/cover change using remote sensing and GIS techniques: A case study of Hawalbagh block, district Almora, Uttarakhand, India. The Egyptian Journal of Remote Sensing and Space Science, 18(1), 77-84.

Subedi, P., Subedi, K. and Thapa, B. 2013. Application of a hybrid cellular automaton-Markov (CA-Markov) model in land use change prediction: a case study of Saddle Creek Drainage Basin, Florida. Appl. Ecol. Environ. Sci., 1, 126-132.

Surabuddin Mondal, M., Sharma, N., Kappas, M., & Garg, P. K. (2013). Modeling of spatio-temporal dynamics of land use and land cover in a part of Brahmaputra River basin using Geoinformatic techniques. Geocarto International, 28(7), 632-656.

Sankarrao, L., Ghose, D. K., & Rathinsamy, M. (2021). Predicting land-use change: Intercomparison of different hybrid machine learning models. Environmental Modelling & Software, 145, 105207.

Sourn, T., Pok, S., Chou, P., Nut, N., Theng, D., Rath, P., Reyes, M.R. and Prasad, P.V.V. 2021. Evaluation of land use and land cover change and its drivers in battambang province, cambodia from 1998 to 2018. Sustainability, 13, 11170.

TAATI, A., SARMADIAN, F., MOUSAVI, A., POUR, C. T. H., & SHAHIR, A. H. E. (2015). Land use classification using support vector machine and maximum likelihood algorithms by Landsat 5 TM images. Walailak Journal of Science and Technology (WJST), 12(8), 681-687.

Takada, T., Miyamoto, A., & Hasegawa, S. F. (2010). Derivation of a yearly transition probability matrix for land-use dynamics and its applications. Landscape ecology, 25, 561-572.

Tadese, S., Soromessa, T., & Bekele, T. (2021). Analysis of the current and future prediction of land use/land cover change using remote sensing and the CA-markov model in Majang forest biosphere reserves of Gambella, southwestern Ethiopia. The scientific world journal, 2021, 1-18.

Wang, S. W., Munkhnasan, L., & Lee, W. K. (2021). Land use and land cover change detection and prediction in Bhutan's high-altitude city of Thimphu, using cellular automata and Markov chain. Environmental Challenges, 2, 100017.

Vanna, C., Yamamoto, T. and Inoue, T. (2020). Evaluation of water shortages in agricultural water use in the Sangker River Basin, Cambodia. IJERD, 11, 32-39.

Yeh, A. G. O., & Li, X. (1999). Economic development and agricultural land loss in the Pearl River Delta, China. Habitat international, 23(3), 373-390.

CHAPTER 6 Assessment of the impact of land use and climate change on water resources

6.1 Introduction

The rapid economic growth of Cambodia (Michinaka et al., 2013) has led to the degradation of forest areas in many regions of the country for agricultural purposes since the civil war ended in 1998. This growth has been driven by factors, such as increasing food demand due to population growth, hydrological drought, and climate variability. Climate change (Estrela et al., 2012; Lu et al., 2019), drought events (Jacobsen et al., 2018; Cunha et al., 2019; Yang et al., 2012), and the conversion of forest cover to agricultural or other land uses (Breuer et al., 2006; Baker and Miller, 2013) have been the focus of numerous studies and documents due to their impact on natural environments and resources, particularly concerning food and water security (Godfray et al., 2010). The impacts of climate change, competition, increasing water demands for agriculture, and other purposes need to be considered when addressing the challenges related to agriculture and water resources.

Battambang province, situated in the western part of Cambodia, is the largest agricultural area and the primary rice crop region in the nation, exerting significant pressure on water resources through irrigation, water supply, and crop productivity. Recent studies have shown that Battambang is more exposed to drought events than other provinces in the country (Abhishek et al., 2021) and faces water scarcity in the irrigation water supply in the Sangker River basin (Vanna et al., 2020). Additionally, the province has been affected by flood and drought due to climate variability between 1994 and 2018 (Sok et al., 2021; Heng et al., 2013). Land use and climate are significant factors influencing hydrological conditions (Li et al., 2009). With the province being designated as Cambodia's fourth economic pole in 2023, focusing on the rice and fish corridor, new regulations by this policy are expected to further strain water resources and ecological systems. Therefore, understanding hydrological changes and having information on water resources under the changing land use and climate conditions are essential for establishing mechanisms for present and future water management.

Several methods have been developed to assess the hydrological effects of environmental changes. These methods include the paired catchment approach, time-trend analysis, and hydrological modeling (Li et al., 2009; Zhang et al., 2018). For more information about these methods, please refer to Zhang et al. (2018).

Using a hydrological model is a common approach to accurately represent and calculate the hydrological processes within a watershed. The Soil and Water Assessment Tool (SWAT) is a widely used spatially distributed hydrological model (Arnold et al., 1998; Gassman et al., 2007). It is commonly used to simulate water resources under changing environmental conditions, such as climate change or land use and land cover (LULC) changes (Zhang et al., 2020; Lin et al., 2015; Bhatta et al., 2019; Narsimlu et al., 2013).

This study was conducted in the Upper Sangker River basin in Battambang province. While detailed studies are needed to understand the available water resources in this basin, there is relatively little information available regarding the effects of climate change on hydrology in this catchment. Monichoth et al. (2014) applied the Hydro-Crop model to assess the possible impacts of climate change on rice production in the Sangker River basin. Oeurng et al. (2019) analyzed the entire catchment of the Sangker River using a SWAT model to examine the climate change effect on the river flow regime. These studies investigated water-related relationships inside the Sangker River basin and the impact of climate variation on future hydrological alterations (Oeurng et al., 2019; Monichoth et al., 2014), but without considering the impacts of land use and land cover changes.

To address this gap, we applied a semi-distributed SWAT model to gain a better understanding of the hydrological processes, taking into account the combined influence of land use and climate change projections. The main objective of the present study is to explore the influence of interrelation between land cover changes and climate variability on water resources. Hence, the specific goals are:

1) to formulate a distributed hydrological model suitable to simulate the effects of land use and climate change.
2) to assess the combined impacts of projected climate and land use changes on water

resources and hydrologic water balance components.

3) to evaluate the influence of reforestation under land use planning projects, on catchment water resources.

These objectives are accomplished by simulating the SWAT hydrological model in which the observed impacts of LULC from 2002 to 2030 were downloaded and predicted Landsat 8 dataset and land use change model, namely Cellular Automata Markov model (CA-Markov), then analyzed and incorporated them into the calibrated model. Besides, the SWAT model simulation in the baseline period (1986-2001) was then against the bias-corrected Global Climate Model-Regional Climate Model (GCM-RCM) of future climate data for the scenario period (2030-2045) for obtaining a better understanding of spatio-temporal climate and land use change effects on hydrologic water balance components and river discharge.

6.2 Methods

6.2.1 Study area

The study area in this chapter covers the upper part of the Sangker River basin. See Chapter 3, section 3.1, for detailed location site and biophysical characteristics of this basin.

6.2.2 Input data

Data scarcity posed a significant challenge for catchment hydrological modeling in Cambodia. Due to the long civil war, limited staffing, and a constrained budget, there was insufficient data available for hydrological model calibration and validation. This was particularly evident in the Sangker River basin, where there was a lack of hydro-meteorological equipment and resources for operation and maintenance. The longest period for which Sangker River water level data was available spanned from 1997. The relationship equation between water level and river discharge (rating curve) was established in 2001 at the Battambang bridge gauging station, which covers an area of 3,062 km^2. Monthly observed discharge data from 2007 to 2018 was used in the study. Although there are four meteorological stations in the study area, the Veal Bek Chan station (Figure 6-1),

operational since 1982, was specifically selected for bias correction of climate model data and climate impact analyses. It was assumed to represent the average spatial distribution of precipitation in the entire catchment area. As hydrological data for the Sek Sork multi-purpose dam and Kang Hot headwork were not publicly available, the SWAT model was calibrated and validated before dam construction in 2018. Spatial data such as the digital elevation model (DEM), land use, and soil maps were also essential inputs for the SWAT modeling, as listed in Table 6-1. Climate data for the study was derived from the Southeast Asia Climate Downscaling/Coordinated Regional Climate Downscaling Experiment-Southeast Asia (SEACLID/CORDEX-SEA) project (Tangang et al.,2020; Tangang et al.,2019). This data was used to assess the impact of future climate on hydrology. The CORDEX-SEA project was developed to enhance the understanding of climate change impact (Herrmann et al., 2020) and vulnerability at local and regional scales. Future climate projection using CORDEX-SEA had been previously conducted in countries such as Malaysia (Tan et al., 2019), Vietnam (Tuyet et al., 2019), Thailand (Tangang et al.,2019), and the Philippines (Magnaye et al., 2023). The climate model data used representative concentration pathways (RCP) scenarios and covered both historical (1951-2005) and future (2006-2099) scenarios, with a spatial resolution of 25 km. As the resolution of the climate model data was coarser than the typical catchment scale, downscaling and bias correction of the data were necessary (Teutschbein and Seibert., 2010; Trang et al., 2017). Land use and land cover (LULC) changes were also considered as influential factors in the hydrological analyses. LULC data from 2014 and 2018 were classified using Landsat 8, and future land use in 2030 was predicted using the CA-Markov model. The predicted land use map in 2030 was analyzed by integrating the provincial government's land use development plan.

Table 6-1 SWAT input data

Data set	Source	Scale
Soil map	FAO-UNESCO	30 m
DEM	ASTER GDEM	30 m
Land use maps	JICA	30 m
Discharge	MOWRAM	2007–2018
Climate	MOWRAM	1986–2018

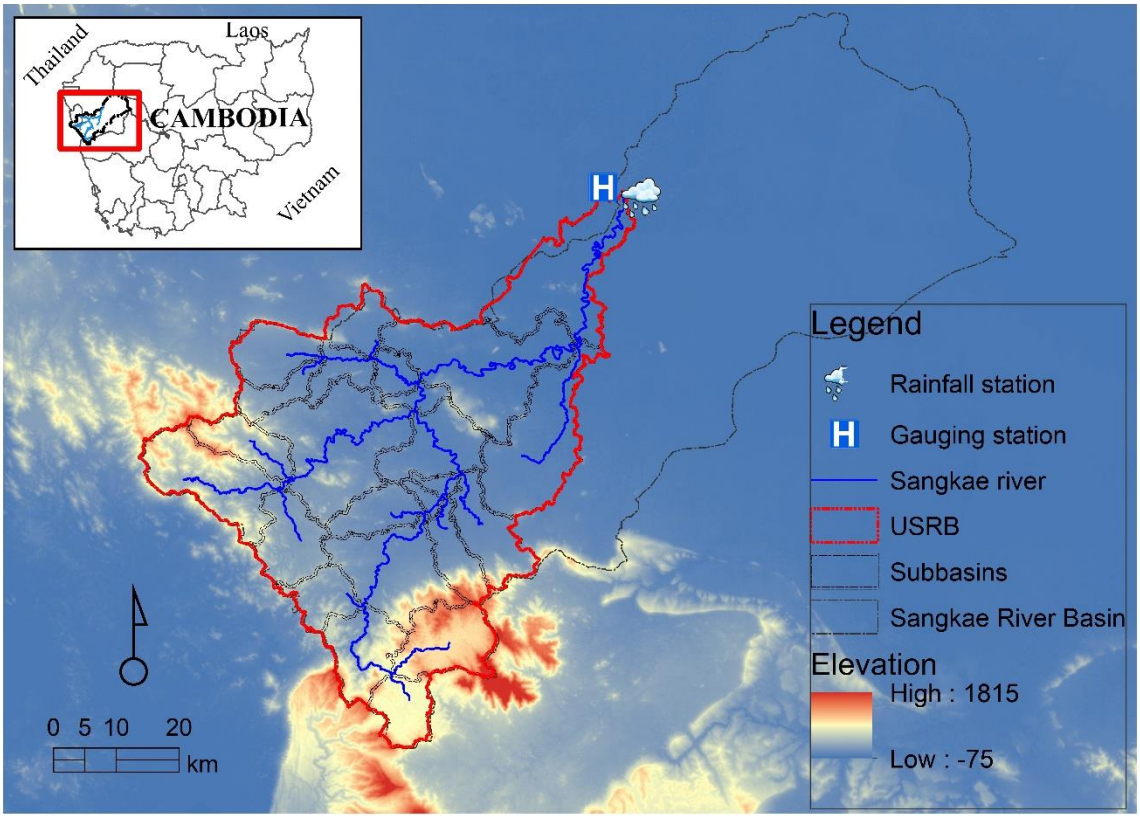

Figure 6-1 Location of Veal Back Chan weather station.

6.2.3 Climate analysis

6.2.3.1 Observed and climate model data

Daily time series of observed rainfall and temperature for the Upper Sangker River basin were obtained from the Ministry of Water Resources and Meteorology, Cambodia (MOWRAM). Long-term observed records at Veal Back Chan station (**Figure 6-1**) from 1986 to 2001 were used as a target dataset for the bias correction methods and as input into the baseline hydrological simulation for climate change impact studies.

Table 6-2 Summary of GCM-RCM model data

GCM	RCM	Emission scenario	Historical	Scenario
CNRM-CM5 (CNRM, France	RCA4 (SMHI, Sweden)	RCP4.5 RCP8.5	1986-2001	2030-2045

Daily rainfall and temperature data from one GCM-RCM model dataset in the CORDEX-SEA project, obtained from the Earth System Grid Federation (ESGF) (https://esgf-data.dkrz.de/search/cordex-dkrz/), were used to estimate the climate change signal cycle (Table 6-2). A total of 2 GCMs were selected and downscaled using 1 RCM with high resolution (25 km × 25 km) for two different emission scenarios, RCP4.5 and RCP8.5, based on the model output availability during the analysis period (Table 6-2). However, the HadGEM2-RCA4 model was excluded from the study due to its unrealistic representation of tropical monsoon climate. After data bias, this model shows heavy rainfall present in the dry season whereas low rainfall exhibits in the wet season months. The term of RCP8.5 corresponds to the pathway with the highest greenhouse gas emissions, while RCP4.5 describes a moderate mitigation pathway (Fix et al., 2018).

6.2.3.2 Downscaling and bias correction

The delta change approach was applied in this study at the station site (**Figure 6-1**) for the baseline/historical period 1986-2001 and the scenario period 2030-2045 due to its considering a robust method to generate climate scenarios (Bosshard et al., 2011; Graham et al., 2007). This method transfers the mean monthly change signal between GCM-RCM historical and GCM-RCM scenario periods to an observed time series (Eisner et al., 2012). The scenario daily precipitation and air temperature time series in the target weather station were given by:

$$P_{Fut}^{(d)} = P_{Obs}^{(d)} \times \frac{\bar{P}_{GCM-RCM}(m)}{\bar{P}_{Histroical}(m)} \quad (6.1)$$

$$T_{Fut}^{(d)} = T_{Obs}^{(d)} + [\ \bar{T}_{GCM-RCM}(m) - \bar{P}_{Histroical}(m)] \quad (6.2)$$

where, $P_{Fut}^{(d)}$ and $P_{Obs}^{(d)}$ represent the future daily and observed precipitation time series used as inputs of the hydrological model, respectively. $\bar{P}_{GCM-RCM}(m)$ and $\bar{P}_{Histroical}(m)$ are mean monthly GCM-RCM and its historical model output. $T_{Fut}^{(d)}$ and $T_{Obs}^{(d)}$ stands for the future daily and observed air temperature, respectively. Whereas $\bar{T}_{GCM-RCM}(m)$ and $\bar{P}_{Histroical}(m)$ are the mean monthly GCM-RCM and its historical model output, respectively.

6.2.4 Analyses of land use change

The upper Sangker catchment has undergone significant changes since the end of the civil war in 1998 (Sourn et al., 2021). A land use map from 2002 was obtained directly from the Japan International Cooperation Agency (JICA) and was used to analyze the land use and land cover (LULC) transitions for this study. Additionally, historical land use maps in the upper Sangker River basin were classified using Landsat 8 dataset images from 2014, 2018, and 2022, obtained from the U.S. Geological Survey (https://earthexplorer.usgs.gov/). These datasets were then used in a supervised classification technique to accurately represent the land cover characteristics for simulation. The LULCs were classified into five categories: forest cover, farmlands, built-up lands, paddy fields, and water (Table 6-3). The changes in land cover in the upper Sangker River basin from 2002 to 2022 are shown in Figure 6-2.

Table 6-3 Description of the LULC classification

LULC	Description
Forest cover	Forest and natural area
Farmlands	Agricultural area not included in paddy field
Built-up lands	Residential/commercial/public facilities
Paddy fields	Rice fields
Water bodies	River, reservoir, lake, and small stream

To forecast the LULC map in 2030, we applied the CA-Markov model using land use maps in 2014, 2018, and 2022 as input for model simulation and projection. The CA-Markov model combined Cellular- Automata, Markov chain, multi-criteria, and multi-objective land allocation to predict land cover change over a specific time (Sang et al., 2011). Human activities, including landmine clearance, economic land concession, and social land concession, were the main factors affected by the dynamic land use change (Sourn et al., 2021). For more details on LULC projection analyses in the upper Sangker River basin, refer to Chapter 5. Moreover, we also presented the projected land use in 2030, considering a combination of simulated land use and a land use development plan from the provincial government.

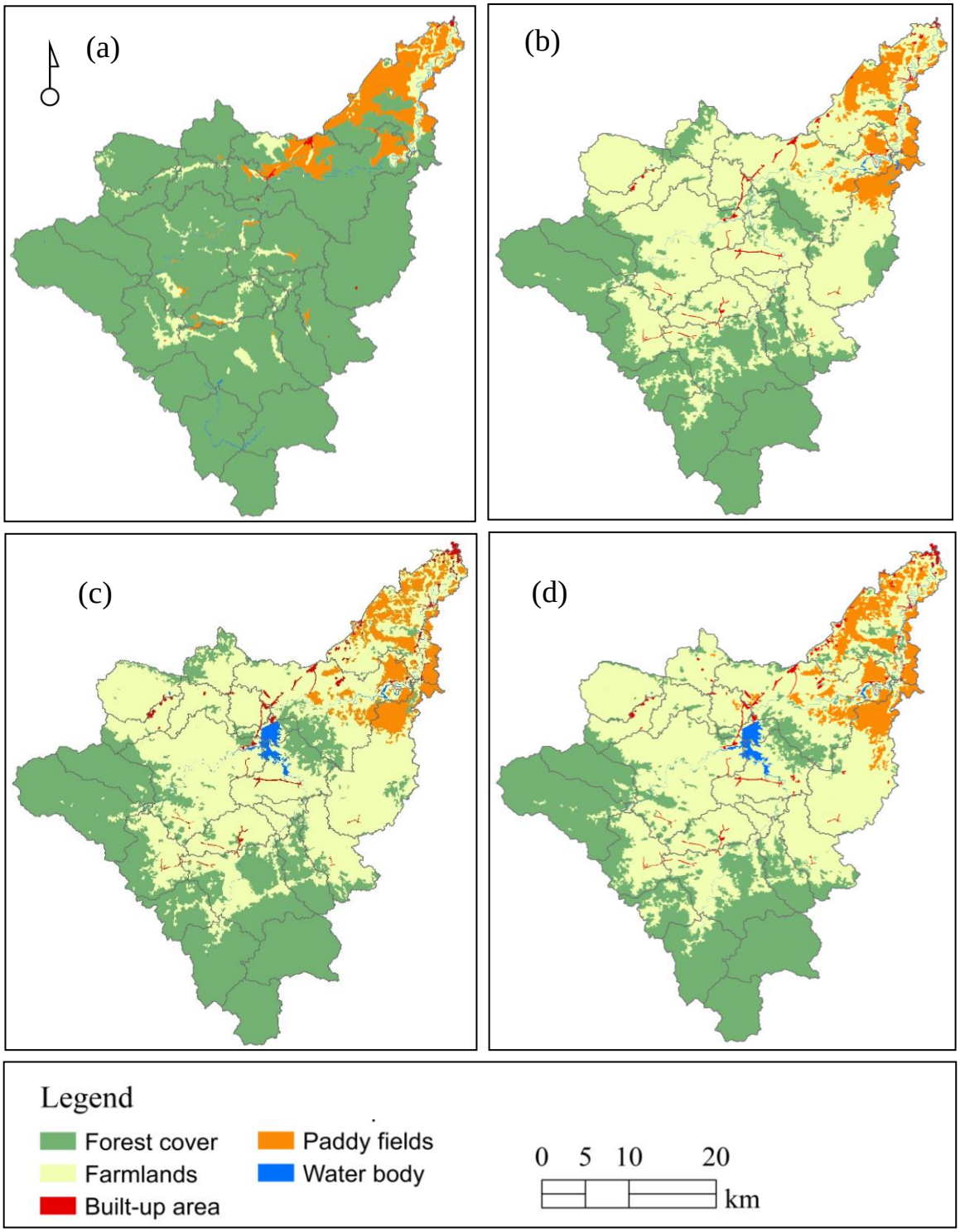

Figure 6-2 Land use and land cover classification for four time steps ranging from 2002 (a) (JICA), 2014 (b), 2018 (c), and 2022 (d).

Table 6-4 Transition of LULC from 2002 to 2030

LULC			Without a land use policy			With a land use policy		
	LU2002		Projected LU2030			Projected LU2030		
	Area (ha)	Area (%)	Area (ha)	Area (%)	Rate of change (%)	Area (ha)	Area (%)	Rate of change (%)
Forest cover	266755.64	87.11	117678.13	38.42	-48.69	120619.33	39.39	0.78
Farmlands	16717.57336	5.46	159570.39	52.12	46.66	150436.29	49.14	−3.05
Built-up lands (high density)	359.426692	0.12	5579.82	1.82	1.70	5538.65	1.81	0.2
Built-up lands (low density)	-	-	-	-	-	6386.96	2.09	100
Paddy fields	21171.92484	6.91	20477.64	6.69	-0.22	20311.63	6.63	−0.02
Water bodies	1208.777961	0.39	2909.35	0.95	0.56	2922.47	0.95	0
Total	306215.34	-	306215.34	-	-	306215.34	-	-

The land use maps for the year 2030 are depicted in Figure 6-3b and Figure 6-3c. A significant decline in natural forests from 2002 to 2030 has been observed and forecasted. The projected land use for 2030 indicates that farmlands will cover 52.12% of the total area of the upper Sangker River basin, followed by forest cover (38.42%), paddy fields (6.69%), built-up land (1.82%), and water bodies (0.95%) (refer to Table 6-4). Compared to 2002, it is expected that natural forests will decrease by 48.69% in 2030, occupying approximately 38.42% of the total area of the upper Sangker River basin. Moreover, the future forest area in 2030 is anticipated to be similar to that of 2022. Over the dynamic period of land use change (2002-2030), the agricultural area, including farmland and rice fields, is projected to significantly increase from 12.37% to 46.44%. However, with the implementation of the land use development policy, the forest cover is expected to experience a modest increase of nearly 0.78% compared to the simulated land use map in 2030, based on historical land use change scenarios (Table 6-4). In this study, the land use and land cover change scenario was developed based on historical trends leading to the projection period. The land use map

for 2002 was used as the reference time, while the projected land use map for 2030 was considered for change impact analysis.

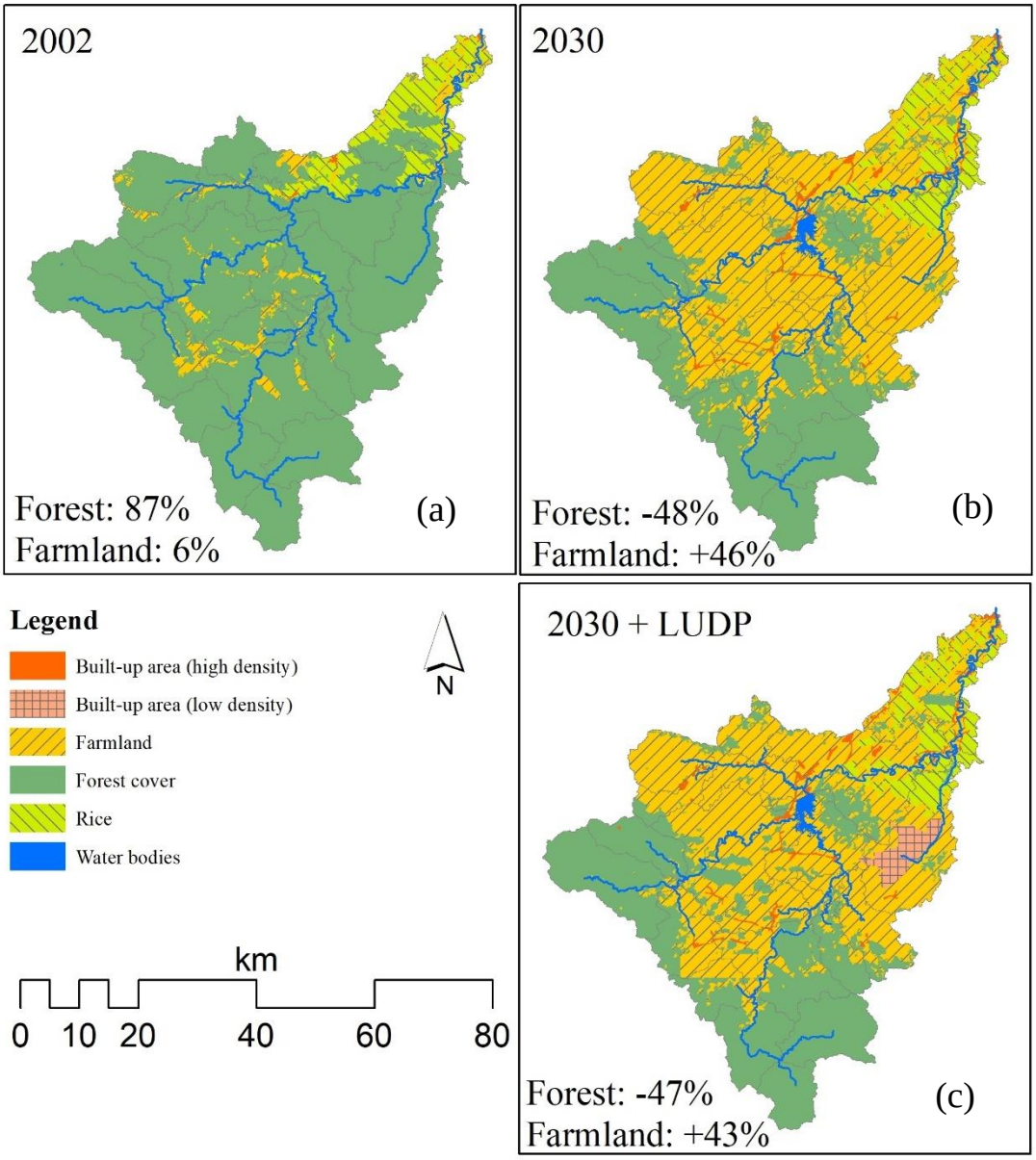

Figure 6-3 Transitional land use from 2002 to 2030 in the upper Sangker river basin: land use in 2002 derived from JICA (a), projected land use in 2030 (b), and projected land use in 2030 with integrated land use development projects.

6.2.5 SWAT Hydrological Modeling

6.2.5.1 The model-soil and water assessment tool (SWAT)

The SWAT model description can be found in Chapter 4, section 4.2.2.1, which provides a detailed explanation of the hydrological cycle and water balance in SWAT. This section includes estimations for various hydrologic water balance components such as surface runoff, peak flow, base flow, channel routing, and evapotranspiration. For detailed SWAT model input data requirements, refer to section 4.2.2.2.

6.2.5.2 SWAT model setup, calibration and calibration

In this chapter, the SWAT model was used to simulate streamflow and hydrologic water balance in the basin. The SWAT model setup, calibration, and validation procedures were consistent with those described in Chapter 4, sections 4.2.2.3, 4.2.2.4, and 4.2.2.5. These sections detailed the model construction, the data input process, and the years over which the model was calibrated and validated. However, for Chapter 6, the model setup was recalibrated using data from only one rainfall station, the Veal Back Chan station (**Figure 6-1**) in Battambang City. This station was selected due to its extensive rainfall and temperature records, which were necessary for projecting future climate conditions through downscaling and bias correction. This was done to analyze the climate and create climate scenarios to study the effects of projected climate changes on hydrologic water balance and water resources. Additionally, updated land use maps were used to establish the hydrologic response units (HRUs). Different land use maps from 2002 (Figure 6-3a) and 2014 (Figure 5-2) were employed in simulating streamflow. The 2002 land use map was used for model input during the calibration period, while the 2014 map was utilized to enhance model validation, reflecting significant changes in land use between 2002 and 2018.

6.2.5.3 SWAT Model Performance Evaluation

The statistical analysis using Nash-Sutcliff efficiency (*NSE*), the coefficient of determination (R^2), and the percent bias (*PBIAS*) were selected to evaluate the performance of SWAT modeling.

$$R^2 = \frac{\sum_{i=1}^{n}(O_i - \bar{O}_i)(S_i - \bar{S}_i))}{[\sum_{i=1}^{n}(O_i - \bar{O}_i)^2]^{0.5}[\sum_{i=1}^{n}(S_i - \bar{S}_i)^2]^{0.5}} \quad (6.3)$$

$$PBIAS = \frac{\sum_{i=1}^{n}(O_i - S_i)}{\sum_{i=1}^{n}(O_i)} \quad (6.4)$$

Where O_i and S_i are the observed and simulated streamflow values; and $\bar{O}$ and $\bar{S}$ are the mean of observed and simulated streamflow values.

The ranges of statistics for model evaluation were followed by Morisai et al. (2007). See Chapter 4 section 4.2.2.6 for detailed NSE equations and statistical ranges.

6.2.6 Scenario simulation

The study involved two scenarios to explore the impact of land use and climate changes on hydrological systems. Fundamental change scenarios were applied for land use and climate changes. The land use maps for 2002 and 2030 represented land use and land cover (LULC) patterns in the study area, serving as the reference or baseline scenario and future scenarios, respectively. Additionally, a future land use impact scenario, known as land use-2030+LUDP, integrated the land use development plan for 2030. Meteorological data, including rainfall and temperature from 1986 to 2001, were considered as the baseline, while the years 2030-2045 were treated as future climate scenarios.

The downscaled climate scenarios in the study utilized GCM-RCM model outputs in CORDEX-SEA, incorporating two climate scenarios: RCP4.5 and RCP8.5.

The projection of land use was simulated using the CA-Markov model, based on historical changes in land use patterns from 2014 to 2018, to predict LULC in 2030.

The SWAT model was executed three times to examine the effects of environmental changes, such as LULC and climatic variability.

Scenario 1 was designed to evaluate the impact of transitioning land use to the year 2030 on the hydrological cycle, without accounting for changing climate.

Scenario 2 was specifically developed to assess the influence of changing both land use and climate on water resources, as well as to investigate the impact of the land use development project (2030) on the hydrological system.

6.3 Results

6.3.1 SWAT calibration and validation

The results of the SWAT model calibration and validation for simulating streamflow using the SUFI-2 calibration approach at the gauging station in Battambang City are depicted in Figure 6-4. The monthly hydrograph of observed and simulated streamflow generated by the SWAT model generally indicates a quite good agreement. The validity of this model is further substantiated by the statistical analysis presented in Table 6-5. According to Moriasi et al. (2007), the model's performance was deemed satisfactory for both calibration (*NSE*=0.63, *PBIAS*=20.8, R^2=0.65) and validation (*NSE*=0.50, *PBIAS*=34.6, R^2=0.57). Notably, during the calibration period, the peak flow was overestimated in 2009 and 2012 but underestimated in 2013. Furthermore, the SWAT model underpredicted during the validation period for 2014-2015 and 2018. The limited number of meteorological stations and their uneven distribution within the watershed contributed to the model's overall satisfactory performance.

Table 6-5 Summary of the statistical quantitative model performance analysis for the model calibration and validation. NES is the Nash-Sutcliff Efficient.

Quantitative statistics	Monthly calibration (2007-2013)	Monthly validation (2014-2018)
NSE	0.63	0.50
PBIAS	20.8	34.6
R^2	0.65	0.57

Table 6-6 presents the components of the hydrologic cycle and water budgets such as evapotranspiration (ET), rainfall, lateral flow, baseflow, surface water, and water yields for the entire simulation period (2007-2018), besides the river flow simulation. Based on the simulation, 68% of the rainfall drop was evaporated into the atmosphere, which is

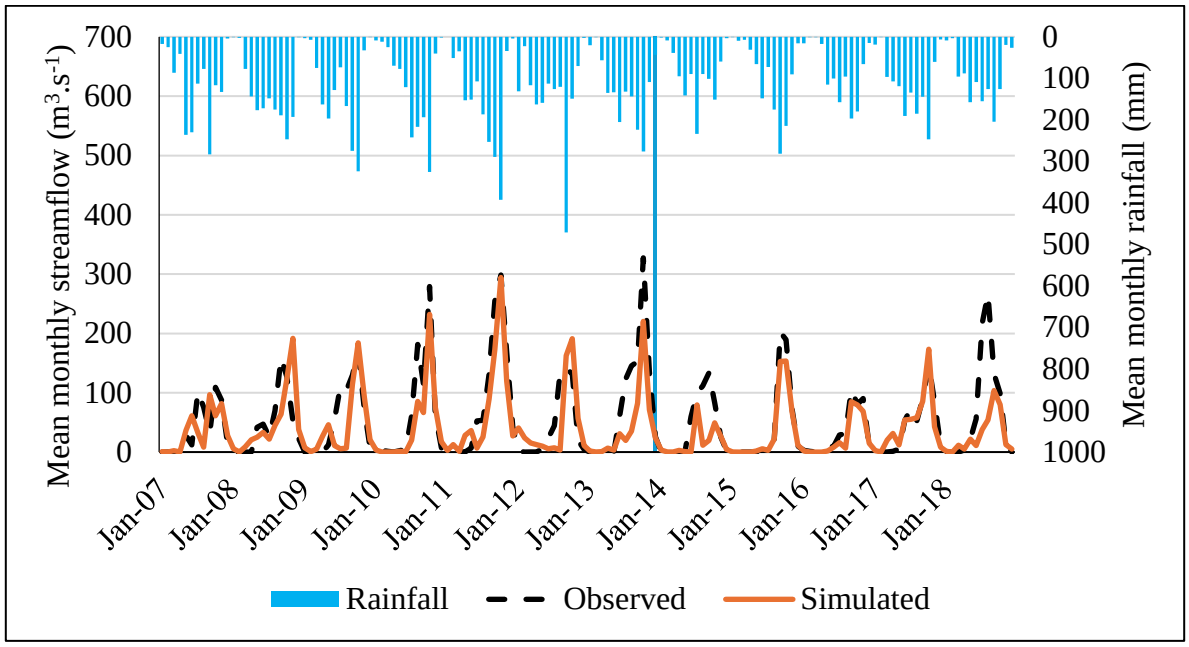

Figure 6-4 Hydrograph of observed and simulated streamflow for the calibration (2007-2013) and the validation (2014-2018)

consistent with the publication of Neitsch et al. (2011). According to Dingman (1994), evapotranspiration exceeds runoff in most watersheds and on all continents except Antarctica. The hydrologic water balance ratios of each component (streamflow/rainfall, baseflow/total flow, surface runoff/total flow, ET/rainfall) were well examined by SWAT Check.

Table 6-6 Components of the hydrologic water balances for the simulation period (2007-2018).

	Hydrologic water balance (mm)
Rainfall	1329.7
Evapotranspiration	908.9
Surface runoff	202.54
Lateral flow	29.4
Baseflow	215.33
Water yield	418

6.3.2 Meteorological Data Analysis

The primary objective of bias correction was to spatially downscale to point data (Maraun, 2016). The downscaling of GCM-RCM to represent climatology in the upper Sangker River basin was achieved through statistical downscaling. Figure 6-5 illustrates the distribution of historical rainfall (1986-2001) and raw simulated CNRM-CM5-RCA4 rainfall (2030-2045) under 2 climate scenarios (RCP4.5 and RCP8.5), along with observed rainfall (1986-2001). The graph of historical rainfall from the climate model output (CNRM-CM5-RCA4) did not closely match the observed rainfall. Additionally, it highlighted the differences between the historical and raw simulated CNRM-CM5-RCA4 rainfall, indicating potential signals of future rainfall change.

The maximum and minimum temperatures in the study area exhibited similar rainfall change signals. Figure 6-6 and Figure 6-7 revealed significant bias between the historical and observed maximum and minimum temperatures of the climate model output. Furthermore, the observed minimum and maximum temperature curves were notably distinct.

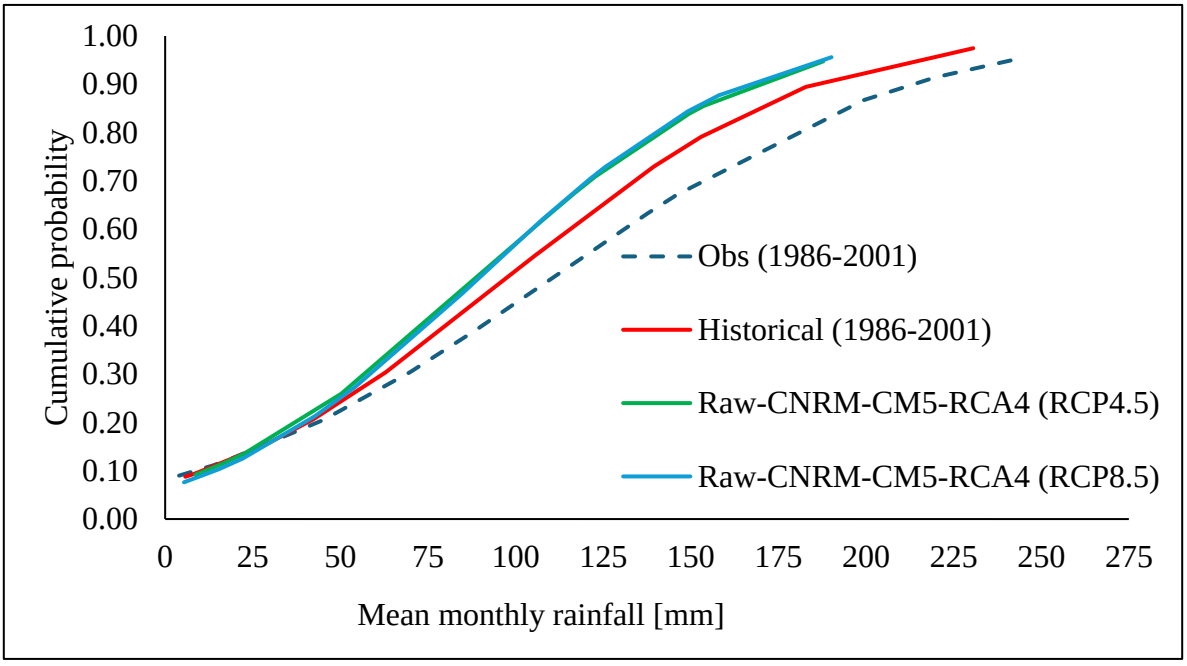

Figure 6-5 Rainfall quantiles (observed and raw data)

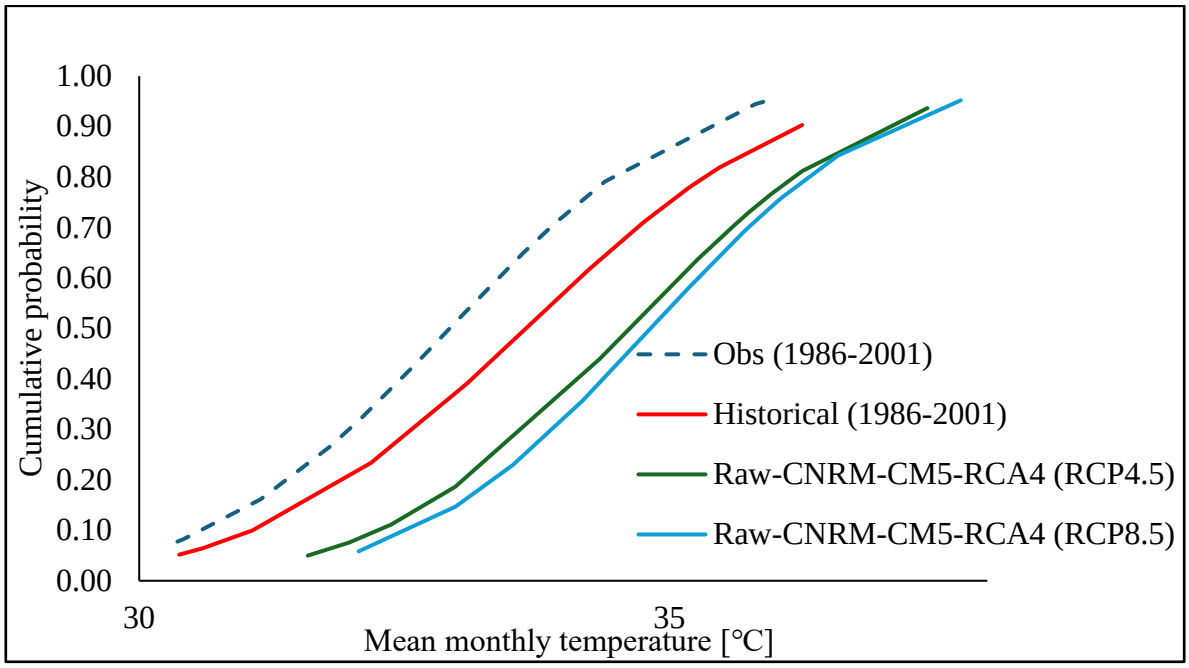

Figure 6-6 Max-temperature quantiles (OBS & Raw data)

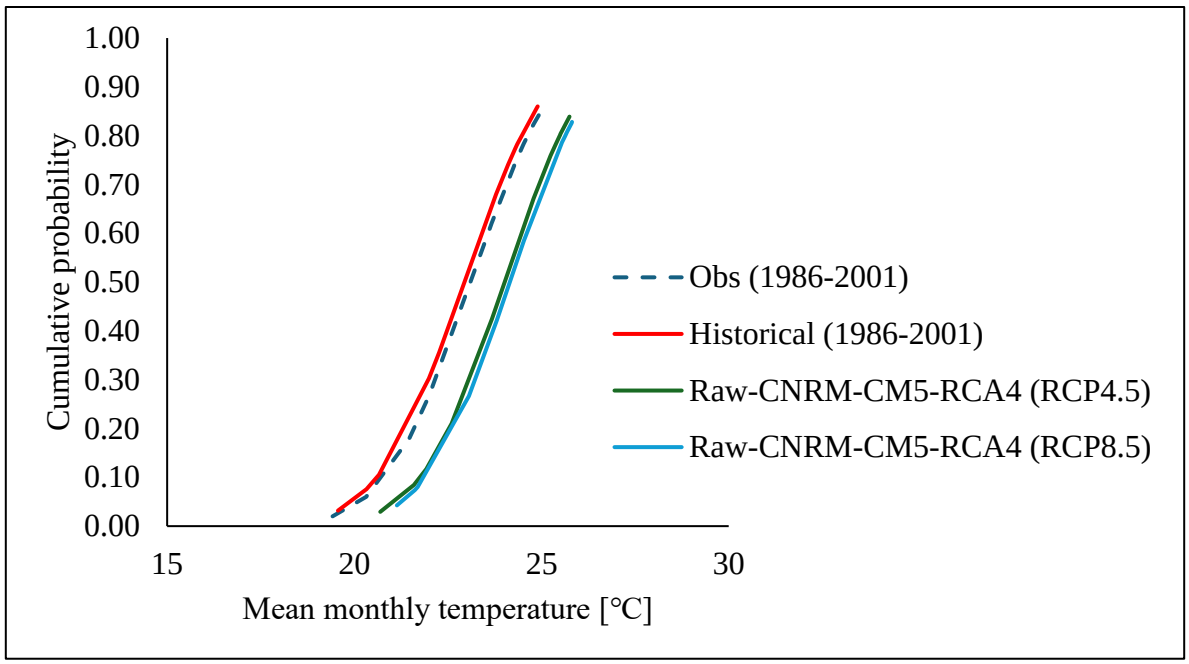

Figure 6-7 Min-temperature quantiles (OBS & Raw data)

6.3.2.1 Projected Changes in Rainfall

The projected change of mean annual rainfall cycle in the catchment for the period of 2030-2045 will undergo a decrease from 1,328 to 1,227 and to 1,231, which accounts for about -7.63% and -7.28% for the RCP4.5 and RCP8.5 respectively, compared to the baseline 1986-2001 (Figure 6-8). Figure 6-8 clearly shows the seasonal rainfall pattern of future changes in mean monthly precipitation produced by CNRM-CM5-RCA4 compared to the observed baseline in the upper Sangker River basin. Rainy season (May-October) rainfall would generally decrease by 4.48% and 9.47% for the RCP4.5 and RCP8.5 respectively. However, there are certain months within the rainy season, such as June, July, and August, where rainfall is projected to increase. In addition, there is a noticeable shift in the timing of peak rainfall, with projected peak rainfall in August as opposed to observed peak rainfall in October, indicating an earlier onset of climate change. The projected change in the dry season indicates a significant decrease of about 22% for the RCP4.5 scenario but a slight increase of 2.65% for the RCP8.5 scenario.

6.3.2.2 Projected changes in temperature

The relationship between the observed maximum and minimum temperatures and their simulations in the upper Sangker River basin exhibited a strong correlation, consistent with the observed temperature trends (refer to Figure 6-9 and Figure 6-10). The data were averaged at the target station for the reference period 1986-2001 and the scenario period 2030-2045. Figure 6-9 and Figure 6-10 indicate a general increase in air temperature across all months, both for maximum and minimum temperatures. It is projected that the maximum air temperature will likely rise by 0.97 and 1.16 degrees Celsius for RCP4.5 and RCP 8.5, respectively, by 2030-2045 compared to the average historical observations between 1986-2001 under intermediate and high emission scenarios. This temperature increase is expected to be most pronounced during the dry season months. Similarly, the minimal air temperature is predicted to increase by 1.08 and 1.22 degrees Celsius for the intermediate (RCP4.5) and high (RCP8.5) emission scenarios, respectively, for the 2030-2045 period. The RCP8.5 emission scenario shows a higher magnitude of change compared to RCP4.5.

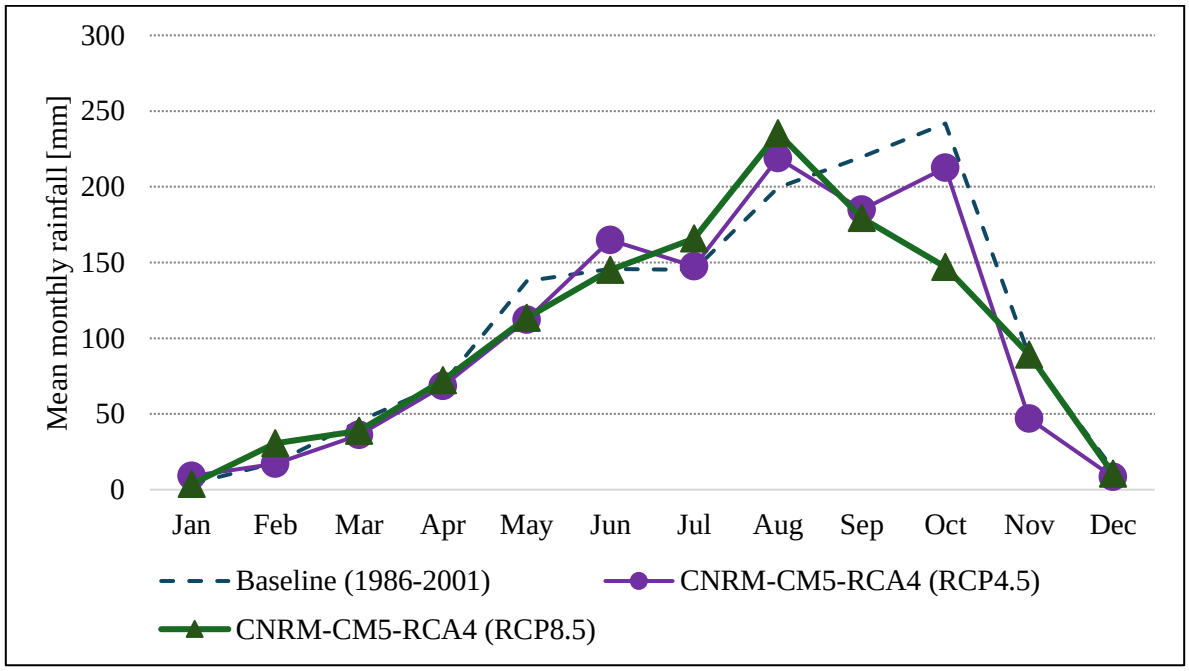

Figure 6-8 Seasonal variation of monthly rainfall represents rainfall distribution in the upper Sangker River basin between baseline (1986-2001) and future (2030-2045).

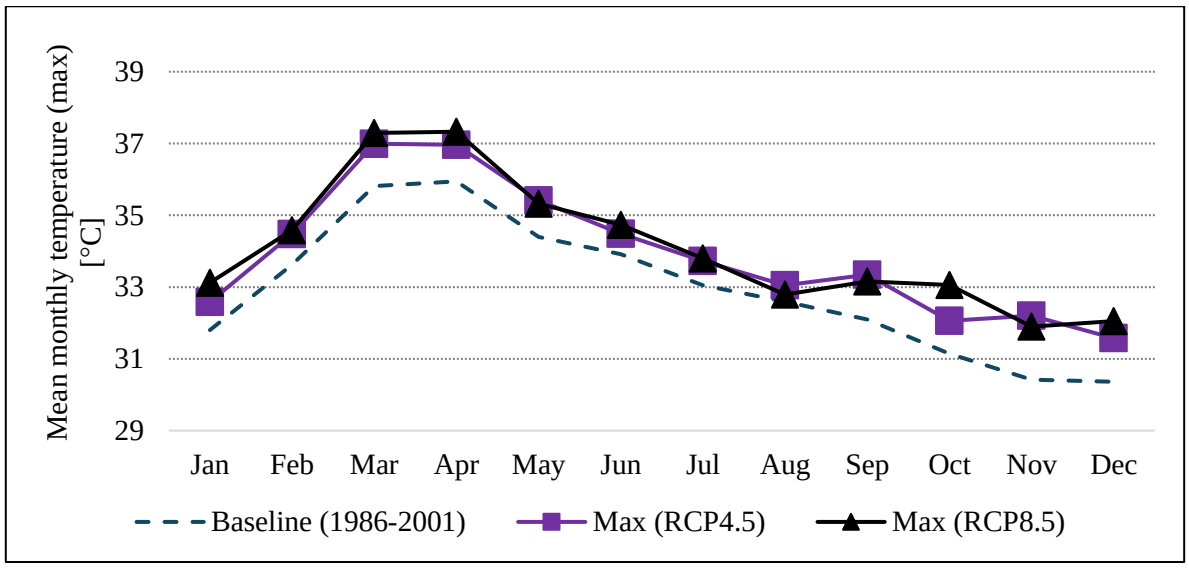

Figure 6-9 Seasonal variation of maximum temperature: baseline (1986-2001) and future (2030-2045).

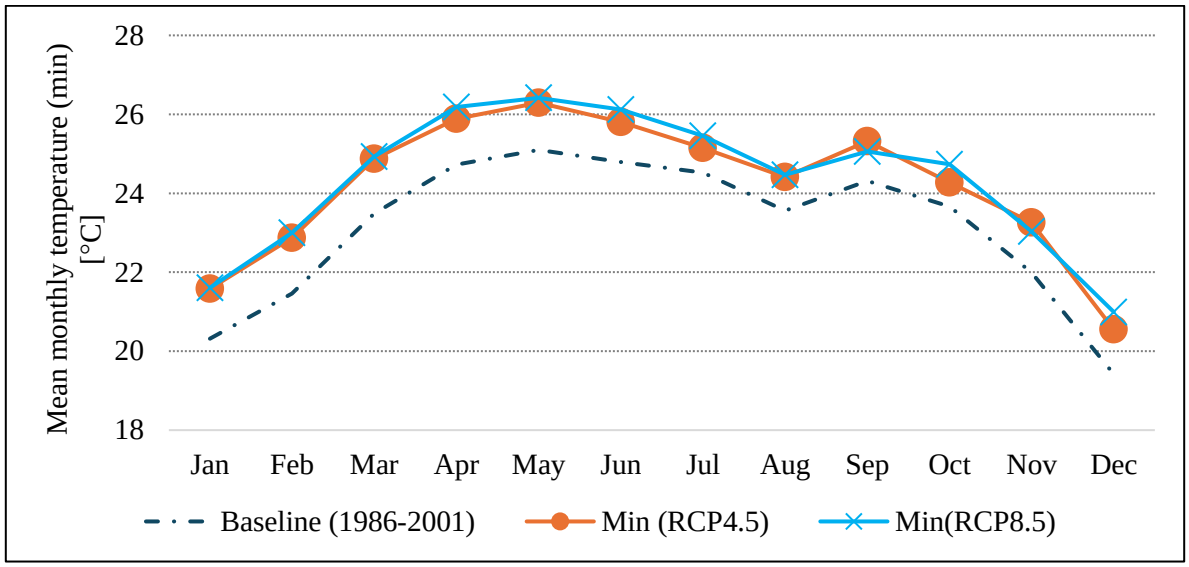

Figure 6-10 Seasonal variation of minimum temperature: baseline (1986-2001) and future (2030-2045).

6.3.3 Hydrological impacts of land use change

The impact of land-use changes on streamflow and hydrological cycle for model scenario 1 is illustrated in Figure 6-11 and Figure 6-12. The mean annual streamflow from the upper Sangker River basin under the baseline (1986-2001) is 33.35 $m^3.s^{-1}$. In Figure 6-13, it is evident that the overall annual streamflow at the outlet (gauging station) remains consistent across all land use (LU) scenario setups. However, the annual streamflow increases for both LU setups (LU2030 and LU203+LUDP). The average annual streamflow sees a 30.89% increase (see Figure 6-13), while the intervention of the land use development project results in a 30.49% increase. This trend of increased streamflow is observed in both wet and dry seasons, with the most significant change occurring in the wet season (May to October). The change to increasing streamflow in the dry season is relatively smaller, likely due to less rainfall during this period. The impact of reforestation on streamflow under land use development projects is shown in Figure 6-13. The data indicates that there is minimal change in streamflow as a result of reforestation. However, it consistently lags behind the expected impact based on historical changes in land cover. When forest cover is converted to agricultural land, there is an increase in river discharge. Therefore, the hydrological simulation shows that streamflow increases in both seasons,

suggesting a clear relationship between the hydrological system and changes in vegetation.

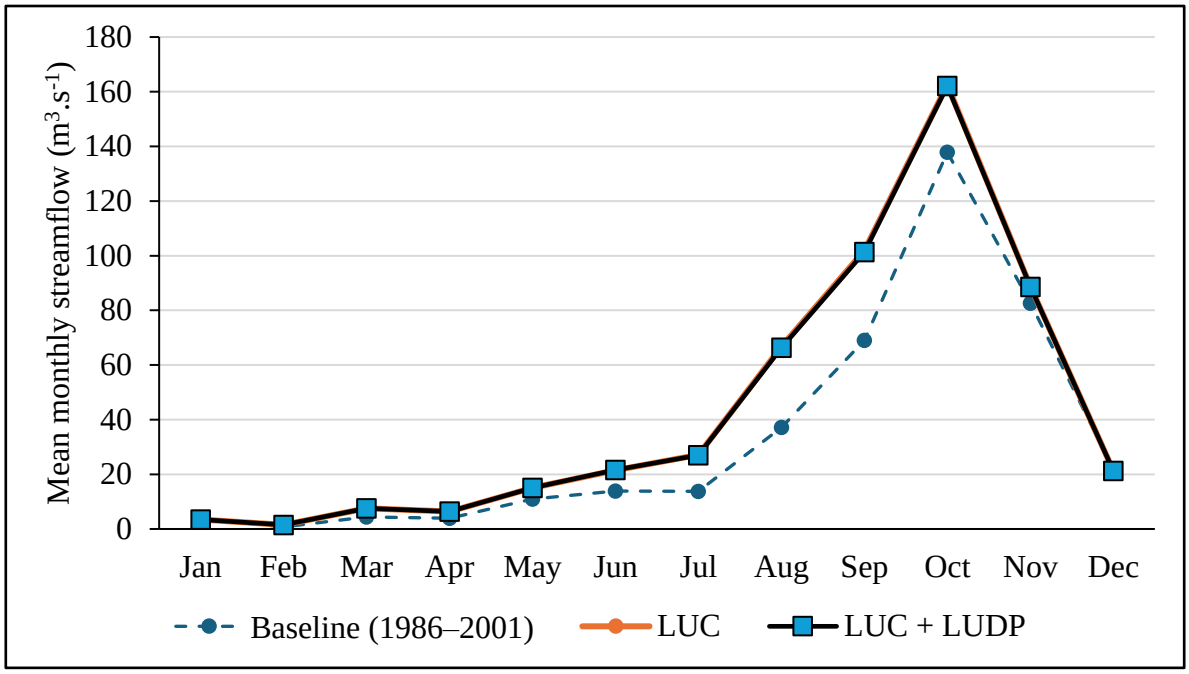

Figure 6-11 Mean monthly streamflow at gauging station in Battambang city within the simulation period (1986-2001).

Figure 6-12 compares the mean annual hydrologic water balance components between the land-use (LU) scenario in 2030 and the baseline LU2002. The figure illustrates the impact of land-use change on various hydrologic water balance components such as water yields, surface water, and evapotranspiration from 1986 to 2001 in the subbasins. It indicates an increase in surface runoff and water yield, predominantly in the farmland area in the middle part of the basin. Specifically, the middle part shows an increase in surface runoff from 0 to 176 mm per year and an increase in average total water yields from 40 to 208 mm. Conversely, evapotranspiration in that area decreases across most subbasins. Changes in water yields and surface water are less noticeable, and most subbasins show a slight decreasing trend. Evapotranspiration varies considerably depending on the variation in soil and land cover characteristics across the basin. Evapotranspiration decreases from the middle to the northern area, which is mainly covered by farmlands. However, there is an increase in evapotranspiration in the forest area, which is characterized as a mountainous area.

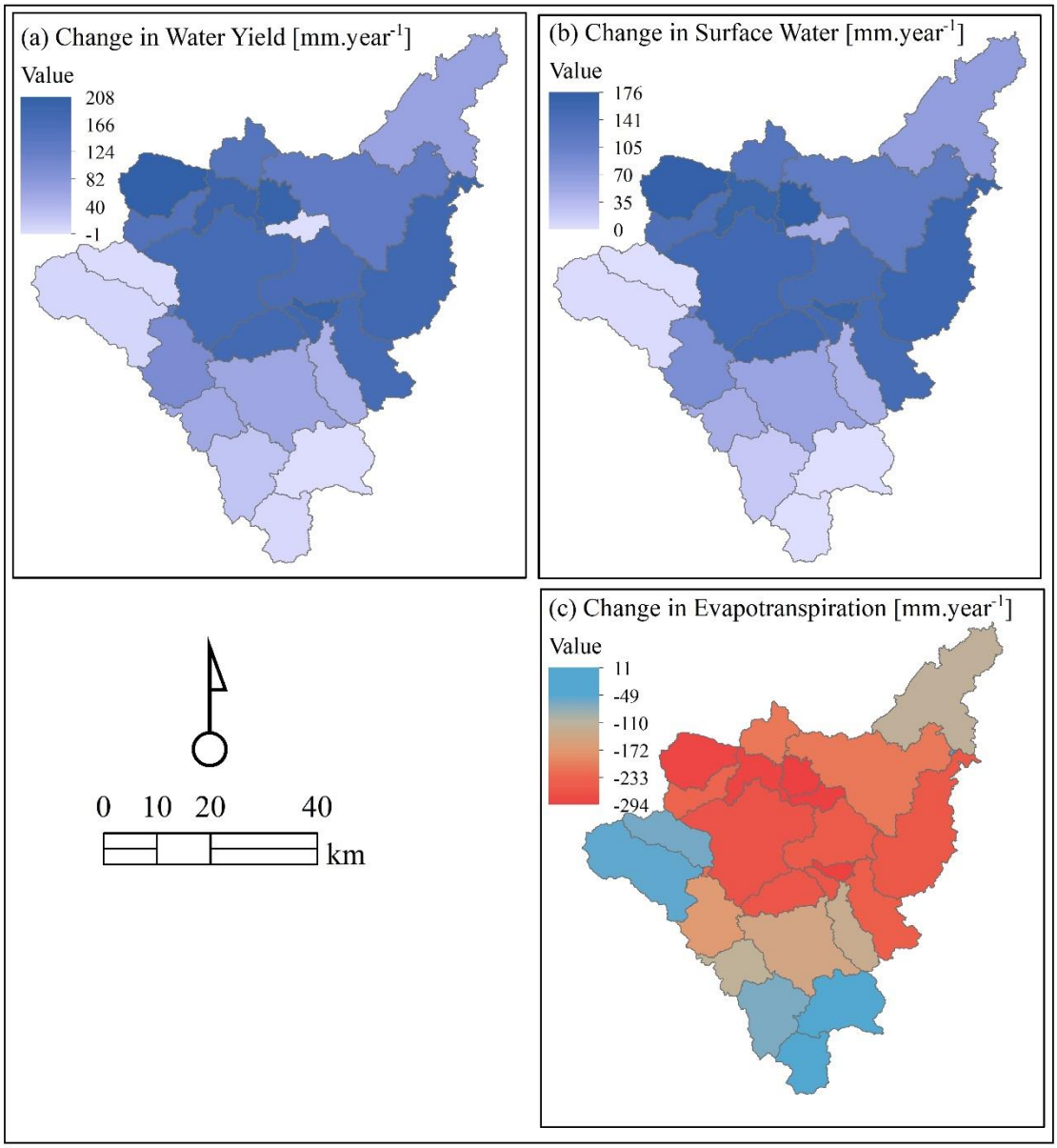

Figure 6-12 Map of the spatial distribution of mean annual values of (a) water yield distribution, (b) surface water distribution, and (c) evapotranspiration for the subbasins within the simulation period (1986-2001) for the land use change to the year 2030.

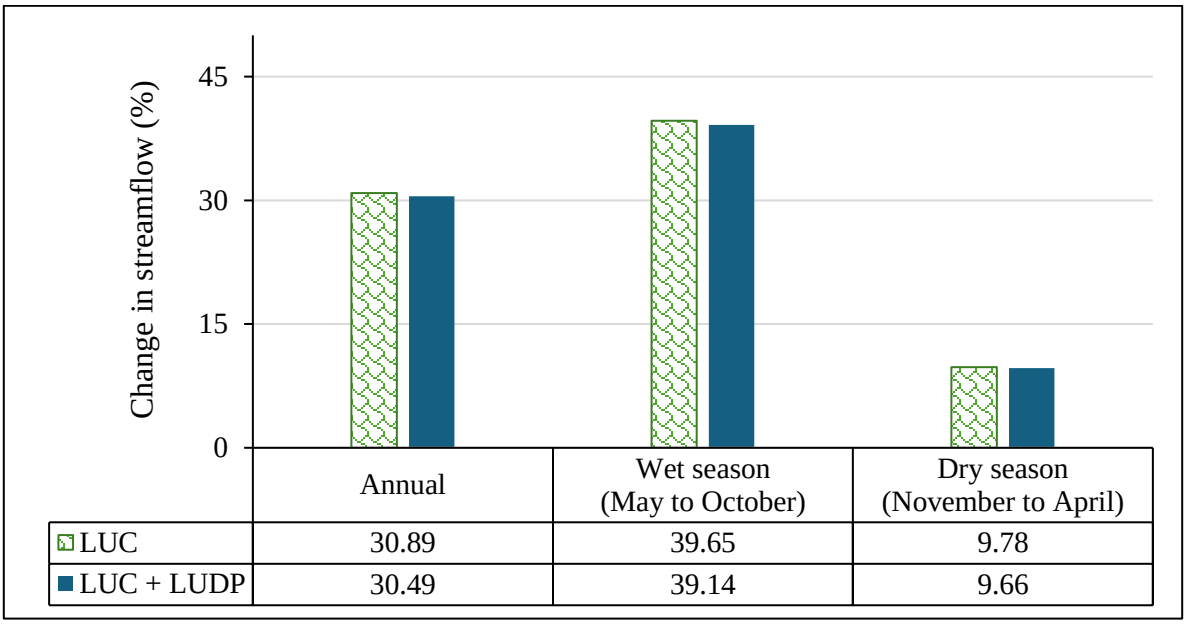

	Annual	Wet season (May to October)	Dry season (November to April)
LUC	30.89	39.65	9.78
LUC + LUDP	30.49	39.14	9.66

Figure 6-13 Percentage change in streamflow within the simulation period (1986-2001) for the land use change to 2030.

6.3.4 Hydrological impacts of combined land use and climate changes

The combined impact of land use and climate changes on water resources is demonstrated in Figure 6-14 and Figure 6-15 by projecting rainfall and temperature data from the GCM-RCM output under RCP4.5 and RCP8.5 climate scenarios and land use map in 2030 was set as land use change scenario. The combined effects show the streamflow is higher from May to October and lower in the remaining months (Figure 6-14), consistent with the pattern of rainfall distribution in the catchment (Figure 6-8). The average annual streamflow is expected to increase by 5.65 % and 3.16% under the RCP4.5 and RCP8.5, respectively, for 2030-2045 compared to baseline 1986-2001 (Figure 6-16). Figure 6-14 illustrates that climate change may have a significant potential impact on streamflow. Climate change has a huge impact on water resources, much more than land use change. Although there is uncertainty in projecting climate estimation, annual streamflow is expected to increase. The most extensive relative changes in streamflow occur in wet season months (e.g., June, July, and August). In the wet season, streamflow is likely to increase by 23.32% and 10.92 for RCP4.5 and RCP85, respectively. Conversely, average streamflow is remarkable, with a high decrease of 36.90% and 15.52% in the dry season for

both climate scenarios (Figure 6-16). Both land use change scenarios exhibit similar results on water resource impacts. The potential impact of integrated land cover and climate variation indicates a substantial increase in the wet season leading to floods caused by an increasing volume of upstream water, and drought risk occurs in the dry season.

Figure 6-15 shows spatially explicit changes to the projected climate data (2030-2045) of water yield (Figure 6-15a), surface runoff (Figure 6-15b), and evapotranspiration (Figure 6-15c) in the upper Sangker River basin. The annual average of water yield and surface runoff shows a generally increasing trend of 5.85% and 23.49% for RCP4.5, respectively, and of 3.27% and 22.87% for RCP8.5, respectively (Table 6-7). In contrast, evapotranspiration is likely to decrease by -16.04% and -14.81% in the annual average percentage change for RCP4.5 and RCP8.5 climate scenarios, respectively.

In the middle part of the basin, which is mostly farmland, the water yield component has increased by more than 34 mm to 118 mm on average annually (Figure 6-15). In contrast, in the south and north, where the land use is dominated by forest area and paddy fields, the water yield has decreased by a range of -7 to -92 mm. The pattern of the overall surface runoff follows a similar trend to water yield, with a decreasing tendency in the south and north of the basin, reaching a low of -59 mm. However, surface runoff mostly tends to increase in the central basin, ranging from 11 to 117 mm, except for one subbasin characterized by a mountain area. Figure 6-15 illustrates a general decrease in evapotranspiration across various subbasins, with values ranging from -20 to -313 mm. The most significant reduction in evapotranspiration occurs in the central part of the basin, while the least pronounced decrease is observed in areas with mountainous terrain covered by forests and in the northern region dominated by mixed residential, farmland, and rice fields.

Based on the results of the land use development project (LUC+LUDP) model simulation, it is evident that there is a minimal impact on water resources. The data reveals a slight decrease in surface runoff, water yield, and evapotranspiration compared to the LU2030 scenario (refer to Table 6-7). The implementation of reforestation has resulted in a reduction in surface runoff, thus aiding in the mitigation of flash floods in the subbasin.

However, Figure 6-17 demonstrates an increase in evapotranspiration within a specific subbasin where the forest communities under the land use policy are situated.

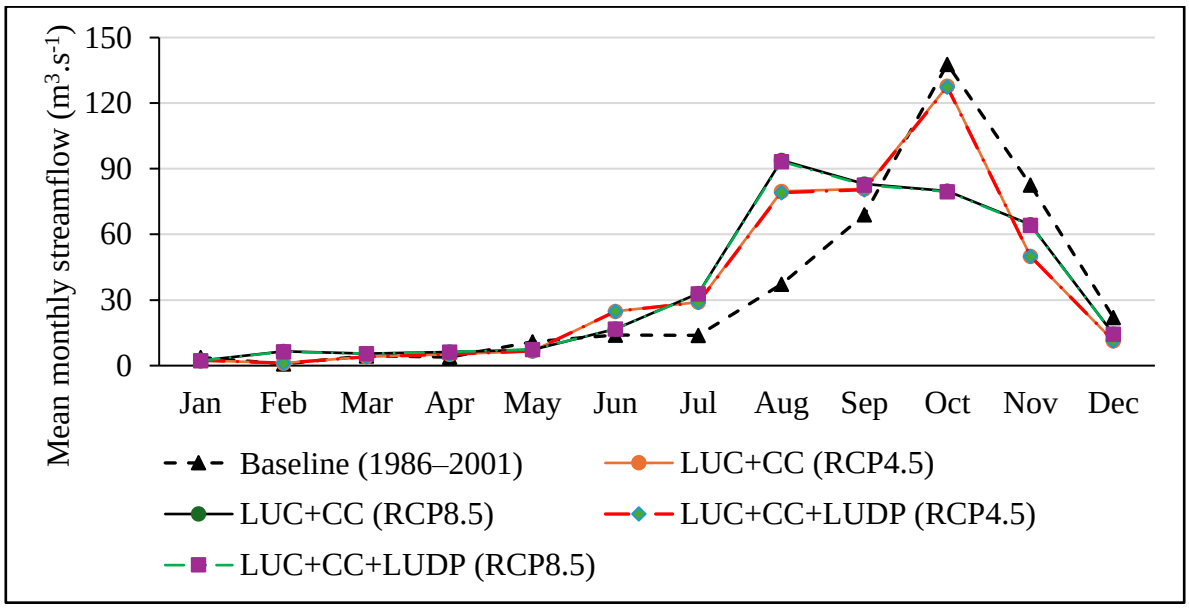

Figure 6-14 Mean monthly streamflow at gauging station between baseline (1986-2001), and future (2030-2045) with climate scenario RCP4.5 and RCP8.5 and simulated using land use map in 2030.

Table 6-7 Projected change of annual average water yield, surface runoff, and evapotranspiration between baseline (1986–2001) and future (2030–2045) based on RCP4.5 and RCP8.5 scenarios. Numbers in parentheses represent the changes in percentage.

Hydrologic water balance components		Change in mm (%) for combined land use and climate change		Change in mm (%) for combined land use change integrated with LUDP and climate change	
	Baseline	RCP4.5	RCP8.5	RCP4.5	RCP8.5
Water yields	359.43	21.02 (5.85)	11.76 (3.27)	21.00 (5.84)	11.76 (3.27)
Surface runoff	175.07	41.12 (23.49)	40.04 (22.87)	40.50 (23.14)	39.45 (22.53)
Evapotranspiration	926.12	-148.57 (-16.04)	-137.15 (-14.81)	-141.33 (-15.26)	-129.92 (-14.03)

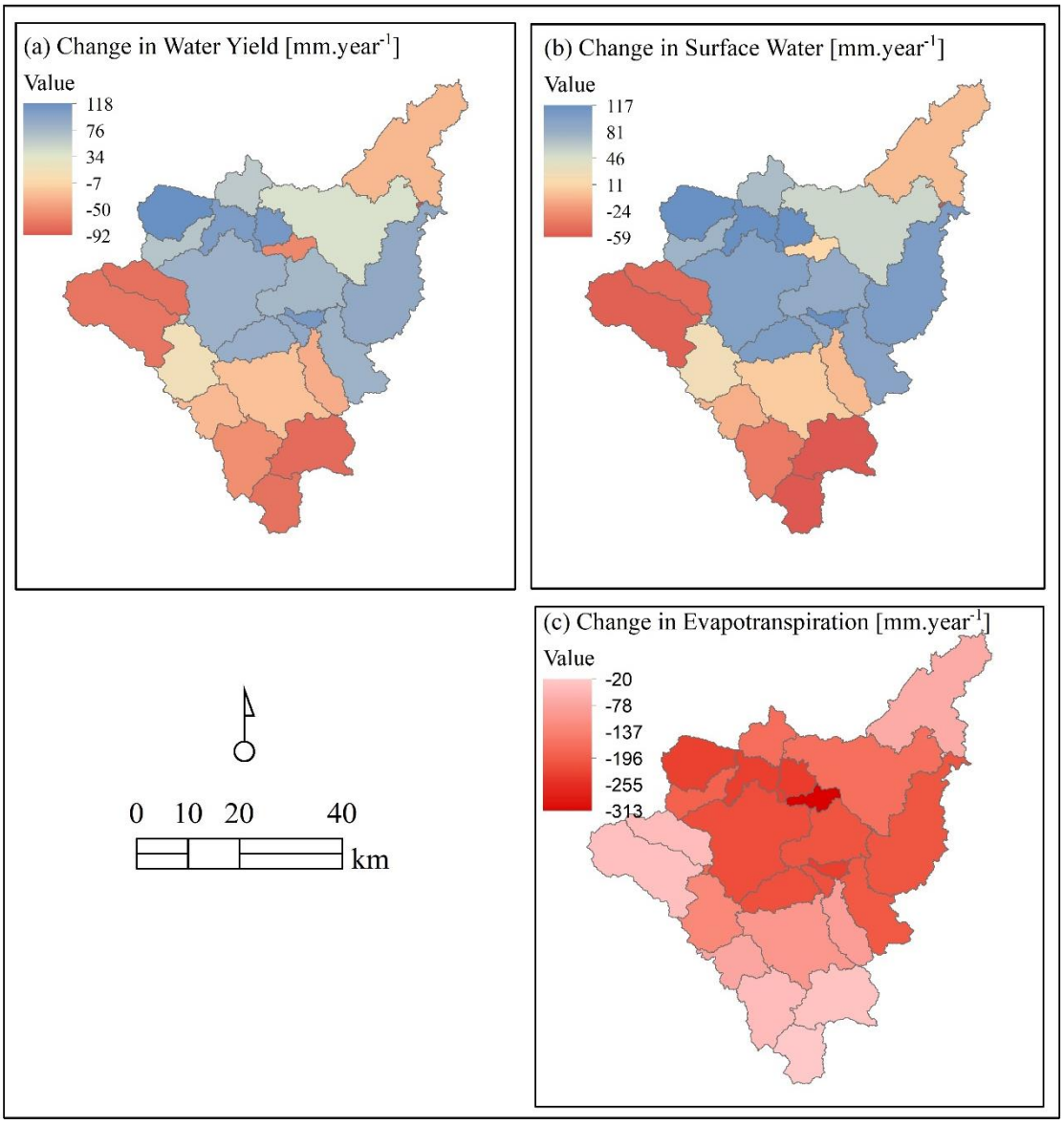

Figure 6-15 Map of the spatial distribution of mean annual values of (a) water yield distribution, (b) surface water distribution, and (c) evapotranspiration for the subbasins for the future (2030-2045) compared to baseline (1986-2001). The model run used LU2030 and climate data for the period 2030 to 2045 with the RCP4.5 and RCP8.5 scenarios as input (Table 6-7).

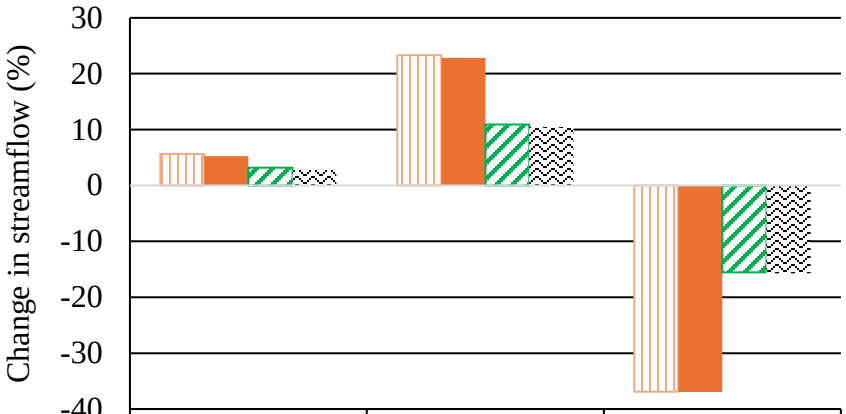

	Annual	Wet season (May to October)	Dry season (November to April)
LUC+CC (RCP4.5)	5.65	23.32	-36.90
LUC+CC+LUDP (RCP4.5)	5.28	22.83	-36.98
LUC+CC (RCP8.5)	3.16	10.92	-15.52
LUC+CC+LUDP (RCP8.5)	2.78	10.45	-15.70

Figure 6-16 The average change in streamflow in percentage at the basin outlet (gauging station) for the future (2030–2045) compared to the baseline (1986–2001).

In the dry season, hydrologic water balance components - water yield, surface runoff, and evapotranspiration - are projected to decrease for all subbasins of the upper Sangker River basin under climate scenario RCP4.5 (Figure 6-18). For the most likely future climate (2030-2045) and changing landscape in 2030, water yield is projected to decline from -29 mm to -54 mm across the basin. The greatest decrease is expected in the north and south of the basin. The pattern of surface runoff is similar, with a decrease ranging from -4 to -26 mm from the upland to the mountain area. Similarly, evapotranspiration is predicted to decrease in every subbasin, with a range of -5 mm to -56 mm. The most likely change in evapotranspiration is expected in the upland area of the central basin.

Nevertheless, the projected change in surface water during the dry season under climate scenario RCP8.5 is expected to lead to an increase of up to 24 mm in all subbasins (see Figure 6-19). This represents a predicted increase of 39.67% for the entire dry season (refer to Table 6-8). The changes in water yield and evapotranspiration associated with this climate scenario show a lesser impact (approximately 50%) when compared to RCP4.5.

Furthermore, evapotranspiration demonstrates an increasing trend of up to 11 mm in the mountain area (southern basin) and in the paddy field (northern basin).

Table 6-8 Projected average change in dry season of water yield, surface runoff, and evapotranspiration between baseline (1986–2001) and future (2030–2045) based on RCP4.5 and RCP8.5 scenarios. Numbers in parentheses represent the changes in percentage.

		Change in mm (%) for combined land use and climate change		Change in mm (%) for combined land use change integrated with LUDP and climate change	
	Baseline	RCP4.5	RCP8.5	RCP4.5	RCP8.5
Water yields	106.17	-37.45 (-35.27)	-16.14 (-15.20)	-37.03 (-37.88)	-15.76 (-14.84)
Surface runoff	33	-12.71 (-38.51)	13.09 (39.67)	-12.59 (-38.16)	13.18 (39.95)
Evapotranspiration	261.19	-27.75 (-10.62)	-11.78 (-4.51)	-27.39 (-10.48)	-11.38 (-4.35)

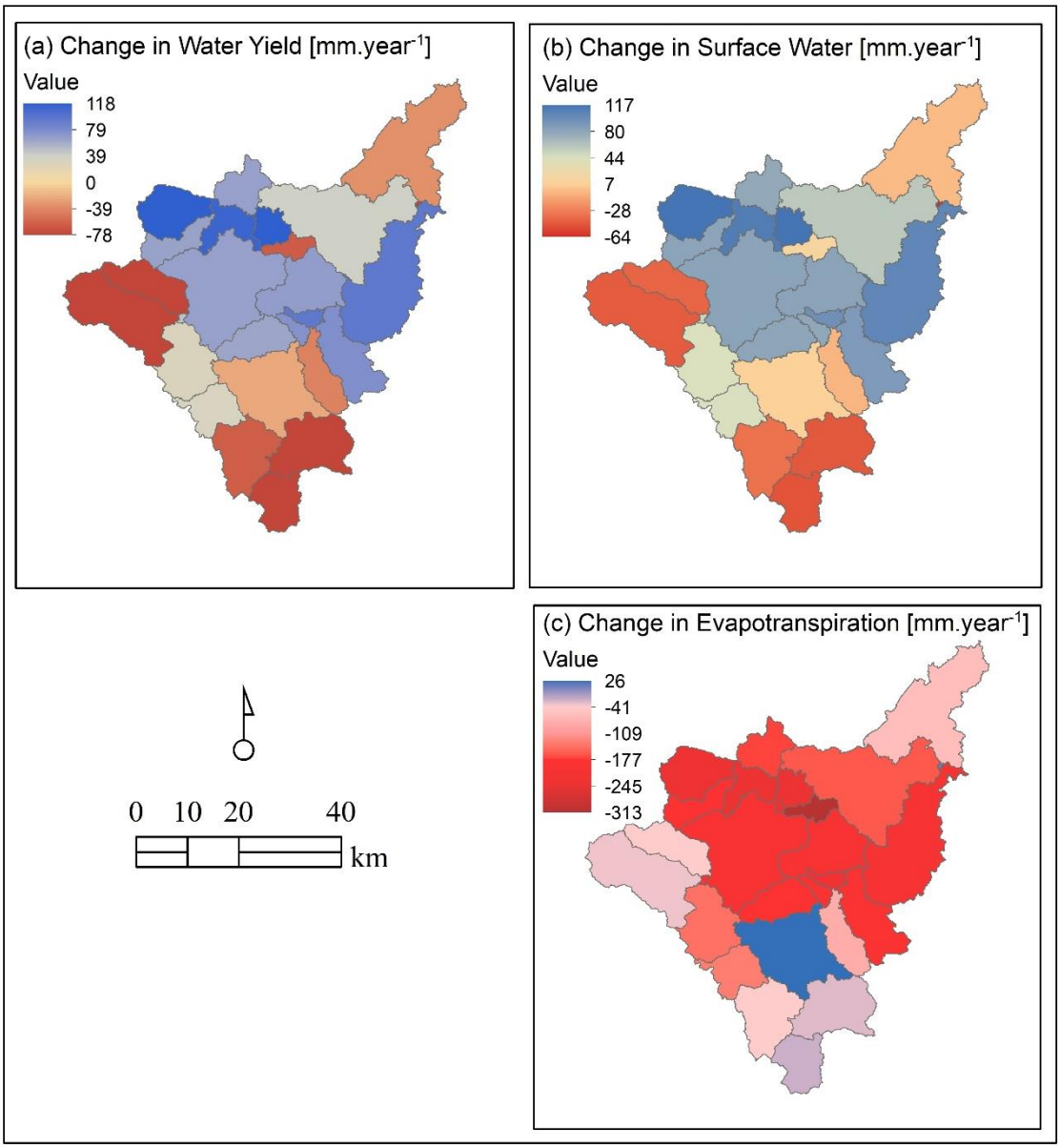

Figure 6-17 Map of the spatial distribution of mean annual values of (a) water yield distribution, (b) surface water distribution, and (c) evapotranspiration for the subbasins for the future (2030-2045) compared to baseline (1986-2001). The model run used LU2030+LUDP, and climate data for the period 2030 to 2045 with the RCP4.5 and RCP8.5 scenarios as input (Table 6-7).

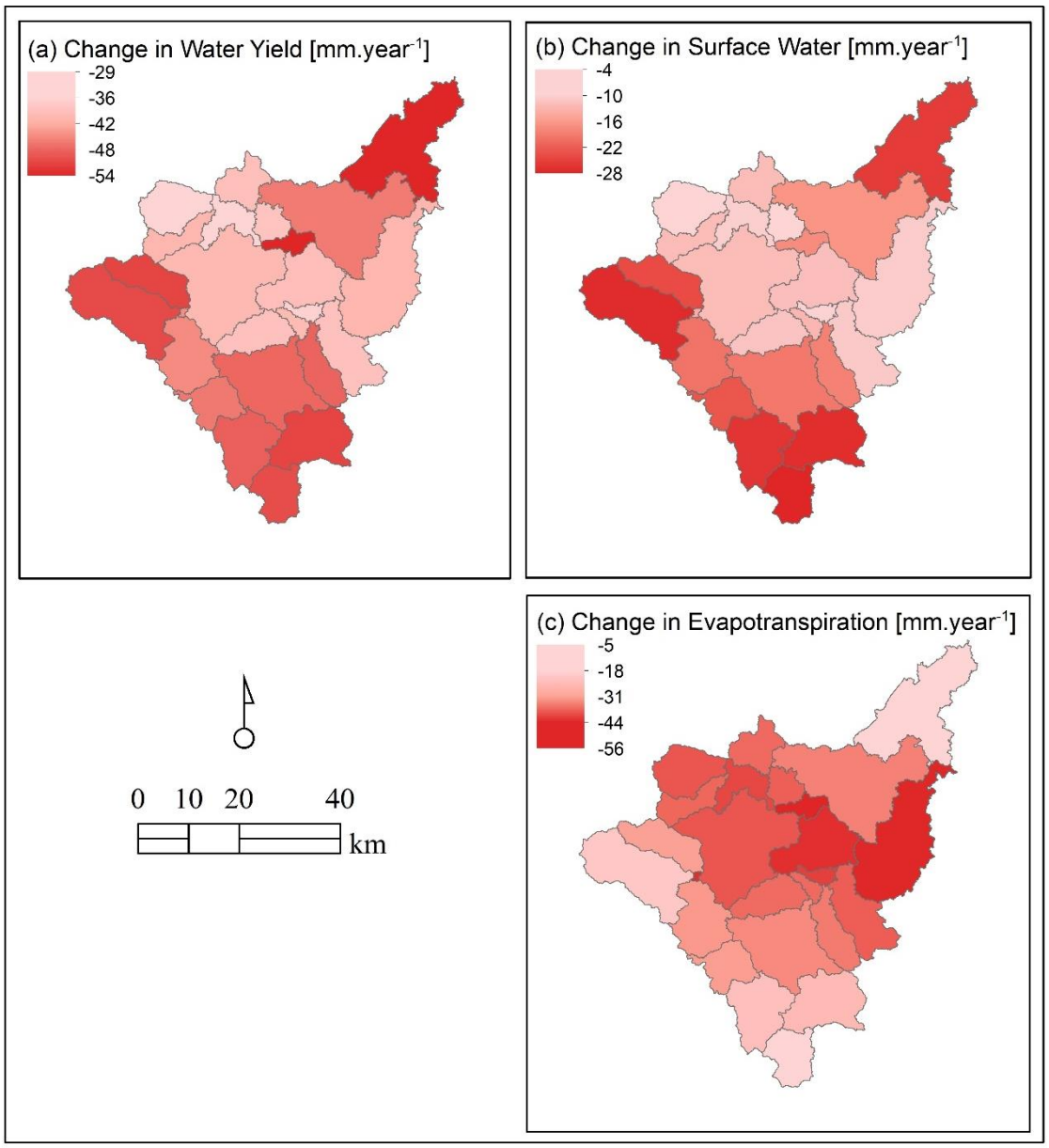

Figure 6-18 Map of the spatial distribution of projected change in the dry season of (a) water yield distribution, (b) surface water distribution, and (c) evapotranspiration for the subbasins for future (2030-2045) based on RCP4.5 scenario compared baseline (1986-2001), model run used LU2030.

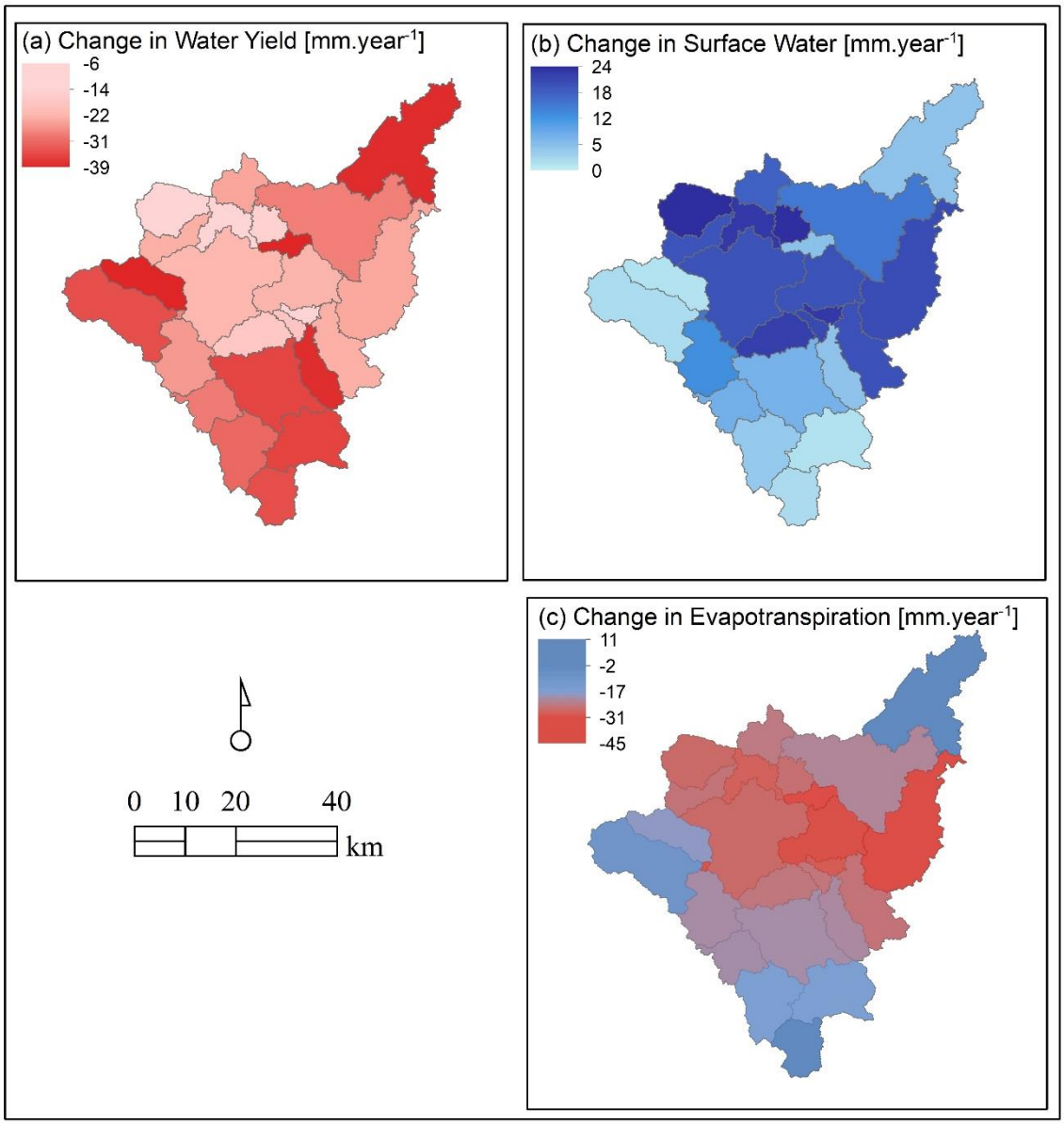

Figure 6-19 Map of the spatial distribution of projected change in the dry season of (a) water yield distribution, (b) surface water distribution, and (c) evapotranspiration for the subbasins for future (2030-2045) based on RCP8.5 scenario compared baseline (1986-2001), model run used LU2030.

6.4 Discussion

6.4.1 Climatology bias

It's important to understand the changes in precipitation extremes because they will have a significant impact on any assessment. This study used the delta change method based on GCM-RCM model output from CORDEX-SEA to downscale future climate statistically. The climate projections for the future (2030-2045) in the upper Sangker River basin are shown in Figure 6-8, Figure 6-9 and Figure 6-10, for rainfall, maximum, and minimum temperatures, respectively. The projected change in annual rainfall for the upper Sangker River basin by 2030-2045 indicates a decrease compared to the baseline 1986-2001 for both climate scenarios (RCP4.5 and RCP8.5). Air temperature is expected to increase across the basin, with the greatest increase being more than 1℃. Global warming and climate change have significantly affected the biosphere (Aizebeokhai, 2009). The projected rainfall and air temperature representing climate for the upper Sangker River basin in Battambang province show a similar trend to the findings of the neighboring province, Siem Reap, from Chim et al. (2021). Chim's investigation showed that average annual precipitation is projected to decrease by 56%, 54%, and 61% according to the RCP2.6, RCP4.5, and RCP8.5 scenarios, respectively. Mean annual temperature is also expected to increase by 1.83℃, 2.38℃, and 3.21℃ from 2018 to 2100 for scenarios RCP 2.6, RCP 4.5, and RCP 8.5, respectively.

The bias correction method is widely used in climate impact modeling (Maraun, 2016). Bias correction using the delta change method has shown consistency and good correlation with observed data after bias correction. Although it is considered a robust method (Bosshard et al., 2011; Graham et al., 2007), climate change signals are scaled and based solely on the observed data signal, resulting in uncertainty in the simulation of regional climate changes and the translation from the global climate model to the basin scale. Therefore, different downscaling techniques should be applied. Due to the limited model output of CORDEX-SEA at the time of our analysis, this study only applied one GCM-RCM output to simulate future climate change. This has a significant impact on

hydrological simulation, while most studies applied a mean ensemble of different GCMs (Trang et al., 2017; Shrestha et al., 2018). Applying the ensemble technique enables better estimation of certain results and can improve accuracy, as climate models describe climatological processes in different ways, and there can be significant variation.

6.4.2 Assessment of land use and climate change on water resources

The alteration of land use has a significant impact on streamflow dynamics and water balance budgets as illustrated in Figure 6-11 and Figure 6-12. The reduction in forest cover and expansion of agricultural land has led to an increase in mean annual and seasonal streamflow within the upper Sangker River basin. The extensive conversion of upstream evergreen forest in recent decades has notably altered the streamflow at the basin outlet. This change is attributed to an increase in surface runoff and water yield in agricultural land (farmland) due to reduced infiltration. This study aims to elucidate the influence of large basins, such as the upper Sangker River basin, on catchment hydrologic water balance over a spatio-temporal scale.

The analysis of individual land use changes indicates that the average annual streamflow is projected to increase by 30.89% (Figure 6-13). Similarly, river flow in both wet and dry seasons is expected to increase by 39.65% and 9.78%, respectively. The upland area covered by farmland has exhibited the most significant changes in surface runoff and water yield, with volumes increasing by 70 to 176 mm and 82 to 208 mm, respectively (Figure 6-12). Notably, upstream deforestation may contribute to exacerbated flood events downstream, particularly during wet seasons. This change is primarily attributed to deforestation activities, expansion of agricultural land, and economic land concessions. Urgent measures are necessary to conserve and protect the upstream forest, which serves as a primary source of rainfall.

The combined impact of climatic and land use changes may lead to the degradation of water resources in the upper Sangker catchment. When assessing the combined influence of land use and climate change, it is projected that the average annual streamflow will experience a modest increase of only 5.65% and 3.16% under the RCP4.5 and RCP8.5

scenarios, respectively (Figure 6-16). This underscores the notion that the impact of climate change surpasses that of land use change. The combined changes in land use and climate are expected to increase surface runoff and water yield for RCP4.5 and RCP8.5, respectively. However, decreased evapotranspiration will exhibit an opposing trend. The combined effects of climate variability and land use change are likely to result in increased river discharge, water yield, and surface runoff during the wet season while causing a decrease during the dry season. Consequently, severe flooding in the wet season and drought in the dry season may be anticipated.

Our findings align with the research by Sok et al. (2021); however, they contradict the results presented by Oeurng et al. (2019). Oeurng et al. (2019) projected changes in river flow for the 2030s, 2060s, and 2090s using different GCMs, such as GISS-E2-R-CC, IPSL-CM5-MR, and GFDL-CM3, to simulate climate change without considering changes in land use during each time horizon. This approach may have led to inconsistent results. Nevertheless, the changing trend of river flow in both the dry and wet seasons remains similar. The development of land use projects, particularly afforestation, is indicated to have a minimal impact on changes in water resources (Table 6-7 and Table 6-8).

The evaluation of the impact of land use and climate change on streamflow and hydrological systems relies heavily on SWAT modeling. The reliability of hydrological models enhances confidence in projected climate change impacts and reduces uncertainty in the associated projections (Krysanova et al., 2018). Data scarcity poses a significant challenge for hydrological modeling in our study area due to constraints faced by the local government, including limited budget and staff. Owing to the limited number of rainfall stations, climate data analysis in this study was based on a single methodological station. The hydrograph (Figure 6-4) and the statistical quantitative analysis (Table 6-5) indicate satisfactory performance of the SWAT model during calibration and validation. However, peak flow during the calibration period was overestimated in 2009 and 2013 and underestimated in 2013. The availability of outflow data from the dam and headwork led to the exclusion of the SWAT simulation. The performance of the SWAT model could be attributed to the structure of the hydrological model and uncertainties in parameter

estimation (Jiang et al., 2007). Additionally, the uncertainty of the climate change signal is reflected in the extensive range of GCM-RCM model runs. Many studies have utilized a combination of global climate models and ensemble approaches to enhance the accuracy of climate projections. This approach allows for the cancellation of errors from different GCMs and the downweighing of poorly performing GCMs (Her et al., 2019; Christensen and Lettenmaier, 2007; Yira et al, 2017; Shrestha et al., 2018; Pierce et al., 2009). This study assessed the impact of future climate change on water resources using a single GCM-RCM (Table 6-2) based on the availability of model output for the time analysis from CORDEX-SEA. However, as noted by Najafi et al. (2011), the uncertainty of hydrological models is considerably smaller than that of GCMs.

This study analyzed a subbasin scale to estimate future streamflow and hydrologic water balance components under the influence of land use and land cover change (LULC) and climate change. The findings reveal that the conversion of forest cover to agricultural land resulted in an increasing trend of river discharge, water yield, and surface runoff in scenarios of land use change. Average annual evapotranspiration is decreasing across the subbasin and is higher in farmland. However, with the combined impact of land use and climate change, the average annual discharge shows a reduction in flow regime, leading to the most significant increasing and decreasing trends in the wet and dry seasons, respectively. While the impact of climate change outweighs the effects of land use change, the contribution of land use development policies, particularly forest conservation, remains substantial.

6.5 Conclusion

The study aimed to evaluate the influence of land use and climate on water resources in the upper Sangker River basin. Despite the limited number of meteorological stations, the use of SWAT hydrological modeling has proven to be an effective method for assessing the impacts of environmental changes, such as climate change and land cover development. A GCM-RCM was employed for climate process simulation for the future (2030-2045), and future land use change in 2030 was projected using the CA-Markov model. The results

indicated a substantial impact of land use and climate change on streamflow, water yield, surface runoff, and evapotranspiration. The individual impact of land use demonstrated an increasing trend in average annual river flow, surface runoff, and water yield for all scenarios, while evapotranspiration exhibited the opposite trend. When considering the combined impact assessment of climate and land use change, the average annual streamflow showed a reduction. Furthermore, the shift from natural forest to agricultural land resulted in a decrease in water yield and surface runoff in the forested areas and paddy fields, with evapotranspiration showing an overall decreasing trend across all subbasins of the upper Sangker River basin. The combined impact resulted in increased river discharge in the wet season and decreased discharge in the dry season, which may lead to both flood events and severe drought.

This study addresses a gap in previous research by assessing the combined effects of climate variability and land use changes in the upper Sangker River basin. It also identifies critical areas for maintaining the ecological system and supporting the socio-economy with respect to water resource benefits. The study underscores the importance of land use development under reforestation projects to help mitigate potential damages from these significant impacts.

Further research is needed to identify flood-prone areas and support sustainable water resource management. The present hydrological simulation suggests that extensive conversion of forest cover to agricultural land over recent decades, combined with climate change, has had an impact on river discharge and hydrologic water balance components in the upper Sangker River basin.

References

Abhishek, A., Das, N. N., Ines, A. V., Andreadis, K. M., Jayasinghe, S., Granger, S., ... & Phanikumar, M. S. (2021). Evaluating the impacts of drought on rice productivity over Cambodia in the Lower Mekong Basin. Journal of Hydrology, 599, 126291.

Arnold, J. G., Srinivasan, R., Muttiah, R. S., & Williams, J. R. (1998). Large area hydrologic modeling and assessment part I: model development 1. JAWRA Journal of the American Water Resources Association, 34(1), 73-89.

Aizebeokhai, A. P. (2009). Global warming and climate change: Realities, uncertainties and measures. International journal of physical sciences, 4(13), 868-879.

Breuer, L., Huisman, J. A., & Frede, H. G. (2006). Monte Carlo assessment of uncertainty in the simulated hydrological response to land use change. Environmental Modeling & Assessment, 11, 209-218.

Bosshard, T., Kotlarski, S., Ewen, T., & Schär, C. (2011). Spectral representation of the annual cycle in the climate change signal. Hydrology and Earth System Sciences, 15(9), 2777-2788.

Bhatta, B., Shrestha, S., Shrestha, P. K., & Talchabhadel, R. (2019). Evaluation and application of a SWAT model to assess the climate change impact on the hydrology of the Himalayan River Basin. Catena, 181, 104082.

Baker, T. J., & Miller, S. N. (2013). Using the Soil and Water Assessment Tool (SWAT) to assess land use impact on water resources in an East African watershed. Journal of hydrology, 486, 100-111.

Chim, K., Tunnicliffe, J., Shamseldin, A., & Chan, K. (2021). Identifying future climate change and drought detection using CanESM2 in the upper Siem Reap River, Cambodia. Dynamics of Atmospheres and Oceans, 94, 101182.

Cunha, A. P. M., Zeri, M., Deusdará Leal, K., Costa, L., Cuartas, L. A., Marengo, J. A., ... & Ribeiro-Neto, G. (2019). Extreme drought events over Brazil from 2011 to 2019. Atmosphere, 10(11), 642.

Christensen, N. S., & Lettenmaier, D. P. (2007). A multimodel ensemble approach to assessment of climate change impacts on the hydrology and water resources of the Colorado River Basin. Hydrology and Earth System Sciences, 11(4), 1417-1434.

Dingman, S. L. (1994). Physical hydrology. Prentice-Hall, Inc., Englewood Cliffs, NJ.

Eisner, S., Voss, F., & Kynast, E. (2012). Statistical bias correction of global climate projections–consequences for large scale modeling of flood flows. Advances in Geosciences, 31, 75-82.

Estrela, T., Pérez-Martin, M. A., & Vargas, E. (2012). Impacts of climate change on water resources in Spain. Hydrological Sciences Journal, 57(6), 1154-1167.

Fix, M. J., Cooley, D., Sain, S. R., & Tebaldi, C. (2018). A comparison of US precipitation extremes under RCP8. 5 and RCP4. 5 with an application of pattern scaling. Climatic Change, 146, 335-347.

Godfray, H. C. J., Beddington, J. R., Crute, I. R., Haddad, L., Lawrence, D., Muir, J. F., ... & Toulmin, C. (2010). Food security: the challenge of feeding 9 billion people. science, 327(5967), 812-818.

Gassman, P. W., Reyes, M. R., Green, C. H., & Arnold, J. G. (2007). The soil and water assessment tool: historical development, applications, and future research directions. Transactions of the ASABE, 50(4), 1211-1250.

Graham, L. P., Hagemann, S., Jaun, S., & Beniston, M. (2007). On interpreting hydrological change from regional climate models. Climatic change, 81(Suppl 1), 97-122.

Herrmann, M., Ngo-Duc, T., & Trinh-Tuan, L. (2020). Impact of climate change on sea surface wind in Southeast Asia, from climatological average to extreme events: results from a dynamical downscaling. Climate dynamics, 54(3), 2101-2134.

Her, Y., Yoo, S. H., Cho, J., Hwang, S., Jeong, J., & Seong, C. (2019). Uncertainty in hydrological analysis of climate change: multi-parameter vs. multi-GCM ensemble predictions. Scientific reports, 9(1), 4974.

Heng, C. H. I. N. D. A., Doch, S. O. T. H. E. A. V. I. N., & Diepart, J. C. (2013). Toward Measuring the Vulnerability of Agricultural Production to Flood: Insight from Sangker River Catchment, Battambang Province, Cambodia. International Journal of Environmental and Rural Development, 4(2), 89-97.

Im Monichoth, S., Tsujimoto, K., Aida, K., Tamagawa, K., Ohta, T., Koike, T., ... & Homma, K. (2014). Water and food security under climate change in Cambodia. TRANSACTIONS OF THE JAPAN SOCIETY FOR AERONAUTICAL AND SPACE SCIENCES, AEROSPACE TECHNOLOGY JAPAN , 12 (ists29), Tn_31-Tn_39.

Jacobsen, A. L., & Pratt, R. B. (2018). Extensive drought‐associated plant mortality as an agent of type conversion in chaparral shrublands. New Phytologist, 219(2), 498-504.

Jiang T, Chen YD, Xu C, Chen X, Singh VP. (2007). Comparison of hydrological impacts of climate change simulated by six hydrological models in the Dongjiang Basin, South China.Journal of Hydrology336: 316 – 333.

Krysanova, V., Donnelly, C., Gelfan, A., Gerten, D., Arheimer, B., Hattermann, F., & Kundzewicz, Z. W. (2018). How the performance of hydrological models relates to credibility of projections under climate change. Hydrological Sciences Journal, 63(5), 696-720.

Li, Z., Liu, W. Z., Zhang, X. C., & Zheng, F. L. (2009). Impacts of land use change and climate variability on hydrology in an agricultural catchment on the Loess Plateau of China. Journal of hydrology, 377(1-2), 35-42.

Lu, Y., Yuan, J., Lu, X., Su, C., Zhang, Y., Wang, C., ... & Sweijd, N. (2018). Major threats of pollution and climate change to global coastal ecosystems and enhanced management for sustainability. Environmental Pollution, 239, 670-680.

Lin, B., Chen, X., Yao, H., Chen, Y., Liu, M., Gao, L., & James, A. (2015). Analyses of landuse change impacts on catchment runoff using different time indicators based on SWAT model. Ecological Indicators, 58, 55-63.

Moriasi, D. N. Arnold, J. G. Van Liew, M. W. Binger, R. L. Harmel, R. D. Veith, T. L. (2007). Model evaluation guidelines for systematic quantification of accuracy in watershed simulations. Transactions of the ASABE, 50(3), 885-900

Maraun, D. (2016). Bias correcting climate change simulations-a critical review. Current Climate Change Reports, 2(4), 211-220.

Michinaka, T., Miyamoto, M., Yokota, Y., Sokh, H., Lao, S., & Ma, V. (2013). Factors affecting forest area changes in Cambodia: An econometric approach. Journal of Sustainable Development, 6(5), 12.

Magnaye, A. M. T., Aragon, L. G. B., Dado, J. M. B., Cruz, F. T., Olaguera, L. M. P., Narisma, G. T., ... & Sopaheluwakan, A. (2023). Process-based analysis of the impacts of sea surface temperature on climate in CORDEX-SEA simulations. Climate Dynamics, 61(9), 4749-4771.

Najafi, M. R., Moradkhani, H., & Jung, I. W. (2011). Assessing the uncertainties of hydrologic model selection in climate change impact studies. Hydrological processes, 25(18), 2814-2826.

Neitsch, S. L., Arnold, J. G., Kiniry, J. R., & Williams, J. R. (2011). Soil and water assessment tool theoretical documentation version 2009. Texas Water Resources Institute.

Narsimlu, B., Gosain, A. K., & Chahar, B. R. (2013). Assessment of future climate change impacts on water resources of Upper Sind River Basin, India using SWAT model. Water resources management, 27, 3647-3662.

Oeurng, C., Cochrane, T. A., Chung, S., Kondolf, M. G., Piman, T., & Arias, M. E. (2019). Assessing climate change impacts on river flows in the Tonle Sap Lake Basin, Cambodia. Water, 11(3), 618.

Pierce, D. W., Barnett, T. P., Santer, B. D., & Gleckler, P. J. (2009). Selecting global climate models for regional climate change studies. Proceedings of the National Academy of Sciences, 106(21), 8441-8446.

Sok, S., Chhinh, N., Hor, S., & Nguonphan, P. (2021). Climate change impacts on rice cultivation: a comparative study of the Tonle Sap and Mekong river. Sustainability, 13(16), 8979.

Shrestha, S., Bhatta, B., Shrestha, M., & Shrestha, P. K. (2018). Integrated assessment of the climate and landuse change impact on hydrology and water quality in the Songkhram River Basin, Thailand. Science of the Total Environment, 643, 1610-1622.

Sang, L., Zhang, C., Yang, J., Zhu, D., & Yun, W. (2011). Simulation of land use spatial pattern of towns and villages based on CA–Markov model. Mathematical and Computer Modelling, 54(3-4), 938-943.

Sourn, T., Pok, S., Chou, P., Nut, N., Theng, D., Rath, P., ... & Prasad, P. V. (2021). Evaluation of land use and land cover change and its drivers in Battambang Province, Cambodia from 1998 to 2018. Sustainability, 13(20), 11170.

Tangang, F., Chung, J. X., Juneng, L., Supari, Salimun, E., Ngai, S. T., ... & Kumar, P. (2020). Projected future changes in rainfall in Southeast Asia based on CORDEX–SEA multi-model simulations. Climate Dynamics, 55, 1247-1267.

Tangang, F., Santisirisomboon, J., Juneng, L., Salimun, E., Chung, J., Supari, S., ... & Yang, H. (2019). Projected future changes in mean precipitation over Thailand based on multi‐model regional climate simulations of CORDEX Southeast Asia. International Journal of Climatology, 39(14), 5413-5436.

Tan, M. L., Juneng, L., Tangang, F. T., Chan, N. W., & Ngai, S. T. (2019). Future hydro-meteorological drought of the Johor River Basin, Malaysia, based on CORDEX-SEA projections. Hydrological Sciences Journal, 64(8), 921-933.

Tuyet, N. T., Thanh, N. D., & Van Tan, P. (2019). Performance of SEACLID/CORDEX-SEA multi-model experiments in simulating temperature and rainfall in Vietnam. Vietnam Journal of Earth Sciences, 41(4), 374-387.

Teutschbein, C., & Seibert, J. (2010). Regional climate models for hydrological impact studies at the catchment scale: a review of recent modeling strategies. Geography Compass, 4(7), 834-860.

Trang, N. T. T., Shrestha, S., Shrestha, M., Datta, A., & Kawasaki, A. (2017). Evaluating the impacts of climate and land-use change on the hydrology and nutrient yield in a transboundary river basin: A case study in the 3S River Basin (Sekong, Sesan, and Srepok). Science of the Total Environment, 576, 586-598.

Yang, J., Gong, D., Wang, W., Hu, M., & Mao, R. (2012). Extreme drought event of 2009/2010 over southwestern China. Meteorology and Atmospheric Physics, 115, 173-184.

Yira, Y., Diekkrüger, B., Steup, G., & Bossa, A. Y. (2017). Impact of climate change on hydrological conditions in a tropical West African catchment using an ensemble of climate simulations. Hydrology and Earth System Sciences, 21(4), 2143-2161.

Zhang, L., Cheng, L., Chiew, F., & Fu, B. (2018). Understanding the impacts of climate and landuse change on water yield. Current Opinion in Environmental Sustainability, 33, 167-174.

Zhang, H., Wang, B., Li Liu, D., Zhang, M., Leslie, L. M., & Yu, Q. (2020). Using an improved SWAT model to simulate hydrological responses to land use change: A case study of a catchment in tropical Australia. Journal of Hydrology, 585, 124822.

CHAPTER 7 General conclusions and recommendations

This chapter provides a summary of the findings, as well as the limitations of the study, followed by recommendations for further research.

7.1 Conclusions and Recommendations

The purpose of this multi-case study is to explore the key considerations in assessing water scarcity and determining the influence of environmental changes on the availability of water resources in the upper Sangker River basin. The conclusions from this study follow the research questions and the findings and therefore address three themes: (1) evaluation of the water balance in the irrigation system; (2) prediction of future land use changes; and (3) assessment of the impact of land use and climate change on water resources on the hydrological watershed.

Evaluation of the water balance in the irrigation system

Analysis of the river discharge and irrigation water (IW) demands from 2014 to 2018 revealed fluctuations in water availability. Shortages of 50–99% of the monthly requirement were observed in the early wet season months (April to June), while excess water was noted in the late wet season months (August to November) between 2014 and 2017. Furthermore, intense rainfall in 2018 led to sufficient water for irrigation supply. These findings underscore the impact of changing weather conditions and precipitation levels on water availability for irrigation, indicating a significant influence of climate patterns on river discharges.

In addition to comparing river discharge and irrigation water demand, the study assessed actual IW supply and requirements. The results showed that 52% and 41% of actual IW experienced deficits for the left and right main canals, respectively, during wet season months (September and October). The study concluded that water shortages are influenced not only by seasonal variations but also by the quality and efficiency of irrigation systems. Field surveys revealed that damaged canals contributed to water losses, highlighting the importance of regular maintenance and management of water infrastructure for sustainable water supply to paddy fields.

Furthermore, hydrological modeling using the SWAT model demonstrated strong performance in simulating observed and predicted streamflow, as evidenced by statistical metrics of NSE = 0.58/RSR=0.64 and NSE = 0.69/RSR=0.55 during the calibration and validation periods, respectively.

However, this research is subject to the limitation of the scope of the data collection. Due to time constraints, the canal discharge observation was conducted within several months. Future studies should further explore this topic in more depth to obtain a more comprehensive understanding of the efficiency and capability of irrigation water supply.

Prediction the future land use changes

The second objective of this study was to analyze the dynamic changes in land cover and predict future land use in the upper Sangker River basin. The findings revealed significant shifts in vegetation conversion following the economic recovery of the past two decades. These changes were predominantly attributed to factors such as population growth, economic development, land concession, and landmine clearance. The study also projected future land use in 2030 based on historical change dynamics and in combination with land use development projects. It was predicted that forests would continue to face deforestation, although the research also highlighted the positive impact of land use policies in increasing forest cover.

The study acknowledged the complexity and challenges of predicting land use, particularly due to uncertainties in government policies and the intricacies of the model. While the CA-Markov model, coupled with remote sensing, demonstrated its effectiveness in trend projection, it was noted that socio-economic factors and unforeseen changes in government policy were not fully accounted for. To address this limitation, the study proposed integrating the model with GIS tools.

Furthermore, the study suggests the potential for advancements in remote sensing and machine learning to enhance land use and cover forecasting. Ultimately, the study provides valuable insights for policymakers to better understand the factors influencing land use changes in agricultural watersheds. It stressed the importance of comprehending these

changes for effective land management and planning and recommended the implementation of forest conservation measures to safeguard ecosystem services and water cycles.

Assessment of the impact of land use and climate change on water resources

The final part of this study explored the complex interrelationships between changing land use patterns and climate change on the availability of water resources in the upper Sangker River basin. The first major finding was that isolated land use change led to increased mean annual and seasonal discharges, surface runoff, and water yield. However, it led to a decrease in evapotranspiration. This result indicated that the removal of forests caused a decrease in the amount of water returned to the atmosphere through evapotranspiration, leading to a change in rainfall patterns. The second major finding was that combined impacts of land cover change and climate variability reduced amounts of mean annual discharge but triggered to a large shift between the wet season and dry season. Moreover, surface runoff and water yield illustrated a decreasing trend in the forests and mixed residential, farmland, and paddy fields. A conclusion to be drawn from these findings is that climate change is more influential than land use change. A large change in river flow between the wet and dry seasons may lead to flooding events in the rainy season and severe drought in the dry season. The third major finding was that hydrological simulation using predicted land use integrated with land use development projects revealed a positive impact on available river flow and hydrological cycle. The importance of reforestation for hydrological and ecological systems was emphasized, along with the need for further research to identify flood and drought-prone areas for sustainable water resource management and development.

The research acknowledged limitations due to the low availability of climate data, as the hydrological model was simulated using only one climate station. This limitation could introduce significant uncertainties in the model results. As the availability and quality of data improve, the hydrological model will become a valuable tool for river discharge estimation and water resource management, even in data-scarce environments.

Overall, the results reveal essential factors affecting water resources in the Upper Sangker River Basin under climate change and land use change. Based on these results, this study suggests the need to promote water-efficient agricultural practices, cultivate climate-resilient crops, and make significant investments in conserving and restoring natural resources.